TOWARD THE DEVELOPMENT OF SYNTHETIC MICROBIAL CONSORTIA UTILIZING ENGINEERED CYANOBACTERIA AND HETEROTROPH INTERACTIONS

By

Derek T. Fedeson

A DISSERTATION

Submitted to
Michigan State University
in partial fulfillment of the requirements
for the degree of

Genetics – Doctor of Philosophy

2018

ABSTRACT

TOWARD THE DEVELOPMENT OF SYNTHETIC MICROBIAL CONSORTIA UTILIZING ENGINEERED CYANOBACTERIA AND HETEROTROPH INTERACTIONS

By

Derek T. Fedeson

Cyanobacteria form the foundation of the trophic cascade of nearly all biospheres on the surface of our planet and are ubiquitous to every known environment. These unique and diverse organisms have recently come to the forefront of contemporary discussions on the sustainable production of fuels, pharmaceuticals, cosmetics, and plastics. This increase in attention is due to many factors including their high photosynthetic capacity, relatively minimalistic growth requirements, genetic tractability, and untapped potential for novel therapeutics. While direct engineering of cyanobacterial species has been the primary focus of present research trends, there is growing interest in utilizing cyanobacteria in the context of synthetic microbial consortia to accomplish similar biotechnological goals. This approach allows for the distribution of metabolic load amongst the different participating species and compartmentalization of specialties that in the context of cyanobacterial driven consortia could mean that the cyanobacteria fulfill the role of providing nutrients to other members of the consortia in the form of fixed carbon or nitrogen. The goal, in essence, would be to create a synthetic symbiotic or commensal/cross-feeding interaction between the cyanobacteria and the other members of the synthetic community. However, there are many considerations that need to be addressed when conceptualizing how artificial consortia might be applied on an industrial scale which include maintaining species specificity in these consortia, facilitating nutrient exchange between species, preventing invasion of contaminating microbes, enabling the use of contaminated water sources, and

identification of compatible metabolisms. Here, I present my work to address many of these questions through: A) the development of a functional surface display system that allows for mediated binding of cyanobacteria to functionalized cells/particles, B) the expansion of the surface display system, C) the creation of a photosynthetic co-culture capable of remediating waste water contaminated with a xenobiotic, and D) the experimental evolution of a heterotrophic species in long term co-culture with alginate bead encapsulated cyanobacteria. These approaches were designed to both mimic naturally occurring microbial partnerships, which utilize spatial co-localization of symbiotic species to ensure partnership stability and ward off potential contaminants, and provide practical utility in an industrial context. Furthermore, this work lays the foundation for comprehensive study of how cell-cell adhesion and long-term co-evolution could influence symbiotic relationships between microbial organisms, with the potential to yield insights into the conditions that eventually led to the endosymbiotic event that gave rise to the chloroplasts found in eukaryotic photosynthetic species.

This dissertation is dedicated to my family.
To my wife and my daughter, I love you both and you are the source of my inspiration. I could not have done this without you and there are no words capable of expressing my gratitude.
To my parents, your support and unwavering faith in me have meant more than you know.
To my siblings, thank you for always being there when I needed you.

ACKNOWLEDGMENTS

During my time here at the Michigan State University, I was fortunate to interact with many wonderful and talented individuals who spurred my development academically and provided the support necessary to develop this research.

First and foremost I would like to thank my mentor, Dr. Daniel Ducat. Without his knowledge and guidance, none of this work would have been possible. His kind and compassionate nature set the tone for my experience here at MSU and I count myself lucky to have been one of his students. Thank you all Ducat lab members for your camaraderie! I would also like to thank my committee members, Dr. Christoph Benning, Dr. Beronda Montgomery, and Dr. Timothy Whitehead for their expertise and constructive feedback on my work over the years. Their perspectives and advice have helped me develop and grow as a scientist. A final thanks and acknowledgment to the many wonderful individuals I have met during my time as part of the PRL community and as a student in the Genetics Program here at MSU.

There are no words to describe the gratitude I feel toward family and friends for all of their support. Julia, Claire, Jodi, Brian, Gwen, Jonathan Sr., Jonathan Jr., Erin, Renee, Amy, Courtney, Joyce, Thomas, Rose, Ryan, Jimmy, Fernando, Stephanie, Martin, and Kristen, you are all amazing and I am blessed to have you in my life.

TABLE OF CONTENTS

LIST OF TABLES

LIST OF FIGURES

CHAPTER 1: INTRODUCTION

"SYMBIOTIC INTERACTIONS OF PHOTOTROPHIC MICROBES: ENGINEERING SYNTHETIC CONSORTIA FOR BIOTECHNOLOGY"

Derek T. Fedeson & Daniel C. Ducat

This work has been submitted and is currently under review.

Author Contributions:

DTF and DCD wrote and edited the manuscript.

Abstract

Natural microbial communities consist of assemblies of species possessing distinct metabolic capacities. Diversification within the consortia leads to division of labor between species, whereby the global population exhibits functional capabilities that are possessed by only a fraction of its members. Furthermore, community diversity is also associated with higher bioproductivities and robustness compared to microbial 'monocultures.' In this review, we highlight both natural and engineered interactions between photosynthetic microbes and other organisms, with an emphasis on learning design principles of microbial communities through the process of building them from the "bottom up." Rational design of relatively simple microbial communities is likely to substantially improve our understanding of much more complex natural consortia that have important ecological significance. Furthermore, a deeper understanding of effective design principles of microbial communities could enable the application of light-driven microbial cultures for a variety of environmental and biotechnological goals.

Introduction

Microbial communities comprise a substantial proportion of the biomass on Earth (Bar-On et al. 2018) and underlie the health and functioning of many different ecosystems. Complex microbial communities contribute to turnover of a number of critical global biogeochemical cycles, including nitrogen, oxygen, carbon, sulphur, and phosphorous (De Roy et al. 2014). Furthermore, the composition of local microbiomes is increasingly recognized to have direct and substantial impacts on the health of multicellular plants and animals (Mueller and Sachs 2015). Indeed, the vast majority of microorganisms live within multi-species communities, yet we have relatively limited knowledge about microbial interactions within these networks and how these interactions shape community properties and ecosystem functions (Chodkowski and Shade 2017). The majority of microbiology research conducted in the 20th century focused upon axenic (single-species) cultures (Jessup et al. 2005). Reductionist microbiology has led to a number of scientific breakthroughs and valuable outcomes, but has also necessarily isolated microorganisms from their natural context, instead emphasizing their behaviors within a test tube (Little et al. 2008).

Within the past two decades, powerful new methodologies have emerged that facilitate systems-level approaches to study microbial community ecology. These methods include improved genomic and transcriptomic sequencing, mass spectrometry-based metabolomics, and proteomics (Franzosa et al. 2015). The development of such technologies has paved the way to begin to approach some of the most ecologically and bioindustrially-relevant microbial communities that are involved in everything from human health to agriculture (Tringe and Rubin 2005). Yet, while these technologies have

greatly expanded our capacity to inventory the total species and reactions within microbial consortia, the complex datasets they generate do not illuminate the structure of these communities. These deficiencies highlight the need to distill generalizable principles that describe fundamental organization of disparate communities. Identification of common themes of microbial interaction that translate across numerous consortia is needed in order to more fully understand consortia behaviors. Furthermore, this knowledge can provide the basis for design principles that may inform the engineering of artificial multi-species consortia. The ability to customize microbial communities or redesign existing microbiomes represents a new horizon in medicine, agriculture, and bioindustry (Costello et al. 2012; Rollié et al. 2012; Gopal et al. 2013; Song et al. 2014b; Lindemann et al. 2016).

In this review, we summarize different approaches that have been used to study microbial communities and inter-species interactions. To productively constrain our discussion within this broad field, we will focus upon natural communities dominated by phototrophic microbes (especially cyanobacteria), and emphasize biotechnological applications relying on these microbes. We first briefly summarize a couple representative natural photosynthetic microbial consortia of ecological significance. This includes interactions between photosynthetic microbes within the open ocean that contribute a large proportion to global biogeochemical cycles, and plant-cyanobacterial symbioses that can influence agricultural productivity. A discussion of these natural communities will also highlight features evident within natural microbial consortia (*e.g.,* high productivity, robustness to environmental perturbations, resistance to invasive species) that are lacking in many current bioindustrial technologies. Yet, the difficulty of dissecting the interaction networks within these natural communities also illustrates current limitations in our

ability to uncover fundamental design principles that underlie desirable traits within these communities.

As an alternative approach for understanding microbial consortia, we will then review the emerging field of synthetic microbial ecology, which advocates the use of a "bottom-up" approach for understanding microbial consortia. Synthetic microbial ecology is a term that broadly describes all rationally designed ecosystems created by assembling two or more defined microbial populations in a well-characterized and controlled environment. By organizing a relatively small number of defined microbes into a consortium, synthetic ecology allows for the creation of greatly simplified interaction networks relative to the highly complex and integrated interactomes of natural communities (Jessup et al. 2004). Furthermore, because the communities are built from the bottom up, member species with established molecular toolkits can be selected. This enables the use of genetic manipulation to systematically dissect the functions of a given microbe within a larger community. In this way, synthetic microbial ecologists are attempting to distill complex interaction networks into broadly-applicable theoretic principles useful for constructing predictive models for microbial communities (Prosser et al. 2007). We will discuss some applications for synthetic consortia, summarize their current limitations, and provide perspectives on the progression of this field.

Part I: Natural photosynthetic microbial communities of ecological and technological relevance

Photosynthetic microbes are found in many symbiotic interactions across most ecosystems, and cyanobacteria appear especially prolific in their capacity to form symbiotic associations with a wide variety of both prokaryotic and eukaryotic partners. Indeed, cyanobacteria have well-documented mutualisms across many kingdoms, including with plants, mosses, fungi, sponges, dinoflagellates, diatoms, and other bacteria (Adams 2000; Usher et al. 2007). Such symbiotic interactions can be with a single other species, or, as is more common in most environments, a collective of other organisms. Cyanobacterial symbiotic interactions can be largely categorized around their capacity to fix atmospheric carbon (CO_2) or nitrogen (N_2) and provide them in bioavailable forms to associated species within their communities. Below, we discuss two representative symbiotic relationships involving cyanobacteria that revolve around their capacity to either provide fixed carbon, or fixed nitrogen for partner species.

Cyanobacterially-driven marine ecosystems

Marine microbial communities are responsible for as much as half of the global cycling of carbon, nitrogen, sulfur, phosphorus, as well as many important micronutrients (Fuhrman et al. 2015). Such communities can be composed of bacteria, archaea, protists, fungi, and their respective viruses, which form the foundation of the food webs comprising larger marine lifeforms (Sherr and Sherr 2002). In many marine environments, primary production is mainly attributable to prokaryotic phototrophs, which in turn are dominated by the large cyanobacterial groups, *Synechococcus* and *Prochlorococcus*. In much of the

surface waters of the open ocean, free-living *Prochlorococcus* are the most abundant organisms in both number and total biomass. Due to the large area of this environment, these cyanobacteria are estimated to be the most abundant photosynthetic cell type on Earth (Partensky et al. 1999). As such, it has been estimated that *Prochlorococcus* accounts for ~4 gigatons of fixed carbon annually, a number equivalent to the primary productivity of all croplands (Biller et al. 2015).

Prochlorococcus is a broad bacterial group that descends from the marine lineage of *Synechococcus* and is classified partially by some unique features that distinguish it from other cyanobacteria. *Prochlorococcus* is unusually small for a photosynthetic prokaryote (typically <1 um in length and width (Morel et al. 1993)), potentially placing it near the physical lower limit of cell size for an oxygenic phototroph (Raven 1994). Furthermore, *Prochlorococcus* has a unique set of divinyl chlorophyll derivatives which allow use of straightforward spectroscopic methods to quantify the abundance of these cyanobacteria in mixed communities (Morel et al. 1993). *Prochlorococcus* can be divided into clades or ecotypes that stratify in the water column (Biller et al. 2015; Johnson et al. 2017) and are classified based on their adaptation to high-light (HL) or low-light (LL) conditions. Within the HL group, the most recently diverged members are found nearest to oligotrophic surface waters where light is abundant, but other essential nutrients are growth limiting (Braakman et al. 2017). Indeed, *Prochlorococcus* appears to have experienced strong selected pressure for survival in low nutrient conditions (Dufresne et al. 2008) and is well-adapted for growth at very low ambient concentrations of nitrogen, phosphate, and iron.

Given *Prochlorococcus*' relatively slow growth rates and nutrient-poor environment, it is somewhat surprising that these cyanobacteria have a high rate of CO_2 fixation relative

to other cyanobacterial species (Hartmann et al. 2014). This appears to be due in part to their secretion of a large amount of soluble carbohydrates (estimated to account for up to ~25% of total fixed carbon; Bertilsson et al., 2005). Indeed, a recent paper posits that under the nutrient-limited environment of the open ocean, *Prochlorococcus* has been selected to minimize nutrient requirements and to increase sugar secretion as a metabolic sink to dissipate excess ATP/NADPH (Braakman et al. 2017). This secretion of carbohydrates may serve a second role in promoting the formation of symbiotic interactions with neighboring species, as it allows *Prochlorococcus* to directly provide carbon (*e.g.,* via secretion) in addition to indirect (*e.g.,* lysis) routes.

A number of heterotrophic microbes co-exist in mutualistic relationships with *Prochlorococcus*, including some of the most abundant marine bacteria, the α-proteobacteria group SAR11 (*Pelagibacterales*; Giovannoni, 2005). Among other traits, SAR11 is classified by the lack of complete glycine and serine synthesis pathways, deficiencies that can be compensated for by supplementation with the metabolic precursor glycolate (Carini et al. 2013). *Prochlorococcus* secretes glycolate, pyruvate, citrate and other organic acids in large amounts (Bertilsson et al. 2005). These are dominant sources of carbon that promote the growth of SAR11 (Giovannoni 2017). In return, *Prochlorococcus* benefits from SAR11 and other heterotrophic "helper bacteria" that can detoxify reactive oxygen species (ROS; Morris et al., 2011; Zinser, 2018). Many SAR11 ecotypes retain catalases that can mitigate hydrogen peroxide, while *Prochlorococcus* has lost the gene for this enzyme. Other heterotrophic bacteria isolated with *Prochlorococcus* have also been shown to greatly improve the persistence of *Prochlorococcus* cells during periods of extended dark (Biller et al. 2016), perhaps by cross feeding metabolites (such as malate

(Braakman et al. 2017)) or by helping to maintain synchrony in the expression of circadian-controlled genes (Biller et al. 2018). These mutualistic interactions may be especially important to *Prochlorococcus* cells that are carried into deep, light-limited regions of the water column by internal waves and oceanic currents (Biller et al. 2015). Overall, it is proposed that such mutualistic exchanges can greatly increase the total biomass productivity of marine ecosystems, with *Prochlorococcus*-derived carbon contributing up to 40% of total bacterial production (Bertilsson et al. 2005). Given the huge surface area of the ocean, mutualisms that increase carbon capture efficiency of *Prochlorococcus* have the potential to greatly impact global carbon cycling and marine ecosystem food webs (Azam and Malfatti 2007; Brussaard et al. 2016; Braakman et al. 2017).

Despite the importance of *Prochlorococcus*-heterotrophic interactions, our understanding of even the best-studied relationships remains relatively limited. There are several complications related to the analysis of *Prochlorococcus*-SAR11 interactions that illustrate the difficulties encountered in research of natural microbial communities in general. First, despite considerable diversity within *Prochlorococcus*, individual isolates do not differ in their 16S rRNA sequences: a standard metric for defining bacterial species. Instead, *Prochlorococcus* isolates are grouped by ecotype clades, and though individual members may share a 'core-genome' of ~1000 genes that are shared across all *Prochlorococcus*, the "pan-genome" is much larger, with tens of thousands of genes predicted (Baumdicker et al. 2012; Biller et al. 2015). Many genes cluster in hypervariable regions of the genome that can differ largely between otherwise closely related strains: indeed a recent analysis of *Prochlorococcus* populations within the same milliliter water sample have shown that there can be hundreds of distinct co-existing subpopulations that

differ substantially in genomic content but which are stably maintained (Kashtan et al. 2014). Similarly, SAR11 is a broad class of α-proteobacteria with equally difficult nomenclature, species "boundaries," and genomic diversity (Giovannoni 2017). Furthermore, relatively few *Prochlorococcus* or SAR11 isolates have been isolated in axenic cultures, and the genetic tools available for these isolates are quite limited. The physical structuring between *Prochlorococcus* and helper bacteria remains unclear, and such physical associations are known to strongly influence interaction dynamics (De Roy et al., 2014; Jessup et al., 2004; Said and Or, 2017; see below).

Finally, as metagenomic approaches to study natural environments become increasingly advanced and exhaustive (*e.g.,* Tara Oceans Expedition; Bork et al., 2015), it becomes ever more clear that the interactions between *Prochlorococcus* and SAR11 are but a small fraction of the total autotroph/heterotroph "interactome" in any given marine ecosystem. Indeed, pairwise studies between *Prochlorococcus* and more than 300 heterotrophic bacteria isolated from marine environments indicated that the majority of these heterotrophs positively influenced cyanobacterial growth, suggesting that mutualisms may dominate autotroph/heterotroph relationships in these environments (Sher et al. 2011). *Prochlorococcus*-SAR11 interactions may occur against a background of other oceanic microbes, yet some estimates suggest that as few as 0.01-0.1% of these marine species can be cultured in the lab with conventional approaches (Connon and Giovannoni 2002). These complex networks defy current metagenomics and bioinformatics approaches to disentangle and assign roles to individual members within the community (Temperton and Giovannoni 2012; Zengler and Palsson 2012), demanding the

development of new approaches to understand such communities at a systems level (Kazamia et al. 2016).

Plant-cyanobacterial symbioses

Cyanobacteria have a rich history of symbiotic interactions with many plants, and are particularly notable for their mutualistic relationships with an evolutionarily wide range of plants in the green lineage, from Bryophytes (*e.g.,* hornworts, mosses), to ferns, to more recently evolved angiosperms (Usher et al. 2007; Bergman et al. 2008). Many of the most tightly integrated symbiotic interactions are formed between the widespread, terrestrial cyanobacterial genera, *Nostoc* and *Anabaena*. Species within these genera are often capable of nitrogen fixation and form differentiated cellular structures called heterocysts that protect nitrogenases from inactivation by oxygen (Zhang et al. 2006). These traits are important because the capacity to provide a source of fixed nitrogen is a core feature of most cyanobacterial symbioses with plants. In addition to providing nitrogen, cyanobacteria can perform a number of other functions that promote plant health and productivity, including secretion of antibiotics that discourage plant pathogens and improvement of soil fertility (Dodds et al. 1995; Adams 2000). As plant-bacterial interactions are a focal topic beyond the context of this dissertation, we do not focus upon this topic at length here, (interested readers are directed to excellent reviews; Adams, 2000; Adams et al., 2013; Bergman et al., 2008; Rai et al., 2000), but instead provide a brief discussion in the broader context of the study of microbial communities.

Unlike the symbiotic interactions between cyanobacteria and heterotrophic bacteria within marine habitats, some of the best studied examples of plant-cyanobacterial

interactions have a high degree of structural definition. Such mutualistic interactions are often initiated by the release of diffusible signals (*e.g.,* hormogonia inducing factor, HIF) from nitrogen-starved plants, these signals stimulate differentiation of nearby cyanobacteria into infective stages (*i.e.*, hormogonia; Meeks and Elhai, 2002). Hormogonia development involves structural changes and the expression of motility genes that allow cyanobacterial filaments to migrate towards the plant, often leading to invasion and colonization of predefined plant cavities, open stomata, or uptake as intracellular endophytes (Rai et al. 2002). Following colonization, inter-species signaling pathways direct further differentiation of cyanobacteria, often leading to enhanced heterocyst formation and improved nitrogen fixation capabilities. In this way, the cyanobiont becomes capable of increased secretion of ammonium or other nitrogen-containing compounds for the benefit of the host plant. "Loose associations" between plants and cyanobacteria are also widespread, where cyanobacteria play important roles in the broader microbial community in rhizosphere surrounding plant roots, or where cyanobacteria grow epiphytically on plant leaves or other surfaces.

In return, the plant provides several benefits for cyanobacterial partners. In most cases, the plant host can become the primary source of carbon for the cyanobiont, secreting carbohydrates into a localized space, or by general secretion of diffusible organic carbon compounds in the broader vicinity of plant structures. For example, it is estimated that many plants secrete a substantial proportion (up to 20%) of the total carbon they fix through the roots, where it can support the growth of nearby microbes (Bais et al. 2006). Cyanobacteria tightly associated with plants can gain other advantages due to the environment that is provisioned by the plant, including supply of additional nutrients (Rai

et al. 2000), and protection from external environmental stresses, such as desiccation (Adams 2000). For example, in one of the better studied interactions between the cyanobacteria *Nostoc azollae* and the free-floating aquatic fern *Azolla*, the cyanobacterium is housed in a dorsal leaf cavity where it is fed carbohydrates and other nutrients. *Nostoc azollae* in turn provides the host plant with sufficient nitrogen to promote its rapid growth even in relatively nitrogen depleted waters (Adams et al. 2013). This symbiotic interaction is of major agronomic significance, particularly in the cultivation of rice, as *Azolla* is widely used as a traditional 'green manure' for fertilization of crop species (Vaishampayan et al. 2001).

Despite a more detailed understanding of some molecular mechanisms of cyanobacteria-plant interactions, these relationships remain difficult to study and relatively poorly understood. In many cases, the co-evolution of the cyanobiont and host has been extensive, leading to the development of complex networks of metabolic exchange and signaling molecules. Many plant derived HIF factors are unknown, while cyanobacteria also employ a range of anti-hormongonia factors (Liaimer et al. 2015) that also are relatively poorly understood. Once in an established mutualistic interaction, the network of signals exchanged is likely extensive, but largely uncharacterized. Efforts to disentangle these networks are sometimes complicated by the limited ability to culture partner species independently and underdeveloped molecular toolkits. As an example, cyanobionts are vertically transmitted in the *Nostoc-Azolla* mutualism. This means that the association between partners is extremely long-lived and stable across generations, to the extent that it is debatable if *de novo* infection occurs in a natural context, and if free-living cyanobacteria can grow independently (Adams et al. 2013). While this level of stability would be desirable

to replicate in engineered microbial interactions, it renders natural mutualisms with this level of interdependency difficult to dissect.

Part II: Promise and current limitations of the application of synthetic microbial communities

Synthetic microbial ecology & microbial ecology theory

Synthetic microbial ecology offers an alternative approach to study fundamental questions concerning microbial interactions and to examine how local interactions between microbes can lead to complex higher-order patterns at the population level. Synthetic microbial ecology uses simple artificial communities that retain features of natural microbial communities, but which display greatly reduced network complexity in terms of the number of interacting species and the degree of connectivity between species (Momeni et al. 2011). Synthetic microbial communities are typically established between experimentally-tractable organisms that can be selected or engineered to interact through defined pathways. The ability to construct ecologies composed of model organisms can be beneficial for a variety of reasons including the short generation times, small genomes, advanced genetic toolkits, and capacity to freeze populations for evolution studies. There are, of course, inherent tradeoffs between the level of control over such artificial systems and the realism of these platforms to natural microbial communities (Figure 1.1).

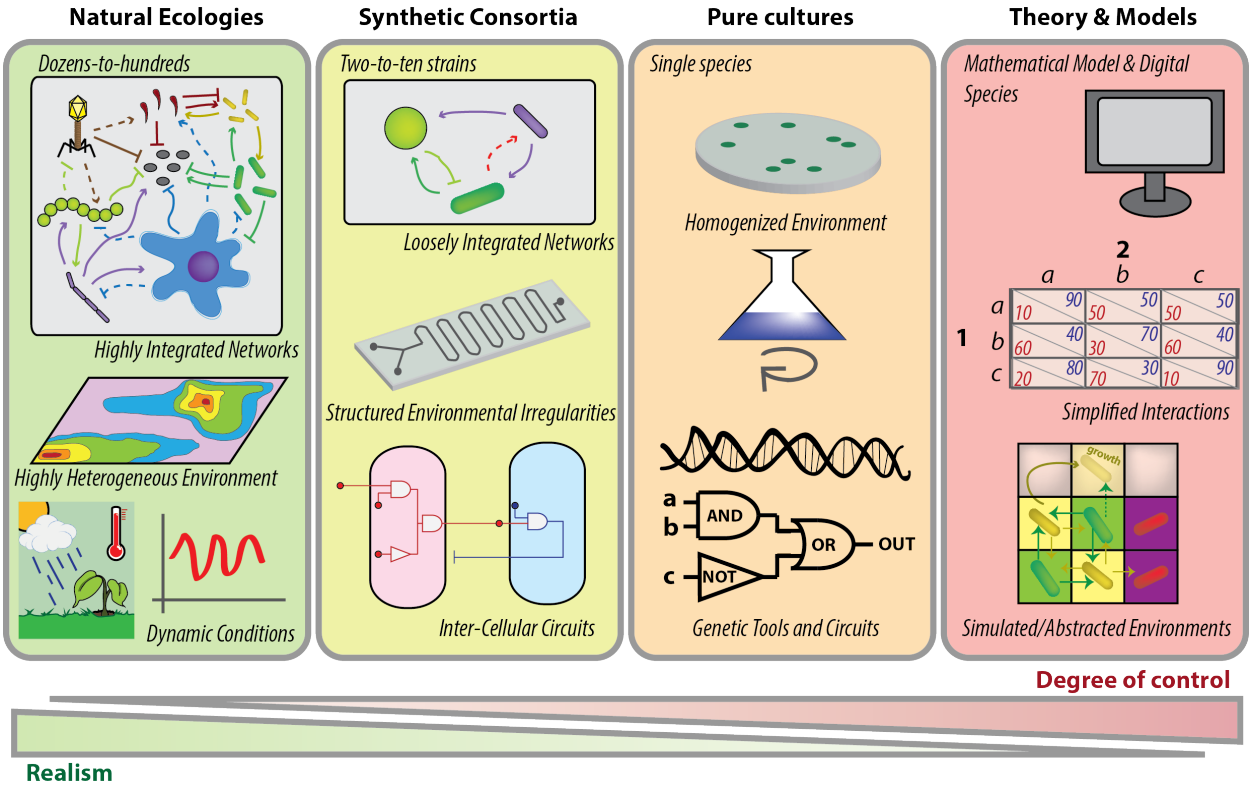

Figure 1.1: Study of microbial ecology at different levels of abstraction

Understanding the factors that shape population-level behaviors of microbial communities requires independent lines of approach. Natural microbial communities are frequently composed of dozens to hundreds of different microbial species, many of which may have co-evolved in the given ecosystem over many generations. Direct (solid lines) and indirect (dotted lines) interactions comprise a complex network between species. Natural environments also display highly irregular physical and chemical properties, which can dynamically shift over time. Different degrees of reductionism have been used to disentangle the complexities of natural systems. Mathematical theories and computational models represent the most abstracted field of research, including low-resolution population-based models, metabolic network models, and individual-based simulations (Song et al. 2014a). Pure microbial cultures allow detailed physiological studies of an isolated species in a highly defined and homogeneous environment. Depending on the microbe, a variety of genetic tools and sophisticated circuits may assist analysis. Synthetic microbial consortia consist of 2 or more microbes that interact through defined pathways. Although other emergent interactions (red dotted lines) are likely to arise between species, the networks are regarded to be much less tightly integrated, and the nature of such interactions can be probed through genetic approaches generally not available during the study of natural ecologies.

Yet, it is recognized that the field of microbial ecology currently has limited theories that can be used to predict the behavior of populations (Prosser et al. 2007; Widder et al. 2016),

and artificial communities are increasingly regarded as an important bridge between abstract mathematical models and the complexity of natural consortia. For some of these reasons, the last decades have seen a steady rise in the use of synthetic microbial communities as a method to study fundamental questions related to the structure and function of ecological networks (Jessup et al. 2005).

In recent years, study of synthetic microbial ecologies has provided a number of useful platforms for study of a variety of variables known to influence natural microbial consortia (De Roy et al., 2014; Jessup et al., 2004; Prosser et al., 2007; Figure 1.1). Natural consortia can be composed of hundreds to thousands of species that interact through the exchange of (often unknown) metabolites and signaling molecules, yet despite these intricate features, such communities display a surprising persistence and resilience in the face of environmental perturbations. This trait is commonly referred to as robustness, or the ability of a community to maintain its functional and structural integrity in the face of fluctuating environmental and biotic conditions. In previously-discussed examples, the *Azolla*-*Nostoc* mutualism can persist through numerous generations (Adams et al. 2013), while *Prochlorococcus*-dominated communities in the open ocean display a surprising degree of regularity in composition from year to year, even cycling through predictable, seasonally-driven states that maintain key features at the population level (Malmstrom et al. 2010). One core ecological theory is that higher diversity contributes to increased community stability; robustness is derived in part by diversity and by redundancy of functions divided amongst multiple community members (Ives and Carpenter, 2007; McCann, 2000). These theories are supported by studies that used a recombinatorial approach to assemble microbial communities with a variable number of phototrophs,

heterotrophic bacteria, and predators, finding that community level features (such as total CO_2 flux or biomass production) became more reliable with increased species diversity (McGrady-Steed et al. 1997; Naeem and Li 1997).

Other studies have emphasized the role of spatial structuring in promoting community stability. For example, multiple synthetic microbial systems for studying predator-prey interactions have been developed and examined for conditions that influence the rate of extinction of one or more partners (Bohannan and Lenski 2000; Kerr et al. 2002). In one notable example, artificial communities of protists were examined for stability under homogenous environments, or under conditions where the same total population size could become subdivided into connected, but locally-differentiated microcosms (Holyoak and Lawler 1996). The results indicated that the heterogenous environment could substantially stabilize the artificial microbial community, providing evidence in support of metapopulation theories that had primarily been examined in mathematical models (Hanski and Hanski 1998). Similarly, a spatially structured environment can also increase the resilience of cooperative behaviors in microenvironments that contain non-cooperating individuals (Doebeli and Hauert 2005). In a homogenous environment, cooperative behaviors that benefit neighboring species but which incur a fitness cost upon the individual (*e.g.,* secretion of a metabolite that requires investment of biochemical resources) are often counter-selected, since non-cooperating community members can reap public benefits without the costs of contributing. Both theoretical and experimental evidence using synthetic microbial consortia have demonstrated that structuring microbial partners into localized communities can stabilize cooperative behavior (Kim et al. 2008; Chuang et al. 2009; Waite and Shou 2012; Allen et al.

2013; Momeni et al. 2013; Kelsic et al. 2015; Pande et al. 2016). Briefly, when exchange of goods between partners is partially restricted to localized environments (*e.g.,* within flocs, or isolated colonies), isolated populations dominated by non-cooperative individuals have weak positive feedback loops, while nearby micro-communities dominated by cooperators can have robust positive feedback and relatively high total growth rates.

The above examples serve to demonstrate how the simplified composition and increased molecular tools of synthetic microbial consortia enable testing of fundamental theories of microbial ecology. Interested readers are directed to several excellent reviews for additional information on synthetic microbial ecology (Jessup et al. 2004; Prosser et al. 2007; Kazamia et al. 2012a; De Roy et al. 2014; Widder et al. 2016).

The biotechnological potential of synthetic consortia

As with the academic literature in microbiology, the majority of current bioindustrial technologies rely on microbial monocultures, although polyculture offers several potential benefits. In particular, if the high metabolic efficiencies and robustness commonly observed in natural consortia could be replicated in synthetic microbial communities, it would have considerable implications for a wide array of industrial, medical, and environmental applications (Goers et al. 2014). Although one common conception in synthetic biology is that improved genetic tools will allow us to reprogram a target biological *chassis* (*e.g., E. coli*) for any desired output, many ecological examples argue that mixed communities should typically outperform a single species (no matter how extensively engineered) in terms of total bioproductivty and robustness.

The concept of biological division of labor is chief among the reasons that increased bioproductivity can be observed in consortia (Brenner et al. 2008; Werner et al. 2014; Hays et al. 2015; Lindemann et al. 2016). Individual members in a complex community adopt specialized roles, allowing niche differentiation and functional complementarity that can enable more efficient resource utilization (Savage et al. 2007). This is reflected in higher bioproductivity yields (*e.g.,* total biomass) from communities compared to populations containing one species, an observation that also applies in rationally designed systems (Eiteman et al. 2008; Shong et al. 2012). Indeed, the improved efficiency of networks containing specialists is a core tenant of biological systems at other scales, including intracellular compartmentalization (Chaijarasphong and Savage 2018), tissue differentiation in multicellular organisms (Ispolatov et al. 2012), and even within social economic theories (Werner et al. 2014). Furthermore, compartmentalization of metabolic reactions across distinct species can mitigate constraints imposed by tradeoffs between different objectives, where increased efficiency in one objective (*e.g.,* metabolic reaction), comes at the cost of another. For example, different enzymes may compete for a common pool of biomolecules (*e.g.,* ATP, NADH, or other precursors and co-factors) and inter-enzyme competition (even between enzymes within a simple, linear metabolic pathway), can result in the accumulation of intermediates and/or constraints in the total flux through desired metabolic steps (Lindemann et al. 2016). In other instances, incompatibilities between one metabolic pathway and another can essentially preclude their simultaneous operation. One example of this is represented by attempts to produce hydrogen gas by using reductant from oxygenic photosynthesis: hydrogenase enzymes are highly oxygen-sensitive, generating many complications when both processes are confined within the

same cell (Ghirardi 2015; Posewitz 2018). Similarly, incompatibilities in metabolic regulation have made it difficult to engineer a single heterotrophic microbe that can efficiently utilize all major sugars released from the hydrolysis of lignocellulosic materials (Eiteman et al. 2008; Minty et al. 2013).

Robustness of natural systems is another feature that is particularly important for biotechnological applications where environmental conditions cannot be strictly controlled. One application where this is the case is in the scaled cultivation of algae and cyanobacteria for the production of fuels, polymers, and other biologics. Algal farming requires increased scaling of the surface area to expand the available input light, which complicates the design of economically-feasible enclosed photobioreactors, especially for the production of commodity goods (Ducat et al. 2011; Chisti 2013). By contrast, the open systems that are deemed more realistic (Sheehan et al. 1998; Chisti 2007) make algal cultures vulnerable to invasive species and largely preclude the possibility of tight environmental control (*e.g.,* temperature; Gupta et al., 2015). Any other biotechnological applications that require release into natural environments (*e.g.,* the application of soil microbes to improve crop yields; Chaparro et al., 2012), will also face the challenge of obtaining a predictable output under highly variable biotic and abiotic conditions.

Most microbial species are not sufficiently robust to be used in a monoculture approach for applications that are exposed to natural environmental fluctuations. Among the largest problems of scaled cultivation of algae and cyanobacteria is the high rate of "pond crashes" caused by invasion of a foreign microbe or virus (Smith et al. 2010; Wang et al. 2013; Carney and Lane 2014). By contrast, natural ecosystems with diverse members can be described as reaching a "climax" steady state, where multiple stable equilibria can

be reached following a perturbation, helping to minimize variation and invasion by foreign species (May 1977; Law and Daniel Morton 1996). If effective ecological principles can be identified and applied to synthetic consortia, higher productivities and "self-regulating" behaviors should be theoretically possible to engineer for biotechnological applications.

Synthetic co-cultures for photosynthesis-driven bioindustry

Given the improbability of maintaining axenic ponds of cyanobacteria or algae, increasing focus is being placed on identifying suitable partner species that will improve productivity or stability of the culture. Many of the current efforts involve prospecting for heterotrophic bacteria which increase total culture yields. As an example, co-inoculation of a bacterial species (*Brevundimonas sp.*) that was isolated as a contaminant of algal cultures, with *Chlorella ellipsoidea* resulted in up to 3 times greater algal growth than that of *C. ellipsoidea* alone (Park et al. 2008). There are many similar examples (Amin et al. 2009; Natrah et al. 2014; Cho et al. 2015), and microbial species that promote growth of cyanobacteria and algae need not be isolated from environments where they grow in proximity to these phototrophs (Hays et al. 2017; Tandon and Jin 2017). The fact that species that do not naturally co-exist with a given phototrophic microbe can also enhance growth in co-culture suggests that there may be generalizable pathways by which heterotrophs perform beneficial functions for algae and cyanobacteria. These pathways may include: mitigation of ROS, increasing dissolved CO_2, cross-feeding of TCA cycle intermediates, increasing accessibility of essential metal ions (i.e., via siderophore secretion), or secretion of soluble vitamins (Natrah et al. 2014; Cooper and Smith 2015; Hays et al. 2017). Identifying a more complete list of common synergistic interactions

between autotroph/heterotroph pairs could benefit from the use of synthetic communities where each partner species has a developed genetic toolkit and robust metabolic models. Deeper understanding of naturally-occurring interactions at the species level could assist in the rational design of partner microbes that could optimize an artificial system (*e.g.,* production in a race-way pond) towards target goals.

One systematic way to explore the design space of synthetic microbial communities is through the development of modular consortia (Figure 1.2).

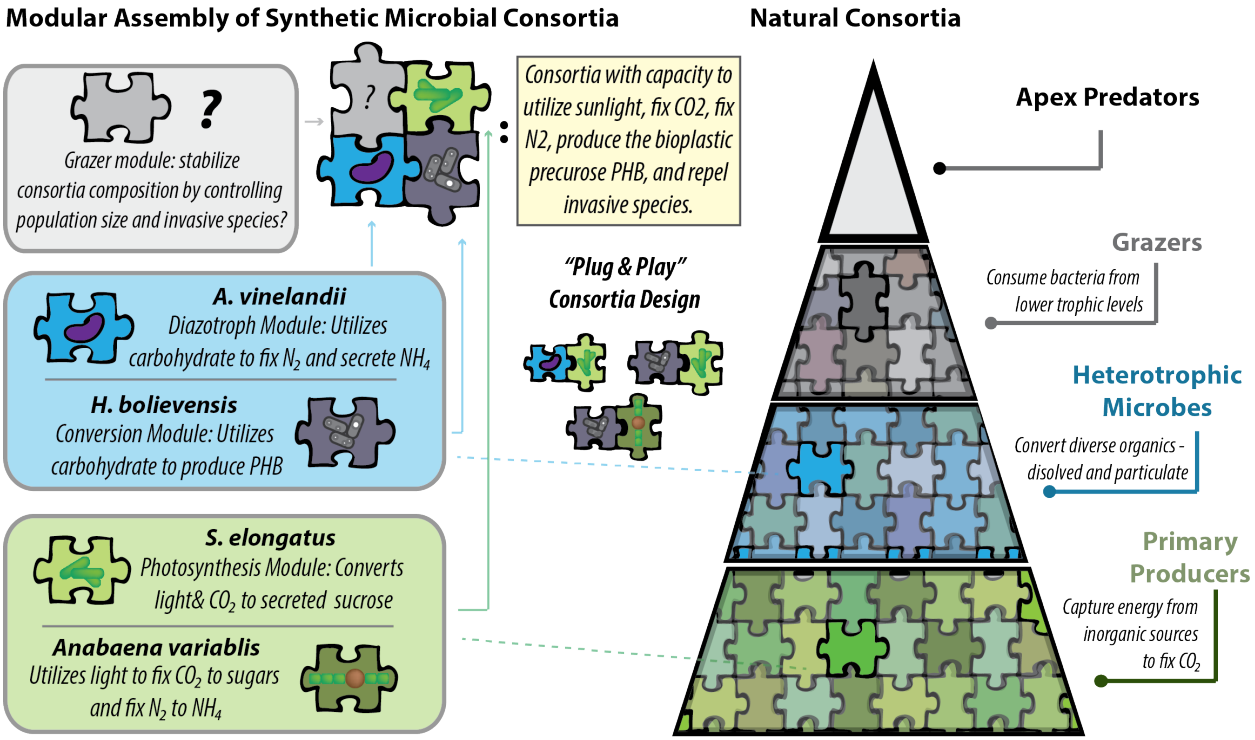

Figure 1.2: Modularity in microbial consortia
Synthetic microbial consortia can be designed in a modular fashion, where each "module" contributes one or more key functions towards the overall capabilities of the community. Compatible modules may be recombined with one another in a flexible, 'plug & play' approach to generate a range of related communities with distinct outputs. This approach has the advantage of allowing cross-comparison of similar synthetic consortia to identify common features and interaction patterns shared across different species pairings. By contrast, natural microbial communities are composed of hundreds to thousands of species: though individual partners may be arbitrarily categorized (*e.g.,* by trophic level),

Figure 1.2 (cont'd)
there is a high degree of functional redundancy. Furthermore, because members of these communities have co-evolved over many generations, interspecies interactions are more likely to be context-specific. This can complicate the ability to define discrete roles or identify predictable interaction patterns for individual species. As the field of synthetic microbial ecology matures, construction of modular communities that more closely mimic natural systems (*e.g.,* composed of species with specialized metabolic modes) may assist in the identification of generalizable design principles.

In synthetic biology, a biological module is defined as a unit of function that can be separated from its native context and repurposed in new networks while retaining fidelity of core functions (Andrianantoandro et al. 2006). While it is a common practice of synthetic biology to conceptualize biological units as 'modular' on the molecular scale (*e.g.,* protein domains, genes, promoter elements), these concepts are increasingly being applied at the level of whole cells, tissues in multicellular organisms, or species within ecosystems (Ortiz-Marquez et al. 2013; Cameron et al. 2014; Ducat 2017). In this context, a given strain within a microbial community would serve a defined set of functions, but could be substituted in a "plug-and-play" fashion with a different species that fulfills those roles. One advantage of developing modular microbial communities is that it streamlines design of new multi-species consortia, and facilitates the identification of common themes of interaction between related communities.

Some recent examples of modular microbial platforms are based off of cyanobacteria that have been engineered to secrete soluble carbohydrates. These engineered strains can behave as a 'carbon fixation module' (Figure 1.2) within synthetic communities that is analogous to natural cyanobacterial symbionts that secrete organic carbon for the community, as *Prochlorococcus* does in marine ecosystems (see above). One example that has been utilized in numerous synthetic co-cultures is a strain of

Synechococcus elongatus sp. PCC 7942 that has been modified to express the sucrose/proton symporter, *cscB* (Ducat et al. 2012). This strain stably exports a large proportion of photosynthetically-fixed carbon as the easily metabolized disaccharide, sucrose (Ducat et al. 2012; Abramson et al. 2016). Multiple labs have shown that photosynthate from these cyanobacteria is sufficient as the sole source of carbon for metabolism and growth of co-cultured heterotrophic microbes. In this design, the heterotroph can be conceptualized as a 'conversion module' to transform the fixed carbon into more valuable bioproducts, including the bioplastic precursors polyhydroxyalkanoate (paired microbe: *Psuedomonas putida*; Löwe et al., 2017), polyhydroxybuterate (*Halomonas bolieviensis*; Weiss and Ducat, 2017, *E. coli*; Hays et al., 2017, or *Azotobacter vinelandii*; Smith and Francis, 2016), fatty acids (*S. cerevisiae* or *Rhodotorula glutinis*; Li et al., 2017), or secreted enzymes (*Bacillus subtilis*; Hays et al., 2017). Of note, in a recent report utilizing synthetic co-cultures of sucrose-secreting *S. elongatus* and *H. bolieviensis*, the designed community was able to continuously produce PHB over the course of more than 5 months while also resisting invasion by a common laboratory contaminant (Weiss and Ducat 2017). Collectively, these results highlight the flexibility and utility of adopting a modular approach to synthetic consortia design (Figure 1.2).

A number of other cyanobacterial strains have been engineered to export carbohydrates, permitting substitution of the "photosynthetic module" in the aforementioned synthetic consortia. For example, *cscB* has been expressed to improve carbohydrate secretion in numerous other model cyanobacteria (Du et al. 2013; Duan et al. 2016; Song et al. 2016). Alternatively, cyanobacteria have been engineered to secrete a variety of other carbohydrates (Niederholtmeyer et al. 2010; Xu et al. 2012; Aikens and

Turner 2013; McEwen et al. 2013; Hays and Ducat 2015), whereas some microalgal strains have been engineered to secrete glycerol (Demmig-Adams et al. 2014). Additionally, many cyanobacterial mutants that are deficient in storing carbohydrates through glycogen synthesis instead secrete a wide array of carbon compounds as overflow metabolism products (Carrieri et al. 2012; Gründel et al. 2012; Xu et al. 2012; Hickman et al. 2013).

Other modular synthetic microbial communities have been generated using strains engineered to fix atmospheric nitrogen and provide it to neighboring species. Some such experiments were originally performed with the diazatrophic cyanobacteria, *Anabaena variabilis,* specifically utilizing mutants where the nitrogenase genes are constitutively derepressed (Spiller et al. 1986). Consequently, these strains maintain nitrogenase activity even after fulfilling their own needs, resulting in the secretion of excess ammonia (Singh and Tiwari 1998). When such mutants were co-cultivated with wheat or rice, they supplemented the nitrogen requirements of the plant and increased crop yields (Latorre et al. 1986; Spiller and Gunasekaran 1990). More recently, a heterotrophic diazotrophic species, *A. vinelandii*, was modified to continuously express nitrogenase and secrete ammonia, and these strains have been used in co-culture with cyanobacteria, algae and with plants (Ortiz-Marquez et al. 2012, 2014; Smith and Francis 2016; Ambrosio et al. 2017). In each case, the partner species effectively gained the benefit of nitrogen-fixing capabilities through the association, leading to enhanced co-culture productivity. Experiments in development seek to combine both the carbon- and nitrogen- fixing modules into a single species by heterologously expressing *cscB* within *Anabaena* strains that also secrete ammonia: such cyanobacterial strains are regarded as promising for

supporting microbial transformations during long-range space flights (Verseux et al. 2015, 2016).

A final class of rationally-designed interactions between a phototroph and a heterotroph involves the exchange of vitamins or other cofactors. Again, co-dependencies can be programmed into selected partners that mimic exchanges that are routinely found in natural environments. In co-cultures of the green algae *Lobomonas rostrata* with the rhizobial bacterium *Mesorhizobium loti*, algae could secrete sufficient carbon to support the growth of the prokaryote, while receiving sufficient cobalamin (vitamin B_{12}) for its own needs (Kazamia et al. 2012b). In each of the above consortia, the mixed autotroph/heterotroph populations exhibited improved bioproduction and/or metabolic functionalities were not available to or achievable by the individual species alone. Furthermore, many of these platforms function as simplified systems to study key exchanges that are found in natural communities in a more methodical fashion.

Limitations in synthetic co-culture approaches and future perspectives

Despite a number of recent advances, the use of synthetic consortia for both academic and applied research is still in its infancy and must overcome a number of limitations to realize their potential. Ironically, while natural consortia display a high degree of robustness, the simplified microbial communities built to mirror them are often highly unstable even under controlled conditions. Furthermore, the majority of published examples of synthetic consortia are composed of only two heterotrophic strains, often that are same species but which have been slightly modified with different genetic constructs (e.g.; Basu et al., 2005; Danino et al., 2010; Goers et al., 2014; Wintermute and Silver, 2010).

Natural communities are composed of individuals from many species and with distinct trophic modes (i.e., chemoheterotrophs, methylotrophs, photoautotrophs, photomixotrophs, and chemoautotrophs). The presence of metabolic specialists can be anticipated to have profound effects on community stability in the face of environmental perturbations. Indeed, a cornerstone ecological principle is that species co-existence in the long-term is impossible if they share the same resources and niches (MacArthur and Levins 1964; Kazamia et al. 2012a). Thus, increasing the number of synthetic microbial platforms that are composed of more than one trophic mode may partially alleviate the problem of instability.

Providing a structured environment is another approach that may be used to increase the robustness of synthetic consortia. As discussed above, there are a number of theoretical and experimental studies that demonstrate that the physical structure and spatial arrangement between microbial partners can increase the long-term stability of interactions that are otherwise prone to collapse (Kim et al. 2008; Chuang et al. 2009; Waite and Shou 2012; Allen et al. 2013; Momeni et al. 2013; Kelsic et al. 2015; Pande et al. 2016). For example, a tripartite heterotrophic community that was unstable when cultivated in well-mixed homogenous environments could be stabilized over long time periods by sequestration of each species into distinct wells of a microfluidic device that were connected by channels allowing exchange of small molecules (Kim et al. 2008). Microfluidic devices also may greatly increase the capacity to test many microbial consortia through recombinatorial approaches by miniaturizing growth chambers (Nai and Meyer 2018). Yet, for some large-scale applications (such as the microalgal ponds discussed above) cultivation in such carefully manufactured conditions may not be economically

realistic. An alternative approach to providing structure within microbial communities would be to engineer the cells to self-organize into higher order patterns. One avenue worth additional exploration in this regard is the refinement of cell-cell attachment systems (Fedeson and Ducat 2016; Zhang et al. 2017; Glass and Riedel-Kruse 2018). Programmable cell adhesion between partner species could allow biologists to better define the spatial positioning and architecture of the community (*e.g.,* programming cells to flocculate, or form structured biofilms), gaining the benefits of a structured environment even in an otherwise homogenized environment.

Finally, the instability of many synthetic microbial communities limits the time scales these consortia have been observed (usually hours to a couple of days; Goers et al., 2014). Increasing the period of observation for stable synthetic communities would offer a new window into the early evolution of symbiotic interactions. While we have learned a great deal from "top down" dissection of specific natural mutualisms (*e.g.,* the chloroplast), the prehistoric origins of these relationships can only be inferred. By contrast, because the partner species in synthetic microbial communities are naïve with regard to one another, stable synthetic ecologies offer a "bottom-up" approach to study the early stages of evolution of a symbiosis (Hom and Murray 2014). For example, Shou et. al. have studied the evolution of synthetic yeast consortia in the early generations to determine what adaptive traits underlie the observed capacity of these populations to evolve towards higher population density limits (Shou et al. 2007). Long-term study of the co-evolution of species within synthetic autotroph/heterotroph consortia could provide new insights into common themes of the early stages of the formation of cyanobacterial and algal mutualisms that are abundant in nature.

Concluding remarks

Synthetic microbial consortia are increasingly being used to disentangle the complex networks of natural microbial communities and program consortia to efficiently perform valuable services. Synthetic microbial consortia offer a biological platform for probing the mechanisms of microbial interactions that is simpler and more easily controlled than natural microbial ecologies. The earliest examples of synthetic microbial consortia have already provided a wealth of information useful for the development of generalizable theories of microbial ecology. Yet, these early examples are often overly simplistic, with limited numbers of metabolic specialists and poor stability. Improvement upon early examples may help to determining effective design rules that increase the robustness and bioproductivity of engineered consortia. The ability to confer these traits on engineered consortia would greatly expand the viability of many microbiology applications across diverse fields, including human medicine, living therapies, bioremediation, and production of sustainable fuels and other commodity products.

CHAPTER 2.1: CYANOBACTERIAL SURFACE DISPLAY SYSTEM MEDIATES ENGINEERED INTERSPECIES AND ABIOTIC BINDING

The work presented in this chapter has been published:

Abstract

Cyanobacteria are uniquely suited for development of sustainable bioproduction platforms, but are currently underutilized in scaled applications in part due to a lack of genetic tools. Here, we develop a surface display system in the cyanobacterial model *Synechococcus elongatus* PCC7942 via expression of modified versions of the outer membrane porin, SomA. Importantly, we demonstrate accessibility of heterologous functional groups on the recombinant porin to the external environment in living cells. We show that this requires the removal of occluding factors that include lipopolysaccharides and a putative surface layer protein. Displayed epitopes on SomA can be utilized to mediate physical adhesion between living cyanobacteria and abiotic surfaces or an engineered *Saccharomyces cerevisiae* partner strain. We show that >80% of cyanobacterial cells attach to functionalized magnetic beads, allowing for magnet-assisted recovery. This work showcases the development of a functional surface display system in cyanobacteria, with wide-ranging applications.

Introduction

Cyanobacteria and algae are increasingly examined as platforms for solar-driven bioproduction due to their favorable traits relative to traditional plant crops. Current photobiological production schemes revolve around microbial conversion of plant-derived sugars (Wyman and Goodman 1993; Papini et al. 2010), creating sustainability concerns regarding arable land and potable water use (Dismukes et al. 2008). Cyanobacteria are an alternative crop species that could disentangle bioindustrial production from agricultural processes (Ducat et al. 2011). Furthermore, cyanobacteria have advantages over other crop species including their high photosynthetic efficiency, genetic tractability, and minimal nutritional requirements (Castenholz 1988; Dismukes et al. 2008; Rittmann 2008; Rastogi and Sinha 2009; Ducat et al. 2011; Kiran et al. 2014). Despite considerable promise, technical and economic barriers to cultivating cyanobacteria have limited their scaled applications (Ortiz-Marquez et al. 2013).

Harvesting cellular biomass is a key concern in the economics of scaled cyanobacterial cultivation. The size, charge, and density of cyanobacteria allow them to remain suspended in stagnant media, and therefore biomass must be harvested through flocculation-induced sedimentation, filtration, or centrifugation (Grima et al. 2003). Initial biomass recovery and subsequent dewatering techniques are energy intensive, limit harvesting rates, and can account for ~20-30% of total production costs (Grima et al. 2003). Rather than using expensive infrastructural approaches, these costs could be potentially mitigated or eliminated through use of engineered cyanobacteria strains. However, the relatively limited cyanobacterial molecular toolkit inhibits our ability to provide biological solutions (Ortiz-Marquez et al. 2013).

Surface display is a molecular tool relevant to scaled biomass recovery that has broad applications in academic and industrial pursuits. For example, surface display systems have been utilized for numerous applications in bacteria and eukaryotic microorganisms, including: bioremediation, live vaccines, biocatalysts, and directed evolution (Samuelson et al. 2002; Kondo and Ueda 2004). A functionalizable cyanobacterial surface would permit the display of useful enzymatic/chemical groups, allowing for selective biomass harvesting techniques and other applications. Previous attempts have been made to functionalize the surface of cyanobacterial cells, but were met with only partial success (Chungjatupornchai and Fa-Aroonsawat 2008; Chungjatupornchai and Fa-aroonsawat 2009; Chungjatupornchai et al. 2011; Ferri et al. 2015), unable to demonstrate that the sequences targeted for surface display were operative, appropriately localized, and accessible. An effective surface display system for any application requires the target protein to localize to the outermost surface of the cell and for this functional moiety to be physically accessible to potential interaction partners and substrates.

Here, we conclusively demonstrate the targeting of a heterologous peptide to the surface of *Synechococcus elongatus* PCC 7942. We systematically investigate potential limitations to effective surface display (*e.g.,* protein expression, localization, and accessibility) to determine the major limiting factors that have likely prevented successful implementation of surface display in previous efforts. We find that several biological barriers occlude outer membrane-localized features and demonstrate that removal of these extracellular components by either chemical or genetic means increases accessibility to the engineered tags. We show that the display peptides facilitate specific attachments of living

cyanobacteria to functionalized beads and other microbes, a technology that has applications in biomass recovery and the development of microbial consortia.

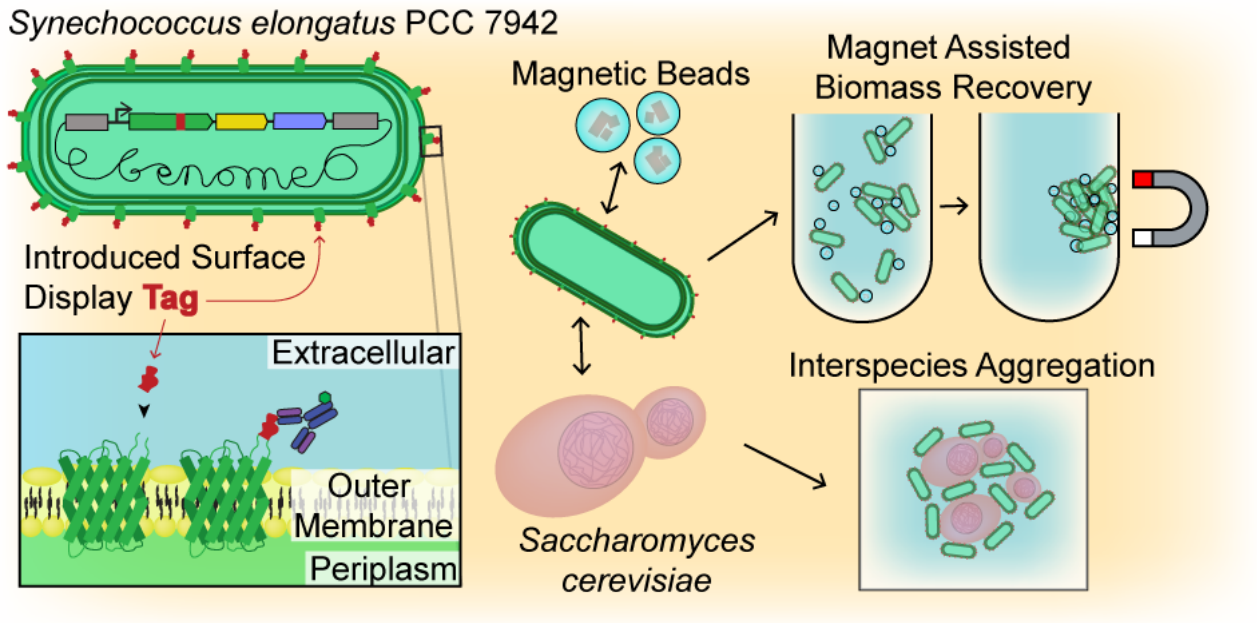

Figure 2.1.1: Graphical abstract

Results

Design and screening of surface display epitopes

Surface display typically utilizes fusion proteins of outer-layer cell components to generate surface display molecules (Boder and Wittrup 2000; Samuelson et al. 2002). SomA, a non-essential, highly-expressed (Rubin et al. 2015) outer membrane porin, was an ideal candidate for engineering a surface display system (Umeda et al. 1996; Hansel et al. 1998). The HHpred secondary structure prediction program (Söding et al. 2005) predicted a 14 transmembrane-strand β-barrel structure for SomA (Figure 2.1a) which differed from previous predictions (Hansel and Tadros 1998), both of which informed our epitope design (Figure 2.1.S1a,c). To minimize the possibility of misfolding or mistargeting (Hagan et al.

2011; Stapleton et al. 2015), we inserted a short peptide sequence in predicted external loops of the full-length protein. Potential external loops were selected from predicted structures (Hansel and Tadros 1998) and we generated in-frame insertions to create a suite of genomically-integrated constructs (R1F-R5F) with the FLAG tag driven by an IPTG inducible promoter (Figure 2.1.2a, Figure 2.1.S1d).

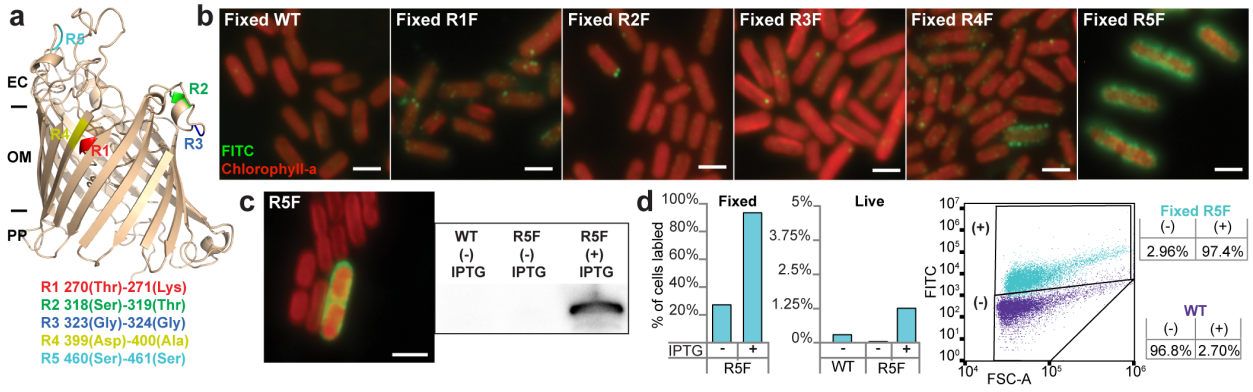

Figure 2.1.2: SomA surface display design and efficacy
(A) HHPred model of SomA showing predicted extracellular (EC), outer membrane (OM), and periplasmic (PP) regions. Epitope insertion sites are labeled and flanking amino acid residues listed in the same color. (B) Representative fixed cell immunostaining of the indicated strains expressing FLAG tagged-SomA at the respective sites. (scale bars = 2 μm). (C) Live R5F cells express recombinant SomA (Western Blot: right), but exhibit impenetrant staining (left). (D) Representative quantification of average percent of cells labeled from fixed (left) or live (middle) populations paired with a flow plot overlay comparing $R5F^{Fixed}$ cells (light blue) with WT^{Fixed} (purple).

We utilized immunofluorescence labeling on fixed cells to screen induced SomA constructs for protein expression and localization (Figure 2.1.2b). Recombinant SomA with inserts in target regions R1-R3 showed very low levels of signal while SomA-R4F appeared to have stochastic signal, with only a small number of strongly fluorescent cells in the population. In contrast, SomA-R5F demonstrated strong and ubiquitous signal with relatively minor variation between cells with induction and strength of expression further confirmed by western blot (Figure 2.1.2b,c and Figure 2.1.S2).

Extracellular factors occlude outer membrane accessibility in living cells

We repeated the immunolocalization in living R5F cells to determine whether the tag remained accessible without permeabilization. We observed that only 2% of living cells were labeled as compared to the 95% of cells in the fixed sample (Figure 2.1.2d). We hypothesized that external cellular components might be sterically occluding the epitope. While cyanobacteria are gram-negative like in that they possess an outer membrane, the outer surfaces of most cyanobacteria – including *S. elongatus* – are poorly characterized, and can differ greatly from the traditional gram-negative classification. However, some examples of extracellular factors that can be found on the surface of cyanobacteria are the lipopolysaccharide layer (LPS), a layer of long-chain polysaccharides covalently linked to molecules in the outer leaflet of the outer membrane (Greenfield and Whitfield 2012), and the surface-layer (S-layer), a paracrystalline shell of a single glycoprotein that encapsulates the cell (Vaara 1982; Schuster and Sleytr 2000; Šmarda et al. 2002). In order to remove peripherally-associated components from the cell surface, we adapted an S-layer stripping protocol which utilizes ethylenediaminetetraacetic acid (EDTA) to strip away metal cations thought to stabilize LPS and S-layers (Sumper et al. 1990; Messner and Sleytr 1992). Immunostaining of stripped R5F cells ($R5F^{EDTA}$) showed staining penetrance comparable to fixed cell levels without the loss of viability (Figure 2.1.2a-b and Figure 2.1.S3), supporting our hypothesis that other external factors were occluding the tagged SomA.

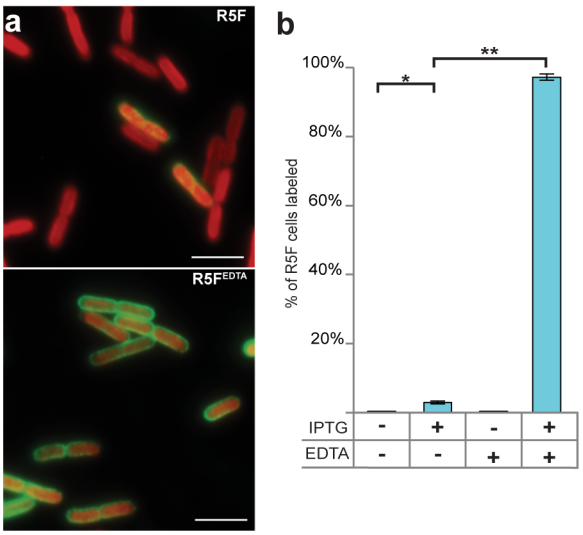

Figure 2.1.3: Surface display epitope is occluded by EDTA-sensitive extracellular factor(s)
(A) Representative images of immunolabeled, induced, live R5F cells before and after EDTA treatment ($R5F^{EDTA}$) (scale bars = 5 μm). (B) Average percentage of labeled cells, quantified via flow cytometry where n=3 independent-day experiments with error bars representing the s.d. (P-values: *<0.05, **<0.01).

LPS extracellular occlusion of epitope

Although EDTA-based stripping protocols can remove occluding factors, genetic ablation of the underlying extracellular factors could constitutively improve epitope availability. We first targeted the O-antigen (OAg), a primary component of the LPS (Greenfield and Whitfield 2012) in *S. elongatus* (Simkovsky et al. 2012) by ablating OAg synthesis and transport genes. We created genetic knockouts (Δ*wbdC*, *Δwzm*, *Δwzt*) of the OAg pathway genes in wild type and R5F backgrounds. No significant changes in viability or morphology were observed (Figure 2.1.S4). We reexamined surface epitope accessibility in living cells via immunolocalization and flow cytometry (Figure 2.1.4a,b). Expressing the tagged SomA in OAg-deficient strains resulted in a moderate increase in the penetrance of immunostaining in live cells (~10%) (Figure 2.1.3b). Interestingly, numerous labeled cells had a patchy appearance (Figure 2.1.4a). Incomplete penetrance and variation between

experimental replicates indicates the OAg may contribute to FLAG epitope occlusion, but there are likely additional occluding factors.

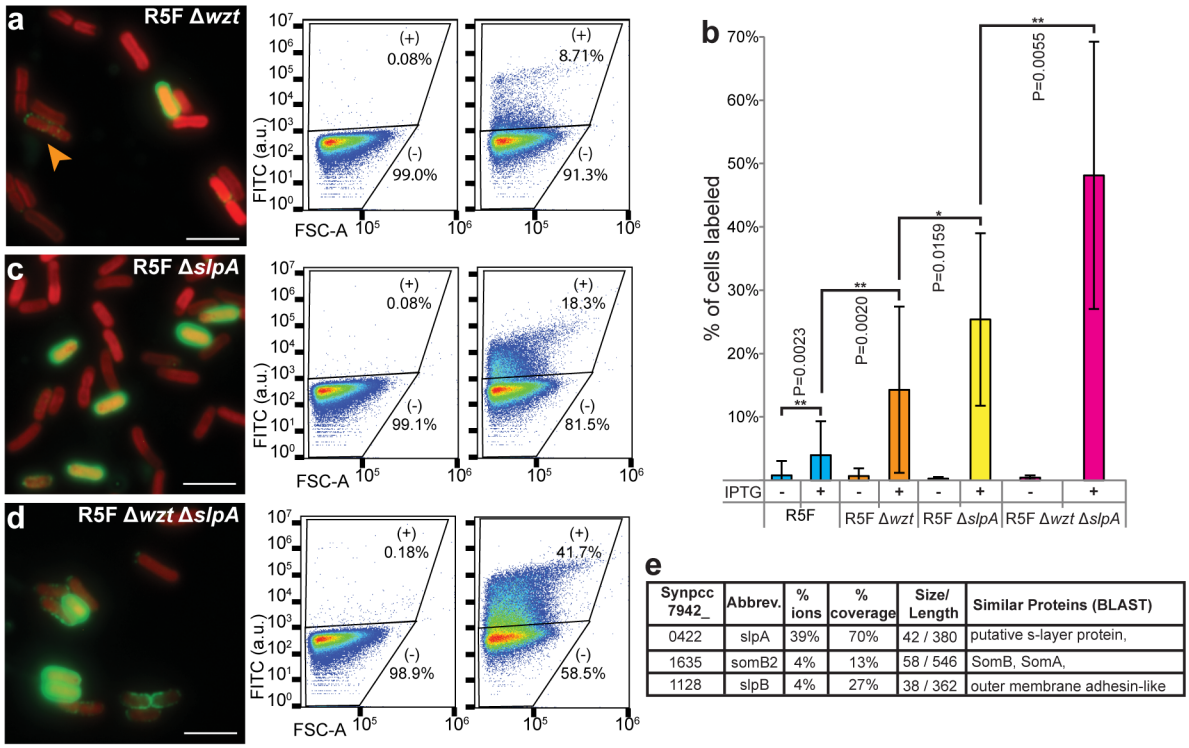

Synpcc 7942_	Abbrev.	% ions	% coverage	Size/ Length	Similar Proteins (BLAST)
0422	slpA	39%	70%	42 / 380	putative s-layer protein,
1635	somB2	4%	13%	58 / 546	SomB, SomA,
1128	slpB	4%	27%	38 / 362	outer membrane adhesin-like

Figure 2.1.4: Removal of OAg synthesis machinery and a putative S-layer protein improves epitope availability

(A-C) Live cell fluorescent microscopy and flow cytometry of the R5F surface display strain in conjunction with gene knockouts. (A) The R5F Δ*wzt* strain shows incomplete penetrance and often patchy staining (orange arrow). (B) Quantification of live cell immunostaining from 12 independent experiments, displaying the mean value with error bars representing the s.d. and significance determined by a two-tailed student t-test (* and ** representing P-values <0.05 and <0.01 respectively). (C) The R5F Δ*slpA* strain shows improved levels of staining, but penetrance is still incomplete. (D) The R5F Δ*wzt* Δ*slpA* strain significantly improves staining of the population, but does not result in full penetrance. (E) The top three LC-MS-MS candidate proteins isolated from EDTA-stripped cyanobacteria; size in kDa, length in amino acids (see Table 2.1.S1).

Identification and deletion of extracellular proteins

We examined proteins extracted by EDTA-stripping for candidate surface proteins that might be occluding the peptide tags. Wild-type and R5F cells were stripped, released proteins separated by SDS-PAGE, and the most abundant bands were excised for LC-MS-MS

analysis (Table 2.1.S1). From the LC-MS-MS data, we identified three top candidates based on their prevalence, examined their predicted homologs by BLAST analysis (Altschul et al. 1990), and evaluated their candidacy for genetic knockout (Figure 2.1.4c-e and Table 2.1.S1). The most abundant candidate with the highest confidence, Synpcc7942_0422 (hereafter: *slpA*), exhibited homology to a putative S-layer protein from *Synechococcus sp.* PCC 7502 (WP_015167719). Although no S-layer has been conclusively documented in *S. elongatus*, metal ion chelators are known to disrupt interactions adhering S-layer proteins to one another and tethering them to the outer surface of gram-negative bacteria (Messner and Sleytr 1992).

We genetically eliminated each of the top candidate proteins to examine changes in R5F epitope accessibility. Knockout lines exhibited normal morphology (Figure 2.1.S5), and Δ*slpA* significantly improved cell live immunolabeling (Figure 2.1.4c). Analysis by flow cytometry showed Δ*slpA* staining levels consistently ranging from 20-35% of the population (Figure 2.1.4b); whereas Δ*somB2* and Δ*slpB* staining levels were unchanged. As the removal of *slpA* resulted in a significant and uniform increase in accessibility of the epitope, it is likely a significant factor in occluding the tagged SomA. However, due to the incomplete penetrance, the SlpA protein is not the only component participating in this occlusion.

Elimination of the putative s-layer and OAg improves surface display availability

If the OAg and the SlpA protein independently contribute to epitope occlusion, elimination of both *wzt* and *slpA* genes would additively increase surface epitope

availability in the R5F strain. We generated the R5FΔ*wzt* Δ*slpA* line (Figure 2.1.S6), and found enhanced immunostaining relative to either single knockout strains, with average cell labeling at ~45% (Figure 2.1.4b,d). Furthermore, we discovered that inducing the cells for three days as opposed to 16 hours significantly increased the number of cells labeled (Figure 2.1.S7). We therefore opted to use the extended induction period for downstream experiments (see Materials and Methods). Together our results suggest there may be numerous extracellular factors on the surface of *S. elongatus* yet to be defined, all of which may contribute to the occlusion of outer membrane proteins.

Surface display mediates interactions with functionalized abiotic beads

The interaction of α-FLAG antibodies with the displayed tag demonstrates that the surface epitope is accessible to diffusing proteins, and therefore other soluble molecules could be targeted to the cyanobacterial surface in an analogous manner. Other useful applications for surface display, such as the specific adhesion of cyanobacteria to large biotic and abiotic surfaces, requires unimpeded access of the surface epitope as the target surfaces are unable to diffuse through any remaining external components. We tested protein A coated magnetic beads as a potential binding partner. Protein A is a *Staphylococcus aureus* surface protein that binds to a conserved region of antibodies (Fc), uninvolved in antigen binding (Sandor and Langone 1982). The beads could bind to cyanobacteria through the mediating antibody bound to the surface FLAG tag. In initial tests, we utilized $R5F^{EDTA}$ cells to provide a uniformly labeled cell population (Figure 2.1.3). In equal mixes of beads and labeled $R5F^{EDTA}$ cells, we observed small cell/bead aggregates

(Figure 2.1.5a). These aggregates only appeared in samples that were both induced and labeled, indicating aggregate formation requires expression of tagged SomA (Figure 2.1.S8).

To determine the number of cells participating in these aggregates, an excess of beads were conjugated to FITC and then incubated with R5F^{EDTA} cells. These mixtures were analyzed via flow cytometry. Under these conditions, R5F^{EDTA} cells are identifiable by chlorophyll autofluorescence (P1) while isolated FITC-conjugated beads solely fluoresce in the green (P2) (Figure 2.1.5b). Mixed populations where the surface epitope was induced showed almost complete depletion of the unbound cyanobacteria population and the appearance of a third aggregate population (P3) (Figure 2.1.5b), indicative of physical association of cells and beads. Since multiple cells can bind to a single bead and vice versa, we cannot accurately assess the bead to cell ratio in a given aggregate. However, FACS analysis indicated ~90% of the cells were removed from the unbound cell population (Figure 2.1.5b). We repeated these experiments with live R5FΔ*wzt* Δ*slpA* cells (Figure 2.1.5c) and found that this strain performed similarly, with over 85% of the cells depleted from the unbound population.

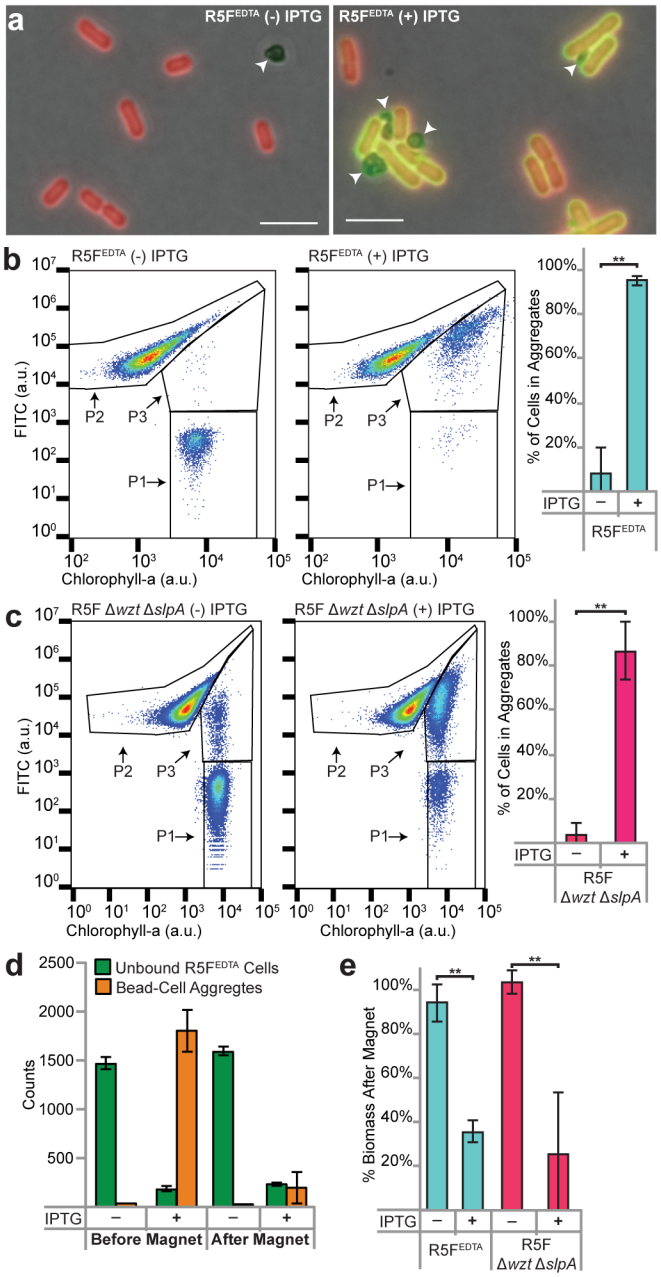

Figure 2.1.5: Surface display can mediate interactions between cyanobacteria and abiotic surfaces

(A) Representative images of uninduced and induced cells with protein A coated beads (white arrows). (B) Flow cytometry of induced or uninduced R5F cyanobacteria treated with EDTA (P1) mixed with beads (P2) shows the formation of a bead-cell aggregate population (P3) in the induced cell state. Bar graphs quantify the percentage of cyanobacterial counts lost from the P1 relative to control cell samples run without beads; this loss is interpreted as the number of cells participating in bead-cell aggregates. Averages of n=3 experiments displayed; error bars represent s.d. P-values: *<0.05, **<0.01). (C) Experiments as in (B), except R5FΔ*wzt* Δ*slpA* strains were used, without

Figure 2.1.5 (cont'd)
EDTA-stripping. (D&E) Magnet assisted pelleting of mixed bead-cell populations, allows for the removal of bound biomass. (D) A representative graph of counts in both P1 (unbound cyanobacteria) and P3 (bead-cell aggregates) gates in mixed $R5F^{EDTA}$ flow cytometry sample, before and after applying the magnet. (E) Quantifying the counts from P1 and P3 relative to control samples without beads, there is induction dependent depletion of biomass. (n=3 experiments, error bars = s.d.)

We examined the capacity for these functionalized beads to facilitate magnet-assisted cyanobacterial biomass recovery. As before, induced and uninduced living R5FΔ*wzt* Δ*slpA* strains were mixed with protein A magnetic beads and incubated with a mediating α-FLAG antibody. A magnetic field was then applied to recover the beads from solution. Comparing supernatant fractions from samples and controls via flow cytometry, we found that ~75% of the cyanobacteria could be removed by magnet-assisted recovery (Figure 2.1.5d), approximately all cells with accessible epitopes. These results definitively demonstrate the ability for this surface display system to mediate binding between the engineered cyanobacteria and functionalized beads.

Surface display mediates binding to engineered yeast binding partners

Since surface display allowed effective binding of cyanobacterial cells to abiotic surfaces, we next examined the potential for this system to enable binding between two distinct microbial species. We utilized *Saccharomyces cerevisiae* as a partner because it possesses a well-characterized surface display system (Kondo and Ueda 2004) that can be used to mediate the interaction. The EBY-100 strain used in this work displays the protein A domain on the surface of its cell wall via expression from an inducible plasmid system (Boder and Wittrup 2000) and is an ideal strain to examine the feasibility of inter-species adhesion of cyanobacteria while allowing for the continued use of tested antibody pairings.

We first verified expression of the Aga2p-proteinA fusion in induced EBY-100 cells via immunostaining and flow cytometry, and observed that ~75% of the population appeared to express the fusion protein (Figure 2.1.S9a). This well-documented inefficiency is an artifact of the expression vectors and dropout media selection which are permissive of plasmid loss (Andreu and Del Olmo 2013). Induced *S. cerevisiae* were mixed with an excess of labeled R5F^{EDTA} cells. Using flow cytometry, we detected the appearance of an aggregate population that possessed the auto-fluorescent properties of cyanobacterial cells with the light scattering properties of yeast-sized particles or larger (Figure 2.1.6a). The formation of aggregates was then confirmed via fluorescent microscopy where we observed multicellular aggregates of yeast and cyanobacteria (Figure 2.1.6b). These experiments were repeated with the R5FΔ*wzt* Δ*slpA* cells, and we obtained similar results with yeast and cyanobacteria association dependent on the expression of the surface display proteins (Figure 2.1.6c). Furthermore, we determined 50% of yeast were bound to one or more cyanobacterial cells by monitoring the loss of unbound yeast cells (Figure 2.1.6a-b). Accounting for the ~25% non-expressing yeast, ~75% of the potential binding yeast have been bound into an aggregate. Aggregate formation only occurred in mixtures containing labeled induced cyanobacteria and induced yeast (Figure 2.1.6b and Figure 2.1.S9b), indicating adhesion specificity. Imaging the resultant population, we observe a range of interactions, from single yeast-cyanobacterial interactions to larger cell aggregates (Figure 2.1.6c and Figure 2.1.S9c).

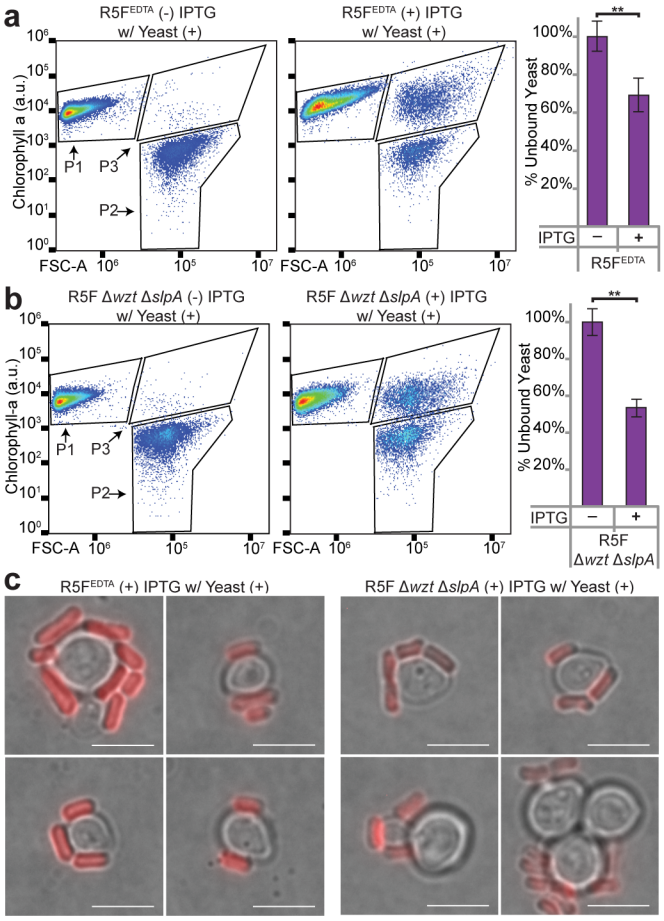

Figure 2.1.6: Surface display mediated adhesion of cyanobacteria to engineered yeast

Mixing induced and antibody labeled (A) R5F^{EDTA} or (B) R5FΔ*wzt* Δ*slpA* cyanobacteria (P1) with induced engineered yeast (P2) results in cyanobacteria-yeast aggregate formation (P3). Average % of unbound yeast in n=3 experiments displayed; error bars represent s.d. P-values: *<0.05, **<0.01) (c) Representative images of varied cyanobacteria/yeast aggregates from flow cytometry samples, (scale bar = 5 μm). (see Figure S10 for additional images)

Discussion

We have developed a surface display system in *S. elongatus* by expressing a modified endogenous outer membrane porin SomA. In order for heterologous affinity tags on the outer membrane of *S. elongatus* to be accessible, we have demonstrated that multiple occluding factors must be removed. After removal of these factors, we

conclusively show that the introduced epitopes are displayed by living cyanobacterial cells and are largely accessible to the extracellular media. While the epitope we introduced to the surface of cyanobacteria lacks inherent functionality, it allows for highly-specific engineered interactions. In proof-of-concept experiments, we have shown that these surface modifications can mediate attachment of cyanobacteria to abiotic surfaces and to other microbes engineered with a complimentary display system. Broadly, this work enables the progression of surface display technology in cyanobacteria and facilitates future academic and industrial applications for *S. elongatus*.

The work presented here is an advance upon previous efforts towards developing cyanobacterial surface display, in part because we document extracellular components that occlude surface accessibility and which may account for the incomplete functionality of previous surface engineering efforts. Chungjatupornchai et al. have conducted the most extensive work on cyanobacterial surface display, utilizing fusions of ice nucleation protein (InP) or N-terminal truncations of SomA to target proteins to direct them to the surface of *S. elongatus* (Chungjatupornchai and Fa-Aroonsawat 2008; Chungjatupornchai and Fa-aroonsawat 2009; Chungjatupornchai et al. 2011). The authors concluded that the majority of surface targeted organophosphorus hydrolase (OPH) (Chungjatupornchai and Fa-Aroonsawat 2008; Chungjatupornchai et al. 2011) and green fluorescent protein (GFP) (Chungjatupornchai and Fa-aroonsawat 2009) remained sequestered within the periplasm/cell wall or were otherwise inaccessible to the external environment. More recently, Ferri et al. (2015) heterologously expressed the *E. coli* antigen 43 (Ag43), an autotransporter protein involved in mediating cell-cell contacts and biofilm formation, in *Synechocystis sp.* 6803. The protein was expressed with its endogenous N-terminus or

truncated and fused with the N-terminal signal peptide of SomA. In both forms, Ag43 was expressed, but did not promote cell-cell adhesion or biofilming. Since the heterologous proteins were susceptible to proteinase K-mediated degradation, it is possible they were localized correctly, but non-functional due to occlusion of Ag43 by extracellular components, such as the previously-characterized S-layer (Trautner and Vermaas 2013). Alternatively, as protease K compromises the integrity of the outer membrane under a variety of conditions (Besingi and Clark 2015), it is also possible that the *E. coli* or truncated SomA signal peptides were inefficient in targeting Ag43 to the outer membrane and some proportion of protein remained within the periplasmic space. These deficiencies in protein outer membrane localization and activity prompted us to pursue internal tagging of SomA, since truncations of the β–barrel porin could exacerbate translocation defects. Here we have confirmed outer membrane localization and accessibility to both diffusible biomolecules and cell-sized tethered surfaces, and found evidence that removal of LPS synthesis machinery and a putative S-layer protein were important to prevent occlusion of the displayed epitopes.

It should be noted that even in our best performing strain (R5F*Δwzt ΔslpA*), the elimination of occluding factors was incomplete; the epitope of ~10-20% of cells remained inaccessible. It is likely that additional components remain on the surface of cyanobacteria that can partially obscure introduced tags. One possibility is that additional exopolysaccharides are being produced as it has recently been shown that cyanobacteria may utilize a variety of components from canonical Wzy, ABC-transporter, and Synthase-dependent extracellular polymeric substance (EPS) secretion pathways interchangeably or redundantly (Pereira et al. 2015). Additionally, while we identified a dominant

extracellular protein with similarity to a putative S-layer protein in *Synechococcus sp.* PCC 7502, conservation of S-layer proteins is extremely poor and it is therefore difficult to assess if alternative S-layer proteins are encoded by *S. elongatus*. Further interrogation of *S. elongatus'* surface proteins may identify additional targets to reduce external obstructions.

From an industrial standpoint, the ability to program materials to have highly specific interactions with cyanobacteria has many possible biotechnological applications. We demonstrate here that surface displaying cyanobacteria can bind magnetic beads, allowing for the majority of biomass to be recovered without centrifugation, chemical flocculants, or filtration. Furthermore, as the interaction between engineered material and cyanobacterial cells can be highly specific, it may be possible to isolate cyanobacteria from non-specific contaminants that are a major problem of scaled reactors (Mata et al. 2010). While our exact approach is not economically viable for large-scale cultivation due to the use of antibodies, these experiments provide evidence that surfaces with appropriate chemistry could be used for novel biomass recovery techniques, possibly ameliorating current biomass recovery problems (Grima et al. 2003). A more thorough exploration of the chemistries/size of peptides that can be displayed on the surface of cyanobacteria would expand the strategies that can be used, including to those that do not rely upon addition of antibodies or other mediating compounds. Furthermore, use of cyanobacterial surface display to recover biomass would be more economical if the binding agents were inexpensive, reusable, and/or the interactions reversible. One material that would meet these criteria is other engineered cells, analogous to the engineered yeast we utilized in these experiments.

Cell-cell attachment is a common theme in nature, where surface ligands and receptors are used to coordinate cell types, from multicellular tissues to microbial biofilms. We show that complementary surface display can be used to program intercellular and interspecies interactions. Beyond biomass recovery, a possible application for these interactions would be to advance previously described synthetic co-cultures of cyanobacteria and heterotrophs, where *S. elongatus*-derived carbohydrates support diverse heterotrophs, including *S. cerevisiae* (Niederholtmeyer et al. 2010; Ducat et al. 2012; Smith and Francis 2016; Hays et al. 2017). Direct attachment of partners in designed communities could potentially increase metabolite exchange and stabilize synthetic commensal relationships. Future strains of both *S. elongatus* and *S. cerevisiae* could be specifically modified to facilitate facile interactions, including the insertion of larger protein domains into SomA (a potential mechanism to enzymatically activate the surface of the cyanobacteria), to eliminate the need for antibodies to mediate binding. Because of the genetic tools within these model organisms, such strains might also be useful as a platform to study and engineer the aggregation dynamics of planktonic microbes into structured, multi-species assemblies.

In summary, this work has shown the development of a surface display system in *Synechococcus elongatus* PCC7942 allows for the specific adhesion of *S. elongatus* to both beads and engineered *S. cerevisiae* cells, with potential implications for both industrial and academic settings.

Materials and Methods

S. elongatus cell culture and strains

Cyanobacterial cultures were grown in baffled flasks in a Multitron Pro (Infors) incubator under constant illumination from fluorescent bulbs (15W Gro-Lux; Sylvania; ~70 μmol/m^2/s), constant temperature (32^{o}C), and 2% CO_2 supplementation and shaking (125 rpm). Cultures were grown in BG-11 media buffered with 1 g/L HEPES (pH 8.3; Sigma). Surface display constructs were obtained by cloning *S. elongatus* SomA into a NSIII integration vector (Niederholtmeyer et al. 2010). The epitope tags and linker coding sequence were inserted using primer directed mutagenesis. Gene knockout plasmids were constructed by cloning ~1 kilobase fragments from upstream and downstream of target genes into a plasmid flanking antibiotic resistance selectable markers. Plasmid assembly was accomplished in all cases through standard isothermal assembly techniques (see Supplemental Materials for Primer List). Transformations were performed as per (Golden et al. 1987) and transformants were selected for on BG-11 agar plates with appropriate antibiotics (chloramphenicol 12.5 μg/ml, kanamycin 16.7 μg/ml, and spectinomycin 100 μg/ml) and verified by colony PCR. Modified somA expression was induced with the addition of 1 mM IPTG (isopropyl-β-D-1-thiogalactopyranoside) to cultures and allowed to incubate overnight (~16 hrs) or over the course of three days (~72 hrs), as indicated.

Immunostaining of cyanobacterial cells

Live cells were pelleted, washed, and blocked (blocking buffer: 5% Bovine Serum Albumin (A9647; Sigma) in PBS) for 30 minutes at room temperature, before incubation with 1:1000 dilution of primary antibody, α-FLAG (DYKDDDDK) tag monoclonal mouse

IgG2b (LT0420; Lifetein) for 1 hour at room temperature. Cells were then washed and resuspended in the dark in blocking buffer with secondary antibody at 1:1000 dilution, as indicated; goat α -mouse IgG Alexa Fluor® 488 (35502; Thermo) for basic expression immunolabeling, goat α -rabbit IgG Alexa Fluor® 647 dye (A-21236; Thermo) for bead-cell adhesion experiments, or rabbit monoclonal M87-3 anti-mouse IgG1, IgG2a, IgG2b H&L (ab125907; abcam) for cyanobacteria-yeast adhesion experiments, were incubated in the dark for 1 hour. Stained cells were washed with PBS three times prior to binding experiments, fluorescent microscopy, or flow cytometry. Fixed cells (Figure 2.1.2) were treated as above, but prior to blocking were resuspended in 500 ul of 100% pre-chilled methanol and incubated at -20^{o}C for 10 minutes. Cells were re-pelleted, washed with 1 ml of PBS, re-pelleted and resuspended in 0.02 mg/ml Lysozyme (0663-10G; Amresco) in Tris-HCl for 30 minutes at room temperature with agitation.

Cyanobacteria-bead binding assays

Magnetic protein A/G beads (88802; Thermofisher) washed and resuspended with 1:1000 Fluoroscein-5-EX succinimidyl ester (F6130; Invitrogen) for 1 hour. Stained beads were washed with PBS to remove excess unconjugated fluorophores and mixed with immunolabeled cyanobacterial cells (primary and goat anti-rabbit IgG Alexa Fluor® 647 dye) for 30 minutes in the dark at room temperature. Mixtures were analyzed by flow cytometry on an Accuri C6 flow cytometer (653119; BD Biosciences) with a minimum threshold of 80,000 FSC-H, or by microscopy on a Zeiss Axio Observer.D1 (491911-0027-000; Zeiss).

Yeast culturing and induction conditions

EBY-100 yeast was cultivated as per (Boder and Wittrup 1997). For induction of fusion protein expression, yeast from overnight cultures were back diluted into SGCAA induction media (Boder and Wittrup 1997) and allowed to induce for 4 hours prior to experimentation. Induction was verified via immunolabeling of induced cells with α-HA-tag-Alexa Fluor 488, monoclonal antibody (M180-A48; MBL) which targets the internal HA tag located in the linker region bridging the Aga2a domain and the protein A domain of the surface display protein (Boder and Wittrup 1997).

Cyanobacteria-yeast binding assays

Cyanobacteria were immunolabeled as described above. EBY-100 yeast cells were harvested, incubated in blocking buffer for 30 minutes at room temperature, and washed in PBS. These cells were then mixed with cyanobacteria, (primary and secondary (rabbit monoclonal M87-3 anti-mouse IgG1, IgG2a, IgG2b H&L)), at room temperature for 30 minutes at a 1:10 yeast:cyanobacteria ratio. Samples were analyzed by flow cytometry or microscopy as above.

Surface component stripping

This protocol was adapted from (Sumper et al. 1990). Briefly, cells were harvested and pelleted from culture at 17,000 xg for 10 minutes. The supernatant was removed and the cells were resuspended in 192 mM EDTA (ethylenediaminetetraacetic acid) in BG-11, and incubated at room temperature for 30 minutes. The cells were then pelleted and resuspended in PBS for recovery. EDTA supernatant was retained for protein analysis by LC/MS/MS.

Western blotting

50 mL of culture adjusted to 0.3 OD_{750} was lysed with a benchtop cell disrupter (Constant Systems Ltd.); three passes at 35 kPa at 4°C. Cell lysates were concentrated using 15 ml 30,000 NMWL Amicon Centrifugal Filter Units (UFC901008; Millipore) spun at 3500 xg for 20 minutes at 4°C. Protein lysate was separated by SDS-PAGE, and transferred to PVDF membrane with the Trans-Blot Turbo Transfer System (1704155; BioRad). PDVF membranes were blocked, and probed with a primary antibody 1:1000, α-FLAG (DYKDDDDK) tag monoclonal mouse IgG2b (LT0420; Lifetein) overnight, and secondary antibody 1:1000, chicken α-mouse IgG secondary antibody HRP Conjugate (SA1-72021; Thermo) for 4 hours. The membrane was imaged using a Chemi Doc MP (1708280; BioRad).

Flow cytometry analysis

Flow cytometry was performed using a BD accuri C6 flow cytometer (653119; BD Biosciences). The particle threshold was set to 80,000 FSC-H for all experiments and flow speed was optimized for fluorescent measurements. Gating was set according to control population samples so as to be inclusive across experiments and exclusive of potential contaminants. The excitation laser used for all measured channels was the 20mW 488 nm Solid State Blue Laser. The optical filters used for fluorescent particles were FL1 533/30 nm (FITC/GFP) for FITC and AlexaFluor488 fluorescence, and FL3 > 670 nm (PerCP, PerCP-Cy™5.5, PE-Cy7) for chlorophyll-α fluorescence. All flow cytometry experiments performed had multiple biological replicates as indicated in the figure legends. Additionally, for each biological replicate, three technical replicates were performed (i.e.

n=3 is an aggregate of 9 sample readings). Combining technical replicates averaged 80,000-100,000 events per biological replicate.

APPENDIX

Appendix: Chapter 2.1 Supplemental Materials

LC/MS/MS

Standard SDS-PAGE of EDTA-treated cell supernatants was conducted, and dominant bands were cut from 4-20% acrylamide gradient gels (456-1094; BioRad). Excised bands were sent to the Michigan State University RTSF Proteomics Core for downstream processing and initial analysis. Gel bands were digested in-gel according to Shevchenko et al. (1996) with modifications. Briefly, gel bands were dehydrated using 100% acetonitrile and incubated with 10mM dithiothreitol in 100mM ammonium bicarbonate, pH~8, at 56C for 45min, dehydrated again and incubated in the dark with 50mM iodoacetamide in 100mM ammonium bicarbonate for 20min. Gel bands were then washed with ammonium bicarbonate and dehydrated again. Sequencing grade modified typsin was prepared to 0.01µg/µL in 50mM ammonium bicarbonate and ~50µL of this was added to each gel band so that the gel was completely submerged. Bands were then incubated at 37°C overnight. Peptides were extracted from the gel by water bath sonication in a solution of 60%ACN/1%TCA and vacuum dried to ~2µL. Peptides were then resuspended in 2% acetonitrile/0.1%TFA to 25µL. From this, 5µL were automatically injected by a Thermo EASYnLC 1000 onto a Thermo Acclaim PepMap RSLC 0.075mm x 250mm C18 column and eluted over 16min with a gradient of 5%B to 30%B in 7min, ramping to 100%B at 8min and held at 100%B for the duration of the run or eluted over 90min with a gradient of 5%B to 30%B in 79min, ramping to 100%B at 80min and holding for the duration of the run (Buffer A = 99.9% Water/0.1% Formic Acid, Buffer B = 99.9% Acetonitrile/0.1% Formic Acid). Eluted peptides were sprayed into a ThermoFisher Q-Exactive mass spectrometer using a FlexSpray spray ion source. Survey scans were taken in

the Orbi trap (35000 resolution, determined at m/z 200) and the top ten ions in each survey scan are then subjected to automatic higher energy collision induced dissociation (HCD) with fragment spectra acquired at 17,500 resolution. The resulting MS/MS spectra are converted to peak lists using Mascot Distiller, v2.5.1 (www.matrixscience.com) and searched against a custom database containing all *S. elongatus* protein sequences available from NCBI (downloaded from www.ncbi.nlm.nih.gov, 2014-10-03) and appended with common laboratory contaminants (downloaded from www.thegpm.org, cRAP project) using the Mascot searching algorithm, v 2.5. The Mascot output was then analyzed using Scaffold, v4.3.4 (www.proteomesoftware.com) to probabilistically validate protein identifications. Assignments validated using the Scaffold 1%FDR confidence filter are considered true.

Mascot parameters for all databases were as follows: allow up to 2 missed tryptic sites; fixed modification of Carbamidomethyl Cysteine; variable modification of Oxidation of Methionine; peptide tolerance of +/- 5ppm; MS/MS tolerance of 0.3 Da; FDR calculated using randomized database search.

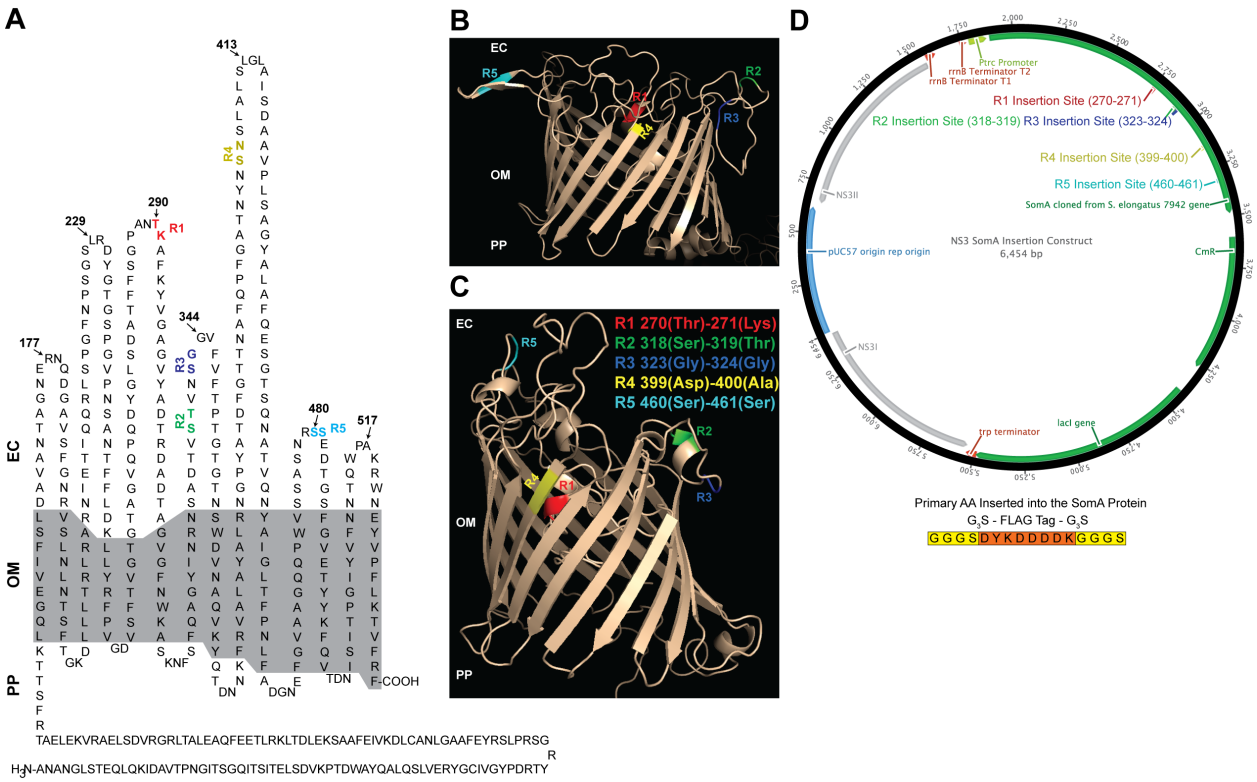

Figure 2.1.S1: Comparisons of SomA models and NS3 tagged SomA insertion construct design

(A) A figure adapted from Mizuno et al. (Umeda et al. 1996) showing the predicted extracellular (EC), outer membrane (OM), and periplasmic (PP) regions of SomA from *Synechocystis* sp. 6803. Regions targeted for insertion are labeled in color with the amino acid residues flanking the site bolded in the same color. R1 [290-291] (red), R2 [338/339] (green), R3 [342/343] (navy), R4 [406/407] (yellow), R5 [480/481] (cyan). Phyre2- (B) and HHPred- (C) generated models, with the same coloring as in (A). (D) Neutral site 3 insertion vector containing the *somA* gene cloned directly from *Synechococcus elongatus* PCC 7942 labeled with target insertion sites.

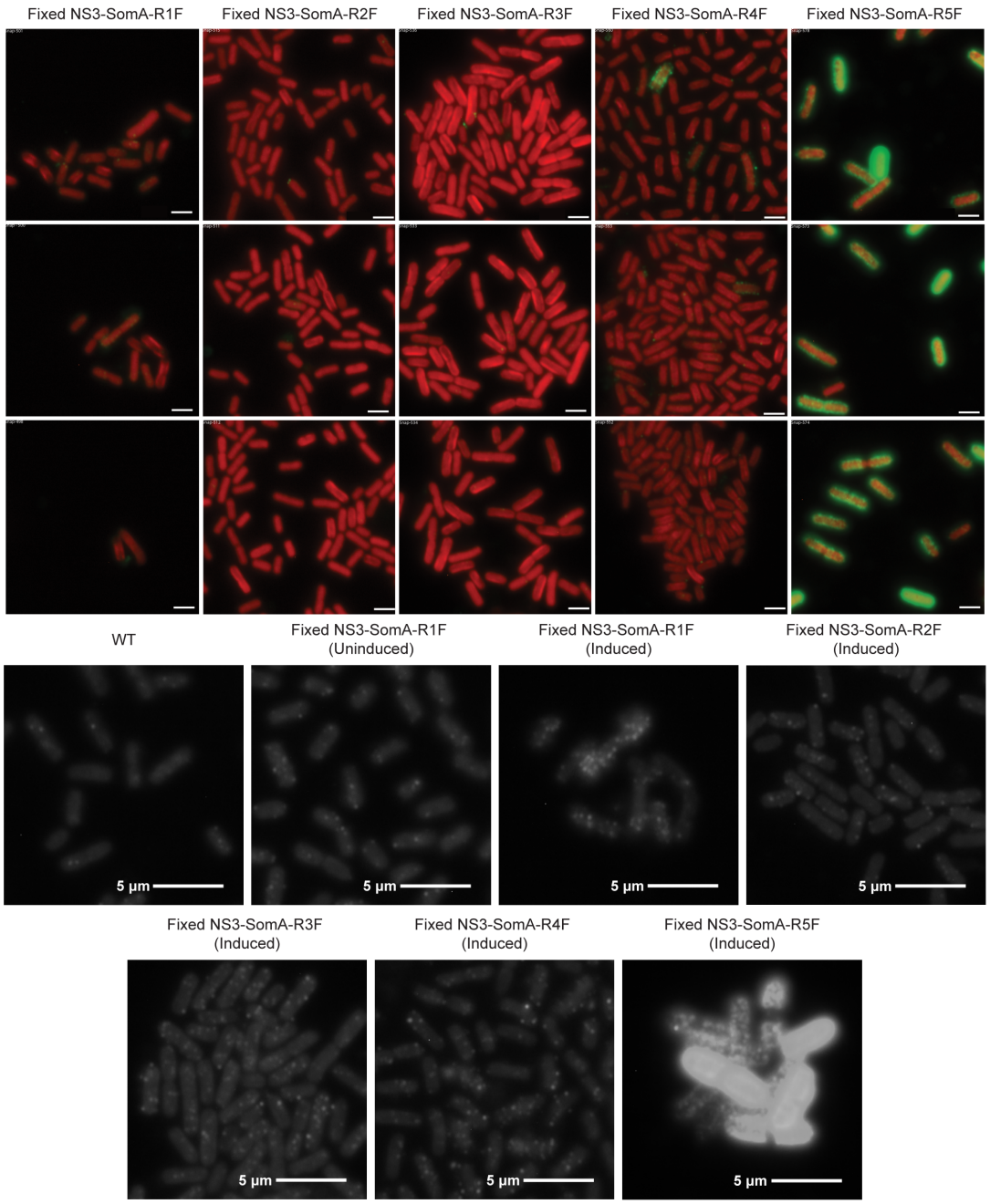

Figure 2.1.S2: Additional representative immunolocalization of indicated tagged SomA constructs in fixed cells

(Top): All cells (red: chlorophyll) are induced (+ 1mM IPTG); the insertion site of the introduced FLAG tag influences the expression and translocation of modified SomA constructs (green: antibody fluorescence). Scale bar = 2 µm. (Bottom): Panels as above, except where only the antibody fluorescence channel (Alexa Fluor 488) is displayed to improve visualization of antibody labeling. Cells are either induced (+ 1mM IPTG) or uninduced, as indicated. Scale bars = 5 µm; as indicated.

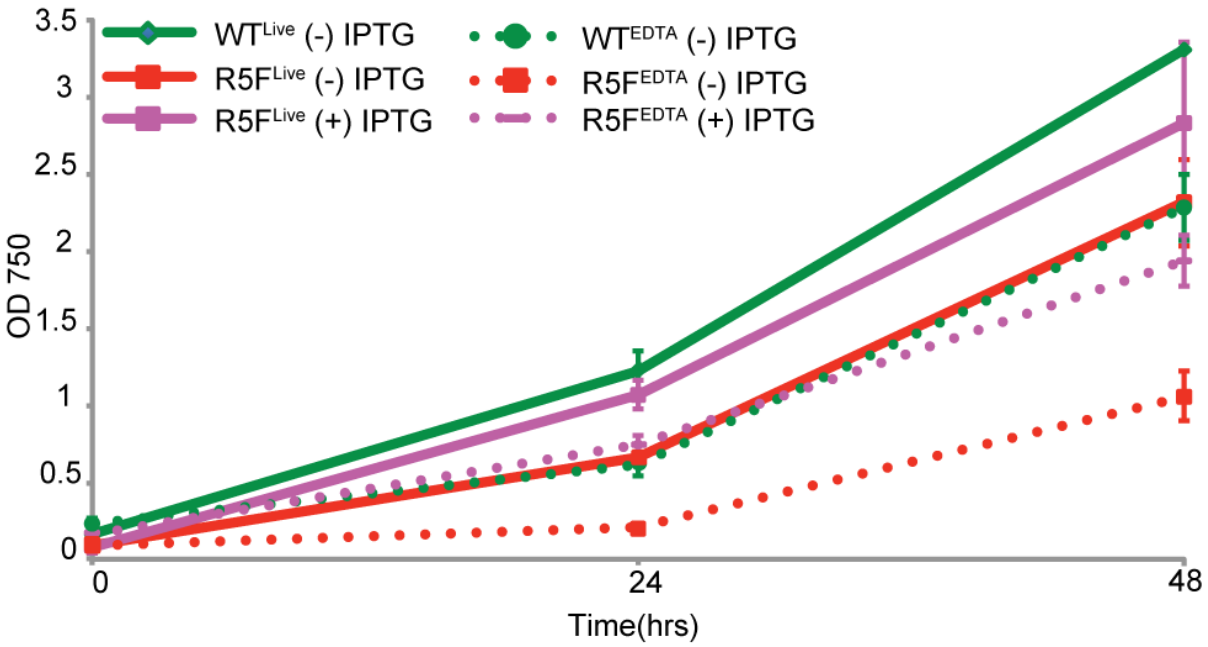

Figure 2.1.S3: Cyanobacterial cell viability following EDTA treatment

Uninduced and induced WT and NS3-SomA-R5F cells were stripped with EDTA to disrupt extracellular structures and inoculated into new cultures. Cells remain viable following EDTA treatment (dotted lines), although EDTA may cause a growth lag, as indicated by the delayed growth in the first 24 hours.

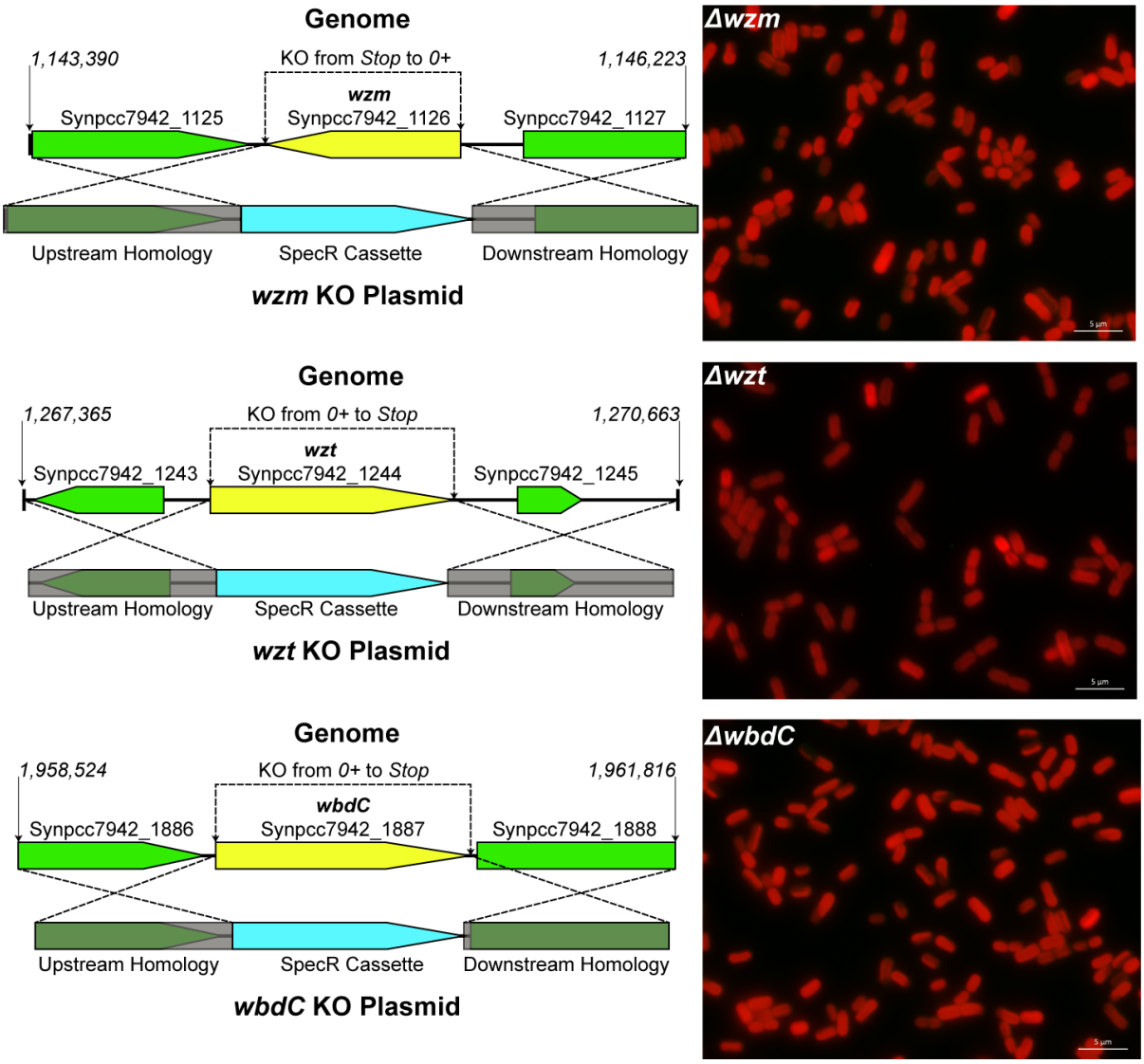

Figure 2.1.S4: O-antigen knockout construct design and cell morphology of resultant knockout strains

OAg KO constructs were designed to replace the target gene with the spectinomycin resistance cassette (left). All knockout strains exhibit normal cellular morphology (right). Scale bar = 5 μm.

#	MS/MS View: 89 Proteins in 84 Clusters	Accession Number	Molecular Weight	Protein Grouping Ambiguity	15+ kDa Band	37+ kDa Band	50+ kDa Band	100+ kDa Band	Complex Sample
1	**hypothetical protein [*Synechococcus elongatus*]**	**gi|499562623**	**42 kDa**		**100% (15)**	**100% (61)**	**100% (6)**	**73% (2)**	**100% (5)**
2	Chain B, X-ray Crystal Structure Of Phycocyanin From *Synechococcus elongatus* Sp. Pcc 7942	gi|459358742	18 kDa		100% (5)	100% (2)	100% (19)	-100% ((0))	100% (22)
3	RecName: Full=C-phycocyanin alpha chain	gi|130028	17 kDa	TRUE	100% (5)	98% (1)	100% (13)	-100% ((0))	100% (18)
4	iron deficiency induced protein A [*Synechococcus elongatus* PCC 7942]	gi|14331111	39 kDa		100% (6)	100% (31)	-100% ((0))	-100% ((0))	19% (0)
5	pili assembly chaperone [*Synechococcus elongatus*]	gi|499696684	15 kDa		100% (13)	100% (9)	100% (6)	44% (2)	85% (4)
6	**porin [*Synechococcus elongatus*]**	**gi|499561624**	**58 kDa**	**TRUE**	**-100% ((0))**	**100% (6)**	**100% (6)**	**-100% ((0))**	**100% (8)**
7	**hypothetical protein Synpcc7942_1128 [*Synechococcus elongatus* PCC 7942]**	**gi|81299937**	**38 kDa**		**-100% ((0))**	**100% (6)**	**100% (6)**	**-100% ((0))**	**100% (5)**
8	porin [*Synechococcus elongatus* PCC 7942]	gi|81300273	57 kDa	TRUE	-100% ((0))	14% (1)	100% (8)	-100% ((0))	100% (12)
9	hypothetical protein [*Synechococcus elongatus*]	gi|499562638	16 kDa		100% (11)	-100% ((0))	-100% ((0))	-100% ((0))	-100% ((0))
10	RecName: Full=Allophycocyanin alpha chain	gi|129994	17 kDa		100% (2)	-100% ((0))	100% (4)	-100% ((0))	100% (5)

Table 2.1.S1: Complete LC-MS-MS peptide reads and predicted protein matches for EDTA-solubilized proteins

The "Protein Grouping Ambiguity" column indicates if there were one or more peptides that could be mapped to more than one discovered protein. Peptide sequences were evaluated by LC-MS-MS (see SI Methods) from total protein, and from four distinct, dominant bands (15, 37, 50, 100 kDa) that were excised from SDS-PAGE gels following EDTA treatment of living *S. elongatus* cells (Messner et al. 2008). Percentiles listed in the individual band columns indicate percent certainty of the proteins' presence in each particular band; the adjacent number in parentheses indicates number of mapped peptides, -100% ((0)) indicating the protein was not detected. The three top candidates (bold) were identified because they were both high confidence hits in the total protein lysate as well as identified as high-confidence hits in excised protein bands of the appropriate size. Furthermore, as the 37+ kDa band was dominant, proteins found in this sample were given additional prioritization.

Table 2.1.S1 (cont'd)

11	SphX [*Synechococcus elongatus* PCC 7942]	gi|496319	36 kDa		100% (3)	100% (2)	-100% ((0))	-100% ((0))	100% (4)
12	hypothetical protein [*Synechococcus elongatus*]	gi|499562813	20 kDa		100% (7)	-100% ((0))	39% (0)	-100% ((0))	100% (2)
13	hypothetical protein [*Synechococcus elongatus* PCC 7942]	gi|24414819	25 kDa		100% (4)	-100% ((0))	-100% ((0))	-100% ((0))	100% (2)
14	Chain B, X-ray Crystal Structure Of Allophycocyanin From *Synechococcus elongatus* Pcc 7942	gi|459358658	17 kDa		100% (5)	-100% ((0))	98% (2)	-100% ((0))	100% (2)
15	alkaline phosphatase [*Synechococcus elongatus*]	gi|499561694	144 kDa		95% (1)	100% (5)	-100% ((0))	-100% ((0))	100% (2)
16	unknown [*Synechococcus elongatus* PCC 7942]	gi|22002502	17 kDa		100% (4)	-100% ((0))	-100% ((0))	-100% ((0))	100% (3)
17	ABC-type nitrate/nitrite transport system substrate-binding protein [*Synechococcus elongatus* PCC 7942]	gi|81300048	48 kDa		-100% ((0))	-100% ((0))	-100% ((0))	-100% ((0))	100% (3)
18	hypothetical protein [*Synechococcus elongatus*]	gi|499563750	20 kDa		100% (9)	-100% ((0))	-100% ((0))	-100% ((0))	100% (2)
19	ANL06 [*Synechococcus elongatus* PCC 7942]	gi|47059644	34 kDa		100% (2)	-100% ((0))	65% (0)	-100% ((0))	100% (2)
20	C-terminal processing peptidase-2 [*Synechococcus elongatus* PCC 7942]	gi|81299523	46 kDa		-100% ((0))	100% (9)	-100% ((0))	-100% ((0))	13% (0)
21	RecName: Full=Superoxide dismutase [Fe]	gi|134647	22 kDa		-100% ((0))	-100% ((0))	94% (2)	-100% ((0))	100% (4)
22	hypothetical protein [*Synechococcus elongatus*]	gi|499563244	43 kDa		-100% ((0))	100% (8)	-100% ((0))	-100% ((0))	-100% ((0))
23	hypothetical protein [*Synechococcus elongatus* PCC 7942]	gi|24414834	19 kDa		100% (8)	-100% ((0))	-100% ((0))	-100% ((0))	-100% ((0))
24	hypothetical protein [*Synechococcus elongatus*]	gi|499563759	37 kDa		100% (3)	100% (3)	-100% ((0))	-100% ((0))	-100% ((0))
25	hypothetical protein [*Synechococcus elongatus*]	gi|499562724	16 kDa	TRUE	100% (6)	-100% ((0))	-100% ((0))	-100% ((0))	8% (1)
26	hypothetical protein [*Synechococcus elongatus*]	gi|499697662	9 kDa		99% (1)	-100% ((0))	98% (2)	-100% ((0))	100% (1)
27	hypothetical protein [*Synechococcus elongatus*]	gi|499562523	30 kDa		100% (1)	-100% ((0))	-100% ((0))	-100% ((0))	-100% ((0))
28	Cluster of photosystem I reaction center subunit II [*Synechococcus elongatus*] (gi|499697090)	gi|499697090	16 kDa	TRUE	100% (2)	0% ((0))	4% ((0))	0% ((0))	89% (1)

Table 2.1.S1 (cont'd)

29	photosystem I reaction center subunit II [*Synechococcus elongatus*]	gi|499697090	16 kDa	TRUE	100% (2)	-100% ((0))	-100% ((0))	-100% ((0))	89% (1)
30	photosystem I reaction center subunit II [*Synechococcus elongatus*]	gi|499562072	12 kDa	TRUE	35% ((0))	-100% ((0))	4% ((0))	-100% ((0))	-100% ((0))
31	unknown [*Synechococcus elongatus* PCC 7942]	gi|25019696	21 kDa		100% (5)	-100% ((0))	-100% ((0))	-100% ((0))	-100% ((0))
32	orf134 [*Synechococcus elongatus* PCC 7942]	gi|454073	14 kDa		100% (4)	-100% ((0))	-100% ((0))	-100% ((0))	-100% ((0))
33	hypothetical protein [*Synechococcus elongatus*]	gi|499561785	35 kDa		47% (0)	100% (1)	51% (0)	23% (0)	-100% ((0))
34	phosphohydrolase [*Synechococcus elongatus*]	gi|499562287	94 kDa		-100% ((0))	-100% ((0))	-100% ((0))	-100% ((0))	99% (1)
35	RecName: Full=Ycf48-like protein; Flags: Precursor	gi|108861977	39 kDa		-100% ((0))	100% (3)	-100% ((0))	-100% ((0))	6% (0)
36	pilin-like protein [*Synechococcus elongatus* PCC 7942]	gi|25019699	20 kDa		100% (4)	-100% ((0))	-100% ((0))	-100% ((0))	-100% ((0))
37	endo-1,4-beta-xylanase [*Synechococcus elongatus*]	gi|499561686	42 kDa		-100% ((0))	100% (4)	-100% ((0))	-100% ((0))	-100% ((0))
38	hypothetical protein [*Synechococcus elongatus*]	gi|499562725	17 kDa	TRUE	100% (4)	-100% ((0))	-100% ((0))	-100% ((0))	4% ((0))
39	purple acid phosphatase [*Synechococcus elongatus*]	gi|499562279	32 kDa		-100% ((0))	-100% ((0))	-100% ((0))	-100% ((0))	100% (1)
40	membrane protein [*Synechococcus elongatus*]	gi|499562143	65 kDa		-100% ((0))	-100% ((0))	-100% ((0))	-100% ((0))	100% (1)
41	rps12 [*Synechococcus elongatus* PCC 6301]	gi|1405430	14 kDa		99% (2)	98% (0)	-100% ((0))	44% (2)	-100% ((0))
42	hypothetical protein [*Synechococcus elongatus*]	gi|499561600	22 kDa		100% (2)	-100% ((0))	-100% ((0))	-100% ((0))	24% (0)
43	peptidylprolyl isomerase [*Synechococcus elongatus*]	gi|499563276	18 kDa		100% (2)	-100% ((0))	-100% ((0))	-100% ((0))	-100% ((0))
44	hypothetical protein [*Synechococcus elongatus*]	gi|499563820	17 kDa		100% (3)	-100% ((0))	-100% ((0))	-100% ((0))	-100% ((0))
45	RecName: Full=Protein RecA; AltName: Full=Recombinase A	gi|123741845	38 kDa		-100% ((0))	-100% ((0))	48% (0)	-100% ((0))	100% (1)
46	Cluster of 30 kD rod-rod linker [*Synechococcus elongatus* PCC 6301] (gi|142124)	gi|142124	30 kDa	TRUE	0% ((0))	0% ((0))	0% ((0))	0% ((0))	100% (1)
47	30 kD rod-rod linker [*Synechococcus elongatus* PCC 6301]	gi|142124	30 kDa	TRUE	-100% ((0))	-100% ((0))	-100% ((0))	-100% ((0))	100% (1)

Table 2.1.S1 (cont'd)

48	Chain A, Solution Nmr Structure Of The Pbs Linker Domain Of Phycobilisome Rod Linker Polypeptide From *Synechococcus elongatus*, Northeast Structural Genomics Consortium Target Snr168a	gi|315113184	16 kDa	TRUE	-100% ((0))	-100% ((0))	-100% ((0))	-100% ((0))	2% ((0))
49	hypothetical protein [*Synechococcus elongatus*]	gi|499563675	18 kDa		100% (2)	-100% ((0))	-100% ((0))	-100% ((0))	-100% ((0))
50	hypothetical protein [*Synechococcus elongatus*]	gi|499561723	19 kDa		100% (2)	-100% ((0))	-100% ((0))	-100% ((0))	-100% ((0))
51	hypothetical protein [*Synechococcus elongatus*]	gi|499697288	19 kDa		100% (2)	-100% ((0))	-100% ((0))	-100% ((0))	-100% ((0))
52	hypothetical protein [*Synechococcus elongatus*]	gi|499561621	18 kDa		100% (2)	-100% ((0))	-100% ((0))	-100% ((0))	-100% ((0))
53	unknown [*Synechococcus elongatus* PCC 7942]	gi|25019695	52 kDa		100% (2)	98% (1)	-100% ((0))	-100% ((0))	-100% ((0))
54	hypothetical protein [*Synechococcus elongatus*]	gi|499562653	56 kDa		99% (1)	100% (2)	-100% ((0))	-100% ((0))	-100% ((0))
55	membrane protein [*Synechococcus elongatus*]	gi|499563531	33 kDa		100% (1)	-100% ((0))	-100% ((0))	-100% ((0))	42% (1)
56	hypothetical protein [*Synechococcus elongatus*]	gi|499562226	16 kDa		100% (1)	-100% ((0))	-100% ((0))	-100% ((0))	-100% ((0))
57	hypothetical protein [*Synechococcus elongatus*]	gi|499561711	14 kDa		100% (2)	-100% ((0))	-100% ((0))	-100% ((0))	-100% ((0))
58	serine protease [*Synechococcus elongatus*]	gi|499562467	43 kDa		100% (2)	-100% ((0))	-100% ((0))	-100% ((0))	-100% ((0))
59	unknown [*Synechococcus elongatus* PCC 7942]	gi|22002557	25 kDa		100% (2)	-100% ((0))	-100% ((0))	-100% ((0))	-100% ((0))
60	hypothetical protein [*Synechococcus elongatus*]	gi|499563369	21 kDa		100% (2)	-100% ((0))	-100% ((0))	-100% ((0))	-100% ((0))
61	phycobilisome core component [*Synechococcus elongatus* PCC 7942]	gi|2655259	19 kDa		-100% ((0))	-100% ((0))	-100% ((0))	-100% ((0))	100% (1)
62	hypothetical protein [*Synechococcus elongatus*]	gi|499561689	47 kDa		-100% ((0))	-100% ((0))	-100% ((0))	-100% ((0))	100% (1)
63	hypothetical protein [*Synechococcus elongatus*]	gi|499563386	19 kDa		100% (1)	-100% ((0))	-100% ((0))	-100% ((0))	-100% ((0))
64	unknown [*Synechococcus elongatus* PCC 7942]	gi|25019697	42 kDa		99% (1)	98% (1)	-100% ((0))	-100% ((0))	-100% ((0))
65	hypothetical protein [*Synechococcus elongatus*]	gi|499562165	21 kDa		99% (2)	-100% ((0))	-100% ((0))	-100% ((0))	-100% ((0))
66	RecName: Full=30S ribosomal protein S8	gi|123556368	15 kDa		99% (1)	-100% ((0))	-100% ((0))	-100% ((0))	-100% ((0))

Table 2.1.S1 (cont'd)

67	unknown [*Synechococcus elongatus* PCC 7942]	gi|25019693	21 kDa		99% (1)	-100% ((0))	-100% ((0))	-100% ((0))	-100% ((0))
68	hypothetical protein [*Synechococcus elongatus*]	gi|499561641	17 kDa		99% (1)	-100% ((0))	-100% ((0))	-100% ((0))	-100% ((0))
69	photosystem I reaction center subunit III [*Synechococcus elongatus*]	gi|499561831	17 kDa		99% (1)	-100% ((0))	-100% ((0))	-100% ((0))	-100% ((0))
70	hypothetical protein, partial [*Synechococcus elongatus*]	gi|499562457	13 kDa		99% (1)	-100% ((0))	-100% ((0))	-100% ((0))	-100% ((0))
71	hypothetical protein [*Synechococcus elongatus*]	gi|499562535	16 kDa		99% (1)	-100% ((0))	-100% ((0))	-100% ((0))	-100% ((0))
72	hypothetical protein [*Synechococcus elongatus*]	gi|499562873	13 kDa		99% (1)	-100% ((0))	-100% ((0))	-100% ((0))	-100% ((0))
73	ABC transporter substrate-binding protein [*Synechococcus elongatus*]	gi|499562957	28 kDa		99% (1)	-100% ((0))	-100% ((0))	-100% ((0))	-100% ((0))
74	hypothetical protein [*Synechococcus elongatus*]	gi|499563689	19 kDa		99% (1)	-100% ((0))	-100% ((0))	-100% ((0))	-100% ((0))
75	hypothetical protein [*Synechococcus elongatus*]	gi|499696874	13 kDa		99% (1)	-100% ((0))	-100% ((0))	-100% ((0))	-100% ((0))

Candidate Proteins	Accession #	BLAST Results	Domains/Families
hypothetical protein [*Synechococcus elongatus*] **(Synpcc7942_0422)**	**gi|499562623**	Hypothetical Cyanobacterial Proteins, Putative S-Layer Protein (WP_015167719.1), Flagellar Hook Length control protein Flik (AIE74170.1),	
porin [*Synechococcus elongatus*] **SomB2 (Synpcc7942_1635)**	**gi|499561624**	Porins, SomB [*Synechococcus elongatus* PCC 6301], SomA [*Synechococcus elongatus* PCC 6301]	SLH Super Family, OprB Super Family
hypothetical protein (**Synpcc7942_1128)** [*Synechococcus elongatus* PCC 7942]	**gi|81299937**	outer membrane adhesin-like protein, Hemolysin-type calcium-binding region, hemolysin-type calcium-binding region, C-type lectin domain-containing protein, cellulose binding protein	DUF4214

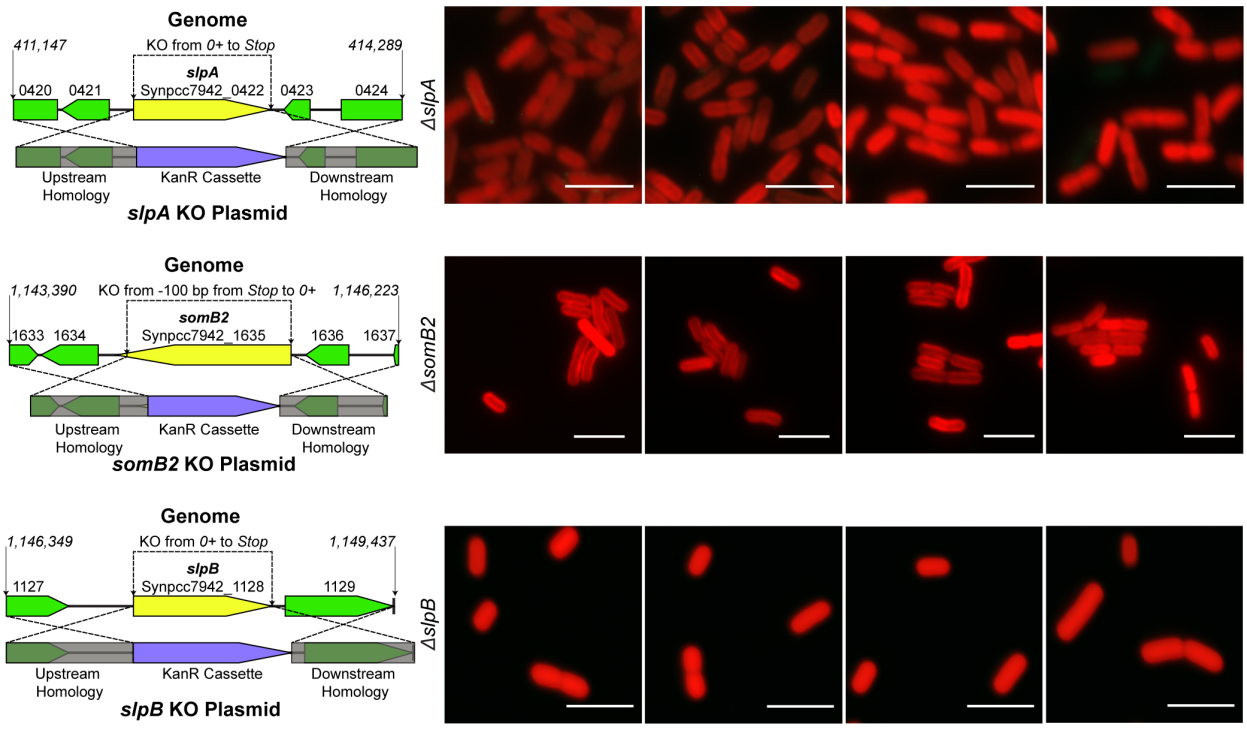

Figure 2.1.S5: Potential surface layer protein vector constructs and morphology
Integration vectors targeting the endogenous gene via ~1 Kb regions of homology flanking the gene of interest were used to delete the genes and replace them with Kanamycin resistance cassettes. In all but one case, we were able to delete the entire gene sequence. However, the GC and secondary structure rich 3' end of *somB2* prevented the design of suitable primers for a complete deletion. This 3' fragment was frame-shifted relative to the original sequence to prevent any potential production of the peptide fragment. Completeness of the transformations was confirmed by genomic PCR and the resultant mutants were screened for gross morphology changes, and none were observed (scale bars = 5μm).

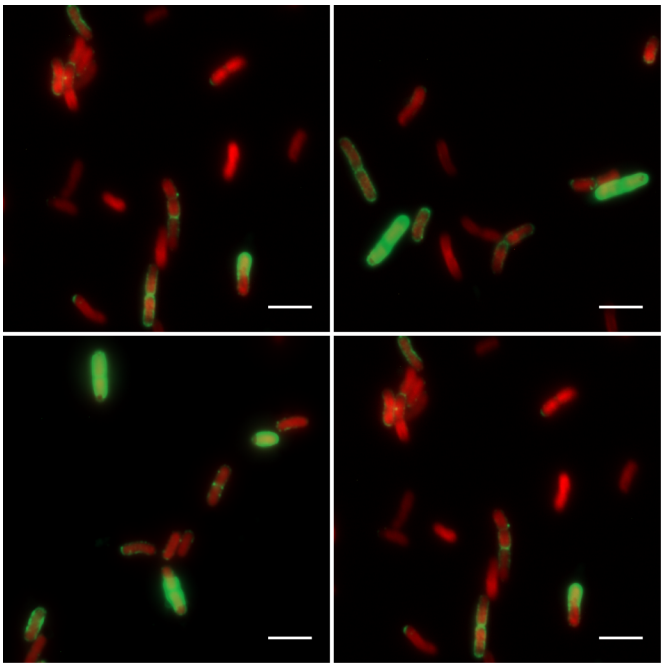

Figure 2.1.S6: Additional representative images of live R5F *wzt slpA* cells
(red: chlorophyll autofluorescence) induced for 16 hours and labeled with FLAG-tag specific antibodies (green). Labeling uniformity is slightly improved relative to single knockouts (Figure 3A,D), and the majority of cells are immunolabeled to some extent (scale bars = 5 μm).

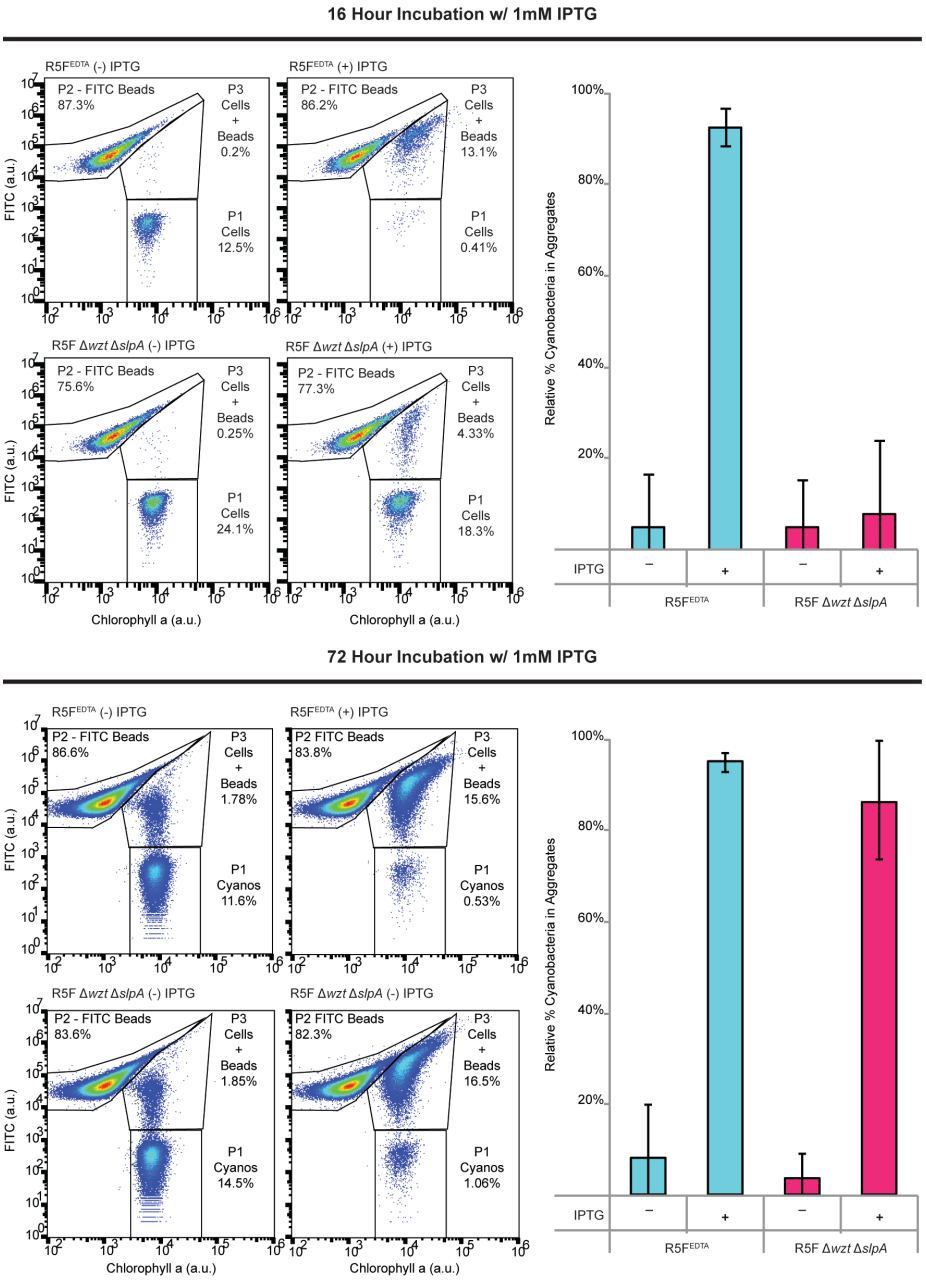

Figure 2.1.S7: Longer induction of SomA-R5F increases epitope availability

(Top) Flow cytometry of induced (16 hours) or uninduced R5F^{EDTA} or R5FΔ*wzt* Δ*slpA* cells (P1) mixed with beads (P2) shows the formation of a bead-cell aggregate population (P3) in the induced cell state. Bar graphs quantify the percentage of cyanobacterial counts lost from the P1 relative to control cell samples run without beads, interpreted as the number of cells participating in bead-cell aggregates. Averages of n=3 experiments displayed; error bars represent s.d. P-values: *<0.05, **<0.01). (Bottom) Experiments as in above, except cells were induced for a total of 72 hours prior to mixing with beads. Extending the induction of cultures increased the availability of the epitope in live cells, as evidenced by increased interaction of the cells with the beads.

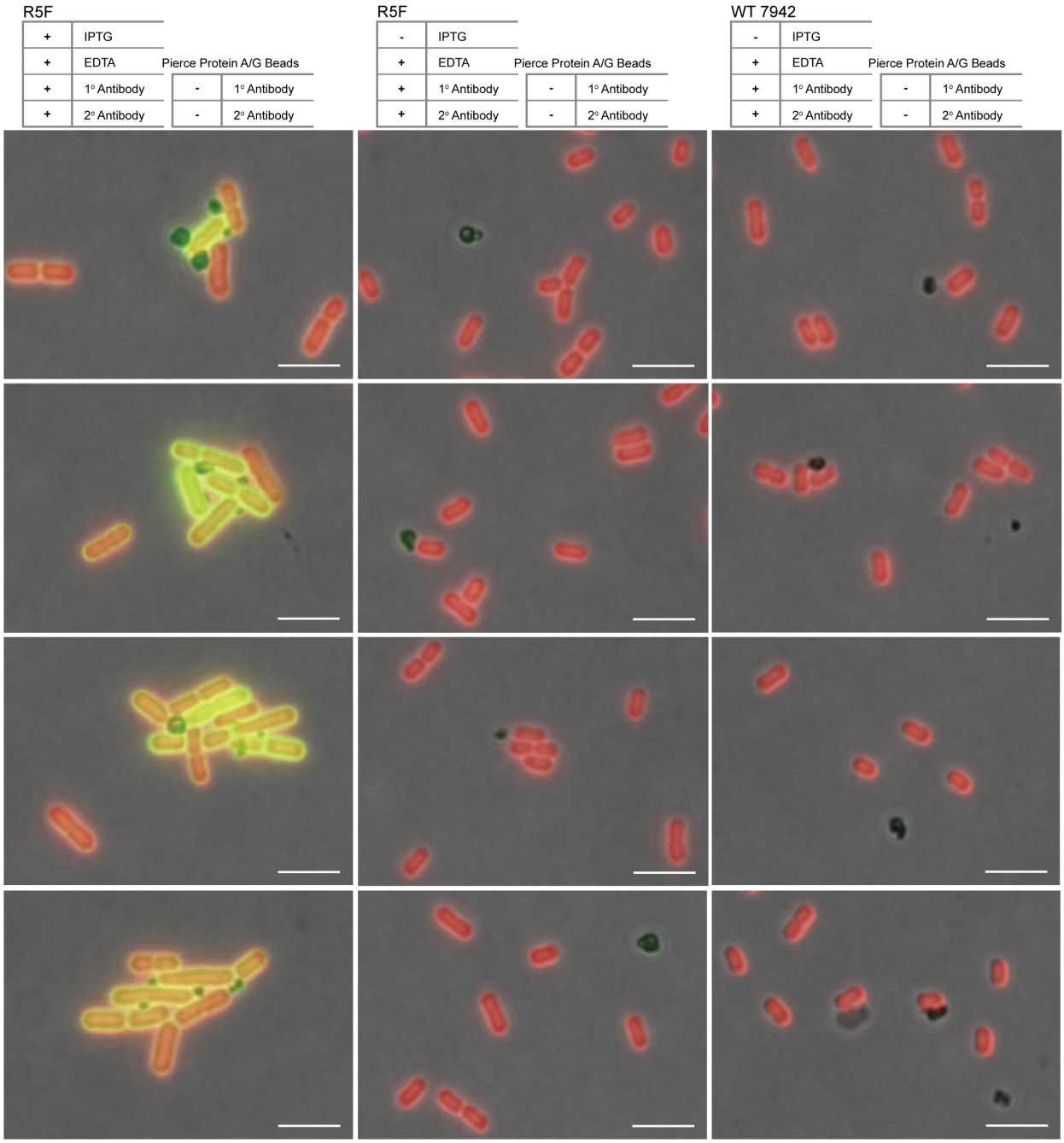

Figure 2.1.S8: Association of R5F^{EDTA} *S. elongatus* cells with magnetic Protein A beads is dependent upon IPTG-induced expression of SomA-R5F and mediating antibodies

Cell/bead mixtures were imaged and analyzed for the formation of aggregates under a number of different combinations of labeling conditions, demonstrating the necessity for antibodies as well as the expression of the modified SomA. Neither wild type cells nor uninduced R5F cells show any affinity for the beads. Aggregates only form under the specified parameters. Scale bars = 5 μm.

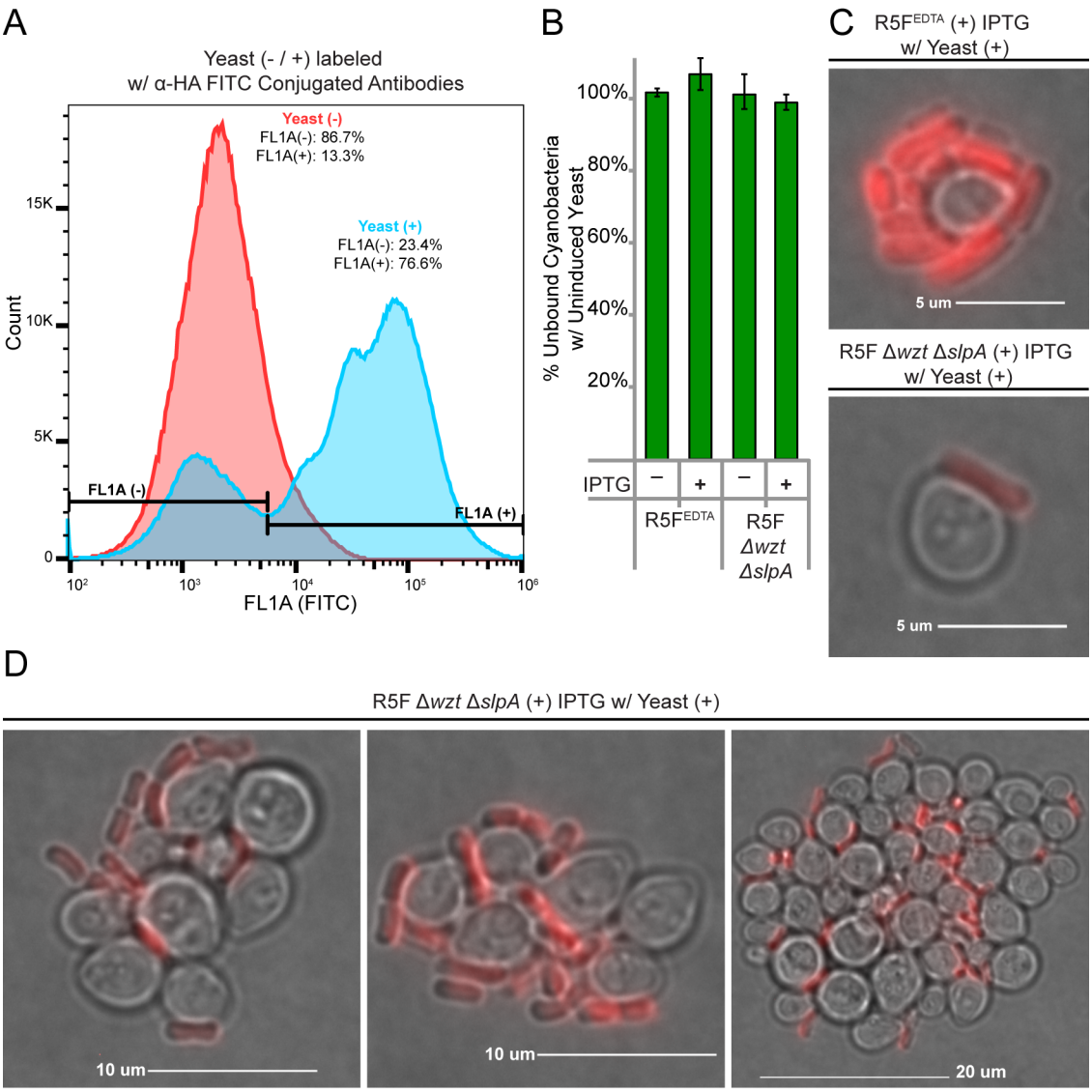

Figure 2.1.S9: Induction of Protein A on the surface of EY100 *S. cerevisiae* and antibody-mediated adhesion of yeast cells to R5F *S. elongatus*

(A) Representative histogram of live EY100 *S. cerevisiae* cells; either uninduced (red) or induced (blue) to express and display HA-tagged Protein A. Cells are labeled with anti-HA antibodies (FITC-labeled). Roughly 23% of the induced population either does not have the expression plasmid or is not expressing the protein as indicated by the lack of antibody staining. (B) An example bar graph of data collected from a flow cytometry experiment showing the lack of binding between cyanobacteria and yeast cells when the yeast cells are uninduced, n=2 biological replicates with 3 technical replicates each. Data was normalized to cyanobacteria control samples without the yeast added. (C-D) Additional examples of R5F *S. elongatus* cells binding to EY100 *S. cerevisiae* in (C) small cyanobacteria-yeast aggregates or (D) larger yeast and cyanobacteria aggregates. Scale bars as indicated.

New #	Pseudonym	Primer Direction	Primer Sequence (5'->3')	Function	5' Homology Target (for Isothermal Assembly)
1	F-somA	Forward	**TCACACAAGGAGGAAAAACATATGTCTAGA**ATGAAACGCCTTTTCTCGGCGCT	PCR *somA* from the Genome	NSIII Vector Backbone
2	R-somA	Reverse	**CTTACGTGCCGATCGGATCCTACGCGGCCG**CCTAGAAACGGAAGACTGTTTTCAGGAAGG	PCR *somA* from the Genome	NSIII Vector Backbone
3	R-NS3	Reverse	TCTAGACATATGTTTTTCCTCCTTGTGTGAAATTGTTATCCGC	PCR NSIII Vector with homology to *somA* insert	*somA* insert
4	R-NS3	Forward	CGGCCGCGTAGGATCCGATCGGCACGTAAGAG	PCR NSIII Vector with homology to *somA* insert	*somA* insert
5	F-R4F	Forward	**ATCCGATTACAAAGATGATGACGATAAAGGAGGAGGATCC**AACCTTGCTCTCTCCTTGGG	Protein Region 4 Site Insertion	FLAG Tag and Linkers
6	R-R4F	Reverse	**TCCTTTATCGTCATCATCTTTGTAATCGGATCCACCGCC**GTTGCTGTTGTAGTTGGTAGC	Protein Region 4 Site Insertion	FLAG Tag and Linkers
7	F-R1F	Forward	**ATCCGATTACAAAGATGATGACGATAAAGGAGGAGGATCC**AAAGCCTTCAAGTATGTCGG	Protein Region 1 Site Insertion	FLAG Tag and Linkers
8	R-R1F	Reverse	**CCTCCTTTATCGTCATCATCTTTGTAATCGGATCCACCGCC**CGTGTTCGCAGGGCCACTG	Protein Region 1 Site Insertion	FLAG Tag and Linkers
9	F-R3F	Forward	**GATCCGATTACAAAGATGATGACGATAAAGGAGGAGGATCC**GGTGTCTTTGGCTTCACCC	Protein Region 3 Site Insertion	FLAG Tag and Linkers
10	R-R3F	Reverse	**TCCTTTATCGTCATCATCTTTGTAATCGGATCCACCGCC**ACCACTGTTGACAGTCGAGAC	Protein Region 3 Site Insertion	FLAG Tag and Linkers
11	F-R5F	Forward	**CCGATTACAAAGATGATGACGATAAAGGAGGAGGATCC**TCTGAAGACACTGGTTCCTTTG	Protein Region 5 Site Insertion	FLAG Tag and Linkers
12	R-R5F	Reverse	**CCTCCTTTATCGTCATCATCTTTGTAATCGGATCCACCGCC**CGAACGGTTAGAAGCGCTG	Protein Region 5 Site Insertion	FLAG Tag and Linkers
13	F-R2F	Forward	**CCGATTACAAAGATGATGACGATAAAGGAGGAGGATCC**ACTGTCAACAGTGGTGGTGTC	Protein Region 2 Site Insertion	FLAG Tag and Linkers
14	R-R2F	Reverse	**CTCCTTTATCGTCATCATCTTTGTAATCGGATCCACCGCCCGA**GACATCAGCAGAGTTGC	Protein Region 2 Site Insertion	FLAG Tag and Linkers
15	F-*somA*-seq	Forward	TGATGTCTCCTTCACTGTTG	Sequencing Primer targeting within the *somA* gene	N/A
16	R-*somA*-seq	Reverse	GCAACTCGGAACTTGTTGTTATCAG	Sequencing Primer targeting within the *somA* gene	N/A
17	F-NS3-seq	Forward	GAGACGATGCGAACCTTCTCC	Sequencing Primer targeting the NSIII Site	N/A
18	R-NS3-seq	Reverse	TCTGGCGACGGGACTACG	Sequencing Primer targeting the NSIII Site	N/A
19	F-FLAGtag-seq	Forward	GGATCCGATTACAAAGATGATGACGATAAAGGAGGA	Sequencing Primer targeting the FLAG Tag Insert in *somA*	N/A

Table 2.1.S2: Primer List

Table 2.1.S2 (cont'd)

20	R-FLAGtag-seq	Reverse	TCCTCCTTTATCGTCATCATCTTTGTAATCGGATCC	Sequencing Primer targeting the FLAG Tag Insert in *somA*	N/A
21	F-*wbdC*-upseq	Forward	CTATCAACTCACCACTGAAACTATTGCC	Sequencing Primer targeting upstream of the *wbdC* gene	N/A
22	R-*wbdC*-downseq	Reverse	ATGATTGTGGAAGGAGGCTCTGG	Sequencing Primer targeting downstream of the *wbdC* gene	N/A
23	F-*wzm*-upseq	Forward	GGCCAGCGATCAATGGCAATTG	Sequencing Primer targeting upstream of the *wzm* gene	N/A
24	R-*wzm*-downseq	Reverse	CTAGCAGTTGTGCCAGTGCCG	Sequencing Primer targeting downstream of the *wzm* gene	N/A
25	F-*wzt*-upseq	Forward	GTTGTTCGGCTGAGAGATTGGC	Sequencing Primer targeting upstream of the *wzt* gene	N/A
26	R-*wzt*-downseq	Reverse	GCAAACGCTTCGCAAGTTTAGG	Sequencing Primer targeting downstream of the *wzt* gene	N/A
27	F-SpecR-Oag	Forward	**ATGCGCTCACGCAACTGG**CGTAGAAGAACAGCAAGGCCGCCAATG	Amplifying Spectinomycin Resistance Cassette for OAg KO Plasmids	Universal Oag Upstream Homology (3')
28	R-SecR-Oag	Reverse	TTATTTGCCGACTACCTTGGTGATCTCGCC	Amplifying Spectinomycin Resistance Cassette for Oag KO Plasmids	N/A
29	F-pUC57-Oag	Forward	CGCGTTGCTGGCGTTTTTC	Amplifying pUC57 Origin for Oag KO Plasmids	N/A
30	R-pUC57-Oag	Reverse	AGATCAAAGGATCTTCTTGAGATCCTTTTTTTCTG	Amplifying pUC57 Origin for Oag KO Plasmids	N/A
31	F-UpH-*wzt*	Forward	**GATCTCAAGAAGATCCTTTGATCT**GATCGATCACAGTAGCGTTGATGGG	Amplifying *wzt* Upstream Homology for KO Plasmid	pUC57 Origin (3')
32	R-UpH-*wzt*	Reverse	**CCAGTTGCGTGAGCGCAT**AGAGGTATTGCCTATCACTCGCC	Amplifying *wzt* Upstream Homology for KO Plasmid	Spectinomycin Resistance Cassette (5')
33	F-DownH-*wzt*	Forward	**CACCAAGGTAGTCGGCAAATAA**GCCATCATGAGAGAGTGGTTGTG	Amplifying *wzt* Downstream Homology for KO Plasmid	Spectinomycin Resistance Cassette (3')
34	R-DownH-*wzt*	Reverse	**AAAAACGCCAGCAACGCG**CCCACTACTGTAGGGCGAACTG	Amplifying *wzt* Downstream Homology for KO Plasmid	pUC57 Origin (5')
35	F-UpH-*wbdC*	Forward	**GATCTCAAGAAGATCCTTTGATCT**GAGGGCTTTGATAATCGCCAGACTG	Amplifying *wbdC* Upstream Homology for KO Plasmid	pUC57 Origin (3')
36	R-UpH-*wbdC*	Reverse	**CCAGTTGCGTGAGCGCAT**CAAAATACTTGTGCTTGGTACTAAAATTGG	Amplifying *wbdC* Upstream Homology for KO Plasmid	Universal Oag Upstream Homology (5')
37	F-DownH-*wbdC*	Forward	**CACCAAGGTAGTCGGCAAATAA**AGCTGTTCGGCAGCTAACGAG	Amplifying *wbdC* Downstream Homology for KO Plasmid	Spectinomycin Resistance Cassette (3')
38	R-DownH-*wbdC*	Reverse	**AACGCCAGCAACGCG**GCTGGAATAGTAGCCCCAGTTGAGG	Amplifying *wbdC* Downstream Homology for KO Plasmid	pUC57 Origin (5')
39	F-UpH-*wzm*	Forward	**GATCTCAAGAAGATCCTTTGATCT**TGGGCTCGTGGATGCAGAACAG	Amplifying *wzm* Upstream Homology for KO Plasmid	pUC57 Origin (3')
40	R-UpH-*wzm*	Reverse	**CCAGTTGCGTGAGCGCAT**GGGCGGAGAGGGACAGCTG	Amplifying *wzm* Upstream Homology for KO Plasmid	Spectinomycin Resistance Cassette (5')

Table 2.1.S2 (cont'd)

41	F-DownH-*wzm*	Forward	**CACCAAGGTAGTCGGCAAATAA**AAATTTGCGACAGGGAGACAGTC	Amplifying *wzm* Downstream Homology for KO Plasmid	Spectinomycin Resistance Cassette (3')
42	R-DownH-*wzm*	Reverse	**AAAAACGCCAGCAACGCG**GTGGTTTCCAGCAAGTGTCC	Amplifying *wzm* Downstream Homology for KO Plasmid	pUC57 Origin (5')
43	F-pUC15-*slpA*	Forward	**CCTCGACGAGTGGCCTCTGACACATGCAGCT**CGGAACTCATTGGCCGGACT	Amplifying pUC15 Origin for *slpA* KO	slpA Downstream Homology (3')
44	R-pUC15-*slpA*	Reverse	**TGGTGATTGACTACTACCTACCGTTACCCAACTTAATCGCC**AGTTGAAACCAGCACCAGC	Amplifying pUC15 Origin for *slpA* KO	slpA Upstream Homology (5')
45	F-KanR-*slpA*	Forward	**GGATCCCTAGTACTCGCT**AGGAAAGCCACGTTGTGTCTC	Amplifying Kanamycin Resistance Cassette for *slpA* KO	slpA Upstream Homology
46	R-KanR-*slpA*	Reverse	**GTTGTGATTTTTCAGTCTGGA**CCATCCCTAACTAAACAGTTGATTCG	Amplifying Kanamycin Resistance Cassette for *slpA* KO	slpA Downstream Homology
47	F-UpH-*slpA*	Forward	**GCGATTAAGTTGGGTAACG**GTAGGTAGTAGTCAATCACCAACGG	Amplifying *slpA* Upstream Homology for KO Plasmid	pUC15 Origin
48	R-UpH-*slpA*	Reverse	**ACAACGTGGCTTTCCT**AGCGAGTACTAGGGATCCCAG	Amplifying *slpA* Upstream Homology for KO Plasmid	Kanamycin Resistance Cassette
49	F-DownH-*slpA*	Forward	**CAACTGTTTAGTTAGGG**ATGGTCCAGACTGAAAAATCACAACTGAG	Amplifying *slpA* Downstream Homology for KO Plasmid	Kanamycin Resistance Cassette
50	R-DownH-*slpA*	Reverse	**AGCTGCATGTGTCAGAG**GCCACTCGTCGAGGCTAGC	Amplifying *slpA* Downstream Homology for KO Plasmid	pUC15 Origin (5')
51	F-DownH-*slpB*	Forward	**CAACTGTTTAGTTAGGGATGG**TCTGAGATAGCTCGTACAGACCG	Amplifying *slpB* Downstream Homology for KO Plasmid	Kanamycin Resistance Cassette (3')
52	R-DownH-*slpB*	Reverse	**GGCCAATGAGTTCCG**CTGGCCACCCAAGTCCTGG	Amplifying *slpB* Downstream for KO Plasmid	pUC15 Origin (5')
53	F-KanR-*slpB*	Forward	**TAAGTTTAAGTCTCTGAGAGTTAAATATT**AGGAAAGCCACGTTGTGTCTC	Amplifying Kanamycin Resistance Cassette for *slpB* KO	slpB Upstream Homology (3')
54	R-KanR-*slpB*	Reverse	**CTGTACGAGCTATCTCAGA**CCATCCCTAACTAAACAGTTGATTCG	Amplifying Kanamycin Resistance Cassette for *slpB* KO	slpB Downstream Homology (5')
55	F-pUC15-*slpB*	Forward	**ACTTGGGTGGCCAG**CGGAACTCATTGGCCGGACT	Amplifying pUC15 Origin for *slpB* KO	slpB Downstream Homology (3')
56	R-pUC15-*slpB*	Reverse	**GCCGCGATCGATTGA**CAGTTGAAACCAGCACCAGC	Amplifying pUC15 Origin for *slpB* KO	slpB Upstream Homology (5')
57	F-UpH-*slpB*	Forward	**GGTGCTGGTTTCAACTG**TCAATCGATCGCGGCATCTAC	Amplifying *slpB* Upstream Homology for KO Plasmid	pUC15 Origin (3')
58	R-UpH-*slpB*	Reverse	**ACAACGTGGCTTTCCT**AATATTTAACTCTCAGAGACTTAAACTTAGAAGAG	Amplifying *slpB* Upstream Homology for KO Plasmid	Kanamycin Resistance Cassette (5')
59	F-DownH-*somB2*	Forward	**CAACTGTTTAGTTAGGGATGG**GAACTCAATCCTCACACCGGG	Amplifying *somB2* Downstream Homology for KO Plasmid	Kanamycin Resistance Cassette (3')
60	R-DownH-*somB2*	Reverse	**GGCCAATGAGTTCCG**TGCCGTTAGGATAGGGGGC	Amplifying *somB2* Downstream Homology for KO Plasmid	pUC15 Origin (5')
61	F-KanR-*somB2*	Forward	**TCGTGACAGCATAGAGG**AGGAAAGCCACGTTGTGTCTC	Amplifying Kanamycin Resistance Cassette for *somB2* KO	somB2 Upstream Homology (3')

Table 2.1.S2 (cont'd)

62	R-KanR-*somB2*	Reverse	**GGTGTGAGGATTGAGTTC**CCATCCCTAACTAAACAGTTGATTCG	Amplifying Kanamycin Resistance Cassette for *somB2* KO	somB2 Downstream Homology (5')
63	F-pUC15-*somB2*	Forward	**CCCTATCCTAACGGCA**CGGAACTCATTGGCCGGACT	Amplifying pUC15 Origin for *somB2* KO	somB2 Downstream Homology (3')
64	R-pUC15-*somB2*	Reverse	**GCAACTCATTCGGTAGATTT**CAGTTGAAACCAGCACCAGC	Amplifying pUC15 Origin for *somB2* KO	somB2 Upstream Homology (5')
65	F-UpH-*somB2*	Forward	**GGTGCTGGTTTCAACTG**AAATCTACCGAATGAGTTGCCCT	Amplifying *somB2* Upstream Homology for KO Plasmid	pUC15 Origin (3')
66	R-UpH-*somB2*	Reverse	**ACAACGTGGCTTTCCT**CCTCTATGCTGTCACGAATGCA	Amplifying *somB2* Upstream Homology for KO Plasmid	Kanamycin Resistance Cassette (5')
67	F-*slpA*-seq	Forward	GAGCGGATTGGCCAACGCATTC	Sequencing Primer targeting within the *slpA* gene	N/A
68	R-*slpA*-seq	Reverse	GCGTACGACCCATCACAACAAAACC	Sequencing Primer targeting within the *slpA* gene	N/A
69	F-*somB2*-seq	Forward	CTAGAACAAGAACTCGGTCTTGAGTACTGGC	Sequencing Primer targeting within the *somB2* gene	N/A
70	R-*somB2*-seq	Reverse	ATGAAAAATCTGTTCAAGGTCATGTTGGCTG	Sequencing Primer targeting within the *somB2* gene	N/A
71	F-*slpB*-seq	Forward	ATGGCTAATCTGAAGATTACTTCTGCTCAGCAG	Sequencing Primer targeting within the *slpB* gene	N/A
72	R-*slpB*-seq	Reverse	TCAAACAATGGCAAGACTGGTGAGGTCG	Sequencing Primer targeting within the *slpB* gene	N/A

For primers involved in isothermal assembly steps: **Bold** = (5' Homology); Underline= (3' Binding Region)

CHAPTER 2.2: ENGINEERING OF PAIRED CYANOBACTERIAL AND HETEROTROPHIC SURFACE DISPLAY FOR INTERSPECIES ADHESION

The work in this chapter is unpublished.

Introduction

Microbial consortia are ubiquitous in nature. In fact, most microbial species have become so specialized they cannot function outside of consortia (Little et al. 2008). These communities are often quite stable when perturbed (Coyte et al. 2015) and play multiple roles in the environment due to the diversity of their constituents (Kato et al. 2005; Coyte et al. 2015; Trivedi et al. 2016). Both enhanced culture stability and the potential for multifunctional cultures are highly desirable features in industrial settings. Thus, there has been increasing interest in developing designer synthetic consortia for the targeted production of valuable biological compounds (Sabra et al. 2010; Ortiz-Marquez et al. 2013); yet, there are few examples of applied artificial consortia at scale (*e.g.,* the production of vitamin C (Ye et al. 2014)). This deficit may be at least partially explained by the absence of parameters that can be used to guide the development of industrially viable consortia. In order to identify the fundamental design principles, a greater understanding of how microbial species behave in both natural and artificial communities is needed.

A number of synthetic consortia have been engineered to explore different types of microbial interactions and how they influence species dynamics within natural consortia (Brenner et al. 2008; Kerner et al. 2012; Ding et al. 2016; Hays et al. 2017; Tecon and Or 2017). A significant portion of this foundational research has been performed with single-species auxotrophs that rely on artificially induced cross-feeding scenarios (Kerner et al. 2012; Tecon and Or 2017). While these consortia are easily tuned, controlled, and measured, they are less realistic and limit the kinds of conclusions that can be made regarding community dynamics. One of the ways in which researchers are attempting to generate artificial consortia more reflective of natural communities is through the selection

of community members with different trophic lifestyles (*e.g.,* phototrophic vs. chemotrophic vs. heterotrophic). Recently, work from our lab and others has explored artificial consortia utilizing a strain of the cyanobacterium *Synechococcus elongatus* PCC 7942 engineered to excrete endogenously synthesized sucrose (Ducat et al. 2012) in combination with different heterotrophic microbes (Smith and Francis 2016; Hays et al. 2017; Löwe et al. 2017a; Weiss et al. 2017). These studies have demonstrated that this engineered strain of cyanobacteria has the ability to stably support a variety of heterotrophs, operating as a flexible photosynthetic co-culture platform.

With sucrose as the exchanged metabolite, any species that either naturally utilizes sucrose or can be engineered to do so (*e.g., Pseudomonas putida* (Löwe et al. 2017b)) could potentially be paired with the *S. elongatus* CscB in a synthetic consortium. However, it leaves the consortia vulnerable to invasion by other microbes also capable of metabolizing sucrose (*e.g., Stenotrophomonas maltophilia* (Weiss et al. 2017)). Additionally, the diffusion of sucrose results in individual heterotrophs experiencing relatively low concentrations of sucrose, which can be problematic when co-cultivating model heterotrophs adapted to growing in high-carbon environments (Kinoshita 1972). To address these limitations I looked to naturally cooperative species and consortia for a method that could be used to potentially stabilize artificial consortia.

One common mechanism used to maintain selectivity between cooperating organisms is spatial organization. This can be seen in a number of natural systems including lichen communities (Pankratov et al. 2017), marine corals (Kvennefors et al. 2017), biofilms (Stoodley et al. 2002), and many more (Kim et al. 2008). Could physical association between the engineered cyanobacteria and their heterotrophic partners increase the

efficiency of carbon transfer and decrease risk of co-culture contamination? In Chapter 2.1, I showed that an engineered recombinant SomA protein with an internal FLAG-tag epitope could be displayed in *S. elongatus*, and demonstrated that this surface tag could be used to adhere the cyanobacteria cells to functionalized magnetic agarose beads or *Saccharomyces cerevisiae*. While this system did demonstrate the potential of biologically encoded adhesion to engineered surface substrates, one of the key caveats to this work was the required addition of monoclonal antibodies to mediate the binding of this cyanobacterial strain. In this chapter, I describe preliminary data on the diversification of the cyanobacterial surface display system developed in Chapter 2.1 with the eventual goal of specific interspecies adhesion in co-culture.

Specifically, I explored the capacity of the SpyTag/SpyCatcher and StrepII/Streptavidin protein domains to mediate direct attachment between a modified cyanobacterium and a heterotrophic partner species. The SpyTag/SpyCatcher system was developed from an immunoglobulin-like collagen adhesion domain (CnaB2) of the fibronectin binding protein (FbaB) in the bacterium *Streptococcus pyogenes* (Zakeri et al. 2012). This domain was one of many extracellular proteins stabilized by intramolecular isopeptide bonds (Kang and Baker 2011). Zakeri et al. split this domain into cognate SpyTag and SpyCatcher peptide sequences. The SpyTag component is 13 amino acids in length and contains the reactive Asp_{117} residue while the SpyCatcher peptide is 116 amino acids in length, constituting the rest of the CnaB2 domain and contains the Lys_{31} that forms the isopeptide bond with the SpyTag Asp_{117}. Recombinant proteins containing the corresponding SpyTag and SpyCatcher sequences covalently bond to one another at a range of temperatures and pH, enabling stable association of independently encoded and expressed proteins (Zakeri et al.

2012; Reddington and Howarth 2015). This split domain has since been used for a number of applications, including enzyme stabilization, immune system stimulation, and protein scaffolding (Reddington and Howarth 2015).

The Strep-tag II is a modified version of the original 9 amino acid affinity tag "Strep tag" which has a high intrinsic binding affinity for the protein streptavidin. Unlike the Strep-tag, Strep-tag II maintains streptavidin binding capabilities even if it is not localized to the C-terminus of recombinant proteins (Schmidt and Skerra 1994). However, the changes to the Strep-tag II amino acid sequence also resulted in a lowered affinity for streptavidin. This was later rectified through the generation of two streptavidin core mutants with improved binding affinity (Voss and Skerra 1997)(Korndorfer and Skerra 2002). In this work, we are utilizing the Streptavidin Core Mutant 2, herein referred to as StrepCoreMut2 (Voss and Skerra 1997), as the basis for our Strep-tag II affinity system. Both the StrepCoreMut2 domain and SpyCatcher domain will be engineered to display on the surface of the partnering heterotrophs. Here we generate modified strains of *S. elongatus*, *E. coli* W cscR, and *S. cerevisiae* EBY100 capable of expressing and translocating recombinant surface display proteins with both SpyTag/SpyCatcher and Strep-tag II/Streptavidin protein domains to their surface.

Results

Design of surface display strains

As described in Chapter 2.1, the cyanobacterial surface display system requires insertion of the displayed moiety into a presumptive extracellular loop of SomA (Chapter 2.1) (Fedeson and Ducat 2016). I therefore cloned the short SpyTag (13aa) or Strep-tag II

(9 aa) peptide sequences into the predicted external loop (R5) of SomA within an IPTG inducible NSIII vector (Chapter 2.1); naming the resulting constructs NSIII-SomA-R5SpyTag and NSIII-SomA-R5StrepII, respectively (Figure 2.2.1A). The NSIII-SomA-R5StreptagII construct simply replaces the FLAG tag epitope (described in chapter 2.1) with the Strep-tag II epitope [NWSHPQFEK]. This insert is flanked on either side by 4 aa linker regions [GGGS] (Figure 2.2.1A). The NSIII-SomA-R5SpyTag construct contains two epitope tags, the SpyTag [AHIVMVDAYKPTK] and the FLAG Tag [DYKDDDDK], both are flanked by the same linker sequence [GGGS] (Figure 2.2.1A). The FLAG Tag was included in this construct to provide an antibody epitope for validating the surface localization of this protein. Here both the SpyTag and Strep-tag II epitopes are generically referred to as ligand domains. Subsequent transformation and chromosomal integration of these constructs in wild-type *S. elongatus* generated the R5SpyTag and R5StrepTagII strains. Transcription of these recombinant genes are controlled by the *trc* promoter utilized in Chapter 2.1 and expression can be induced with the addition of IPTG as previously described (Fedeson and Ducat 2016). Inducing both of these strains overnight with 1 mM IPTG, live cells were harvested from culture the following day, stripped of extracellular components as previously described with an EDTA-based stripping buffer (Fedeson and Ducat 2016), and then immunostained with primary and secondary antibodies. Fluorescent microscopy of these samples showed fluorescent antibody localization, indicating that the antibodies were able to interact with the inserted peptide sequences (Figure 2.2.1B).

Both *S. cerevisiae* and *E. coli* have extensive histories with surface display systems (Pepper et al. 2008; van Bloois et al. 2011) that we could modify for our purposes, and can also be stably co-cultivated with *S. elongatus* CscB (Ducat et al. 2012; Hays et al. 2017).

Therefore, we adapted strains of these model heterotrophs to display compatible ligand pairs to the cyanobacterial R5SpyTag and R5StrepTagII strain surface tags.

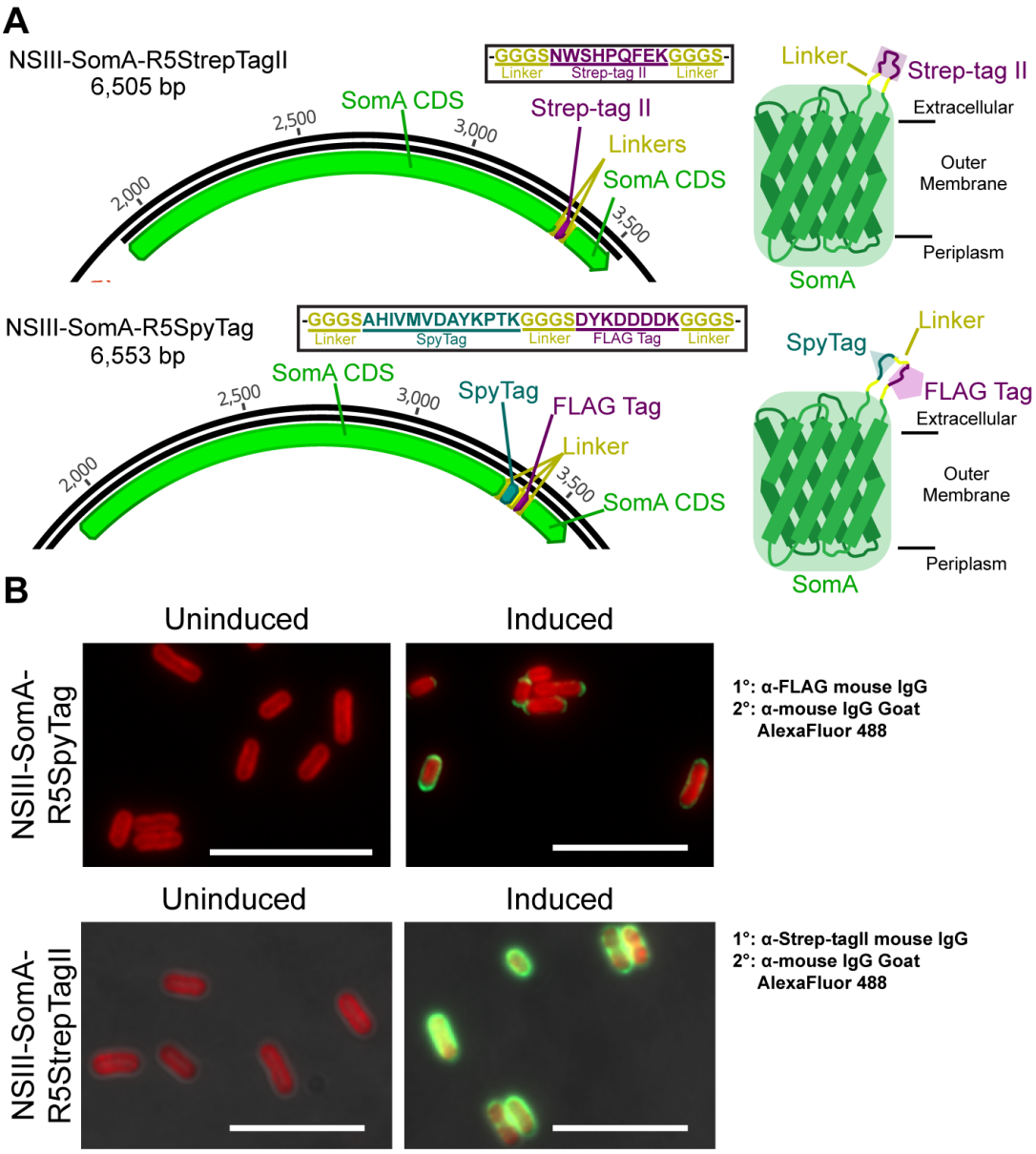

Figure 2.2.1: *S. elongatus* SpyTag and Strep-tag II surface display constructs
(A) Transcription of both the SomA-R5StrepTagII (Top) and SomA-R5SpyTag (Bottom) genes is driven by the IPTG inducible trc-promoter from the neutral site III of the *S. elongatus* chromosome (Chapter 2.1). Each tag is flanked by a set of GlyGlyGlySer linkers. (B) Live cell immunostaining of the NSIII-SomA-R5SpyTag with α-FLAG tag monoclonal mouse IgG2b (LT0420; Lifetein) (Top) and NSIII-SomA-R5StrepTagII (anti-Strep-tagII) (Bottom) show that the integrated NSIII-SomA cassettes are inducible and that the protein is translocated to the cell surface.

To display appropriate binding domains on *S. cerevisiae*, we modified the published yeast display plasmid (pETCON-Aga2p-proteinA; (Boder and Wittrup 2000; Fedeson and Ducat 2016)), replacing the protein A domain with sequence for Streptavidin Mut2 or SpyCatcher (See constructs pETCON-Aga2p-StreptavidinCoreMut2 and pETCON-Aga2p-SpyCatcher; Figure 2.2.2A). Additionally, both protein sequences contain a c-terminal c-Myc peptide tag for the purpose of immunohistochemistry and western blotting. These constructs were introduced into chemically competent *S. cerevisiae* EBY100 cells to create StrepCoreMut2 and SpyCatcher yeast surface display strains. Protein expression from these plasmids was induced by exposing the cells to SGCCA medium for a duration of 4 hours as was done in (Chapter 2.1 Methods) (Fedeson and Ducat 2016). These cells were then immunostained with primary α-cMyc antibodies and AlexaFluor 448 conjugated secondary antibodies (Chapter 2.1 Methods) (Fedeson and Ducat 2016). Imaging of these strains revealed that both constructs display the recombinant proteins on their surface (Figure 2.2.2B).

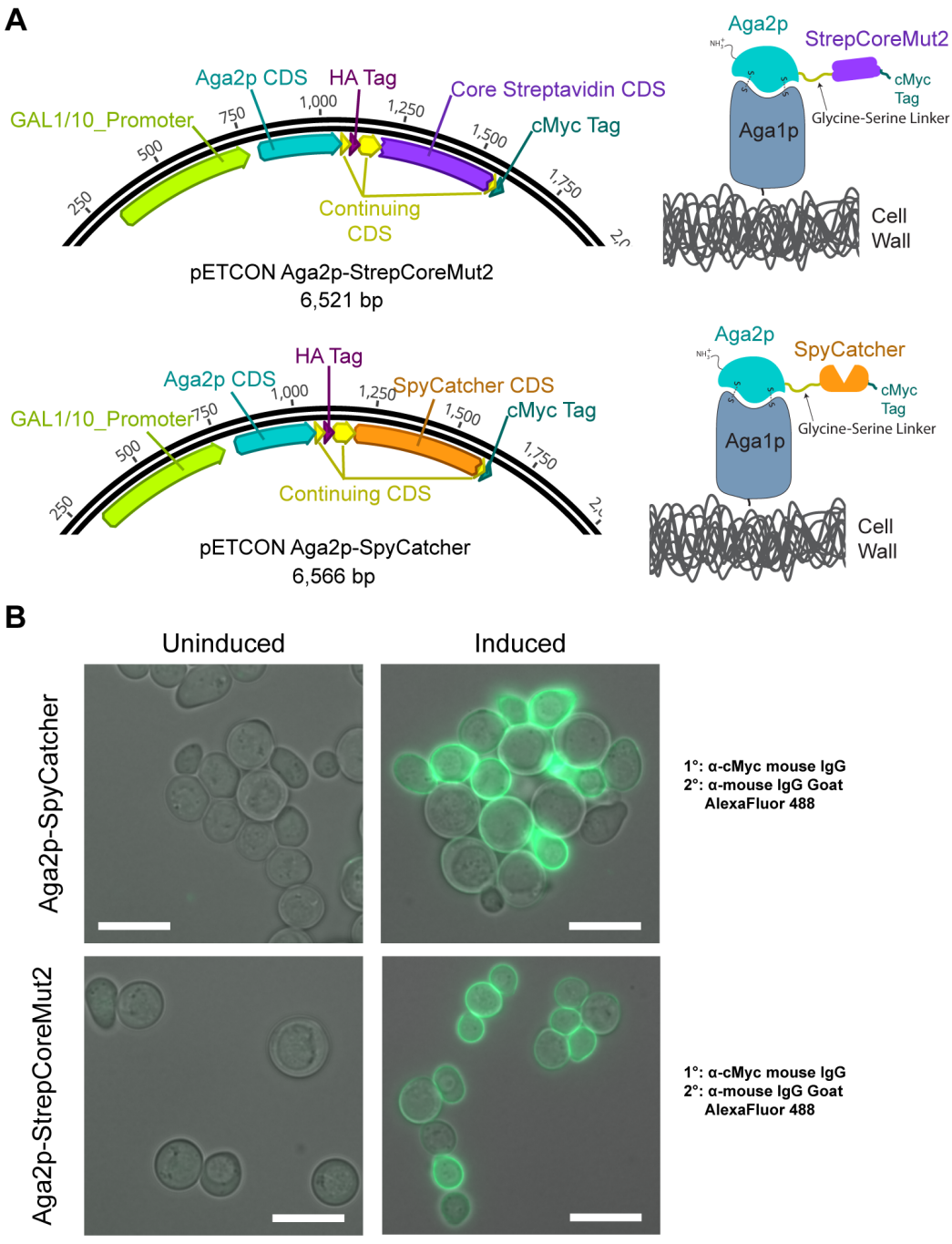

Figure 2.2.2: *S. cerevisiae* SpyCatcher and StrepCoreMut2 surface display constructs
(A) Sequence design for the Aga2p-StrepCoreMut2 surface display protein (Top) and the Aga2p-SpyCatcher surface display protein (Bottom) are both derivatives of the pETCON-Aga2P-proteinA expression plasmid utilized and described in Chapter 2.1. (B) Immunostaining of uninduced and induced *S. cerevisiae* cells containing these constructs with anti-cMyc monocolonal antibodies and AlexaFluor488 conjugated anti-mouse secondary antibodies (as per Chapter 2.1 methods) show that both the SpyCatcher and StrepCoreMut2 constructs are successfully displayed on the surface of the yeast cells.

For display of compatible binding domains on the surface of *E. coli*, we explored two conventional systems. The first system we designed uses a combination of native *E. coli* protein sequences, specifically a lippopolyprotein signal peptide fragment (Lpp'), and a truncated outer membrane protein A (OmpA), the N-terminus of which is fused to the protein of interest that is to be displayed (van Bloois et al. 2011). Using this framework, we generated two constructs that would express Lpp'-OmpA'-SpyCatcher or Lpp'-OmpA'-StrepCoreMut2. However, upon induction and immunostaining of transformed strains no immunofluorescent labeling was observed, indicating that the protein was not being displayed on the surface of the cells. We therefore decided to change surface display systems and obtained the plasmid pAIDA1 through Addgene. This surface display system utilizes the signal peptide, and C-terminal translocation unit of the AIDA-I *E. coli* adhesin to transport and display passenger domains on the surface of *E. coli* (Jarmander et al. 2012). The AIDA-I protein has been used previously for the expression of recombinant proteins, enzymes, and enzyme inhibitors on the cell surface (Jose et al. 2001, 2002; Jose and Zangen 2005). We designed and constructed the pAIDA1-SpyCatcher plasmid using by inserting the *E. coli* codon-optimized SpyCatcher DNA-fragment via Gibson Assembly at the N-terminus of the $AIDA1_c$ domain (Figure 2.2.3A). Immunostaining of *E. coli* transformed with this construct with the same combination of primary α-cMyc antibodies and AlexaFluor 448 conjugated secondary antibodies showed high levels of fluorescence, indicating that the protein was being translocated to the cell surface (Figure 2.2.3B).

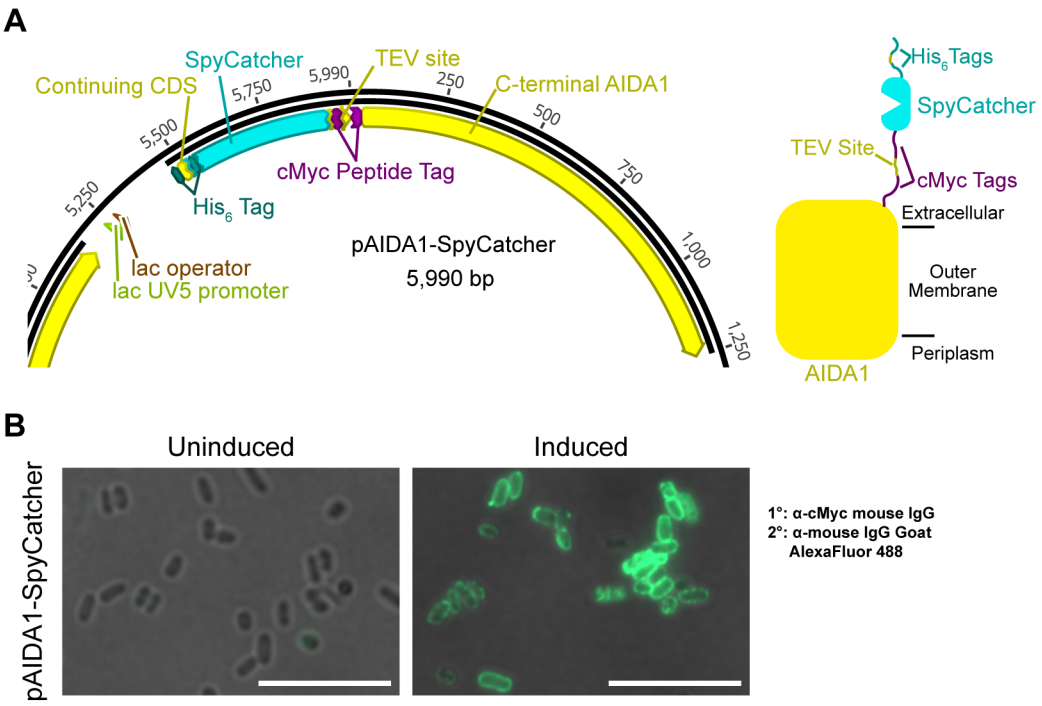

Figure 2.2.3: *E. coli* W cscR SpyCatcher surface display construct
(A) The pAIDA1-SpyCatcher construct was generated by inserting the DNA fragment encoding the SpyCatcher into the pAIDA1 plasmid at the N-terminus of the $AIDA1_c$ domain. (B) Transforming this construct into the *E. coli* W cscR strain and inducing the cells with 1 mM IPTG triggered the production of the fusion protein. Cells were immunolabeled with an anti-cMyc monoclonal mouse antibody and anti-mouse IgG Goat secondary antibody conjugated to AlexaFluor 488.

Evaluating the ability of the surface displayed moieties with soluble conjugate proteins

While the immunostaining experiments indicate that the antigenic tags on both the cyanobacterial and heterotrophic surface display proteins are accessible, this did not directly confirm the binding activity of the displayed moieties. To directly assay the capacity of surface tags to bind to cognate binding domains, we generated constructs encoding soluble recombinant mNeonGreen fluorophores fused with either the SpyCatcher domain or a combination of the SpyTag and Strep-tag II moieties (Figure 2.2.4A).

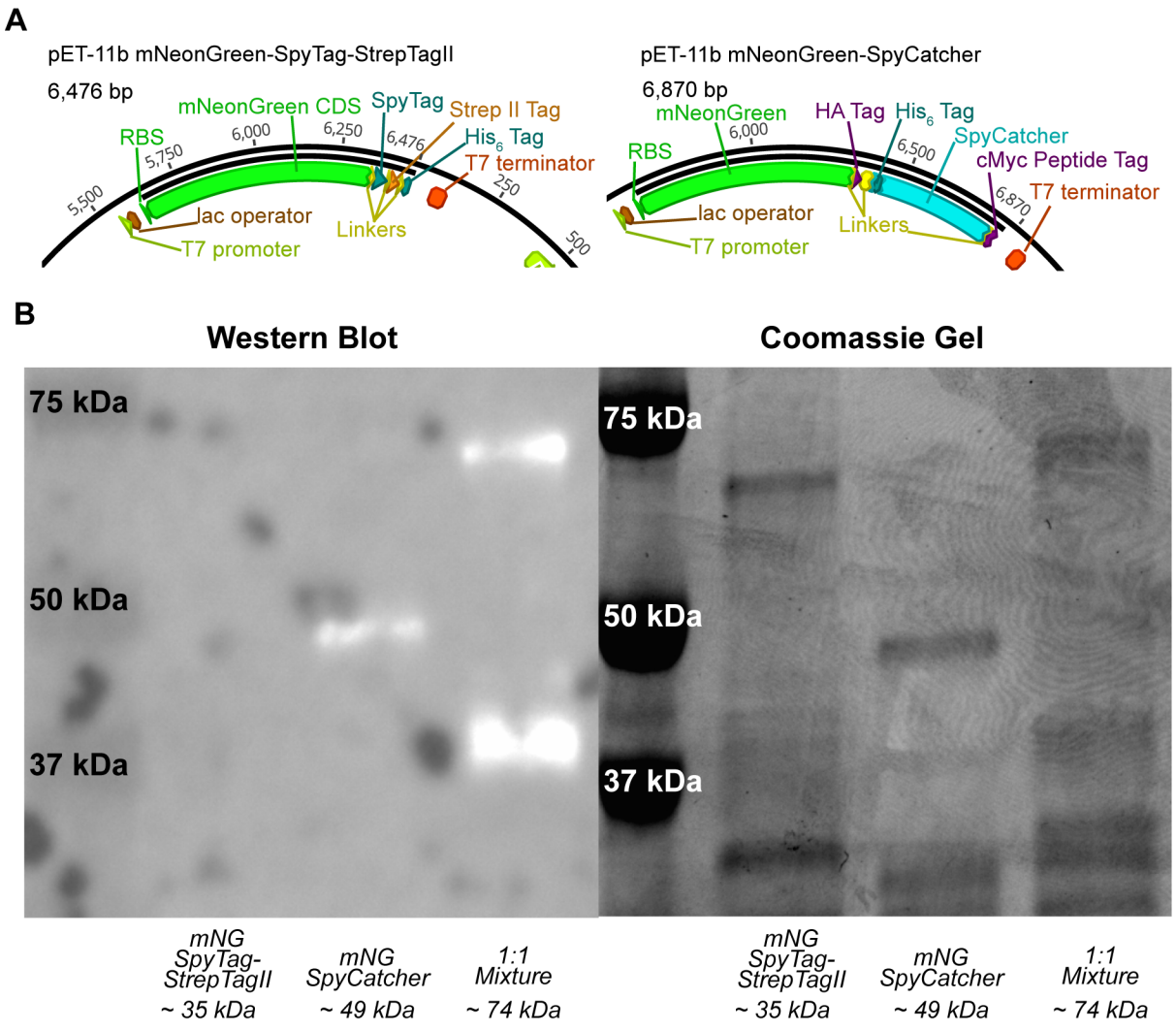

Figure 2.2.4: Protein reagent development

(A) Construct maps of both pET-11b plasmids containing either the mNeonGreen-SpyTag-StrepTagII fusion protein (Left) or the mNeonGreen-SpyCatcher fusion protein (Right). (B) A preliminary EMSA western blot (Left) and paired coomassie gel (Right) that confirmation of the purified mNeonGreen proteins are able to interact through the SpyTag and SpyCatcher domains. This membrane was incubated with anti-cMyc monoclonal mouse antibody and then the anti-mouse IgG goat antibody conjugated to Alexafluor 488. The mNG-SpyTag-StrepTagII runs at ~35 kDa on the SDS-page gel where as the mNG-SpyCatcher protein runs at ~49 kDa. In a 1:1 mixture of these two protein reagents we see the depletion of the mNG SpyCatcher band and the appearance of a band higher up on the gel at ~74 kDa. While slightly less than the predicted combined weight of these two proteins (~84 kDa), this shift indicates that these two reagents maintain affinity for one another under experimental conditions.

The proteins were additionally encoded with His_6 tags, expressed off of pET-11b plasmids in the *E. coli* BL21 D3 cell line. Thereafter, the reporter proteins were purified from cell lysates using a Nickel-affinity column. These purified fluorescent proteins would allow us to examine whether the surface displayed SpyTag, SpyCatcher, and StrepCoreMut2 domains could bind to freely diffusible cognate binding partners. To verify activity of the purified mNeonGreen-SpyCatcher protein, both the mNeonGreen-SpyCatcher and mNeonGreen-SpyTag-StrepII protein were mixed in equal ratio. This mixture was then used to perform a western blot mobility shift assay as the two reagents reacted, forming the predicted isopeptide covalent bond. This assay demonstrated that the two recombinant proteins did indeed bond together (Figure 2.2.4B).

Given the previous success of the *S. cerevisiae* surface display system (Chapter 2.1) and limited time and resources, only the *S. cerevisiae* strains were tested with the purified protein reagent. The *S. cerevisiae* SpyCatcher display strain was induced in SGCCA medium (as in Chapter 2.1) and then incubated with purified mNeonGreen-SpyTag-StrepII protein. This demonstrated that the SpyCatcher domain is displayed in a manner that is sufficient to bind and react with the diffuse mNeonGreen-SpyTag-StrepII protein (Figure 2.2.5A). However, repeating the same experiment with the *S. cerevisiae* StrepCoreMut2 display strain did not show signs of mNeonGreen localization to the cell surface, indicating that either the StrepCoreMut2 domain was non-functional or that the location or orientation of the Strep-tag II on the fluorescent protein prevented binding (Figure 2.2.5B). Similarly, our initial attempts to localize the mNeonGreen-SpyCatcher protein to the surface of the cyanobacteria also appeared to be unsuccessful (Figure 2.2.5C).

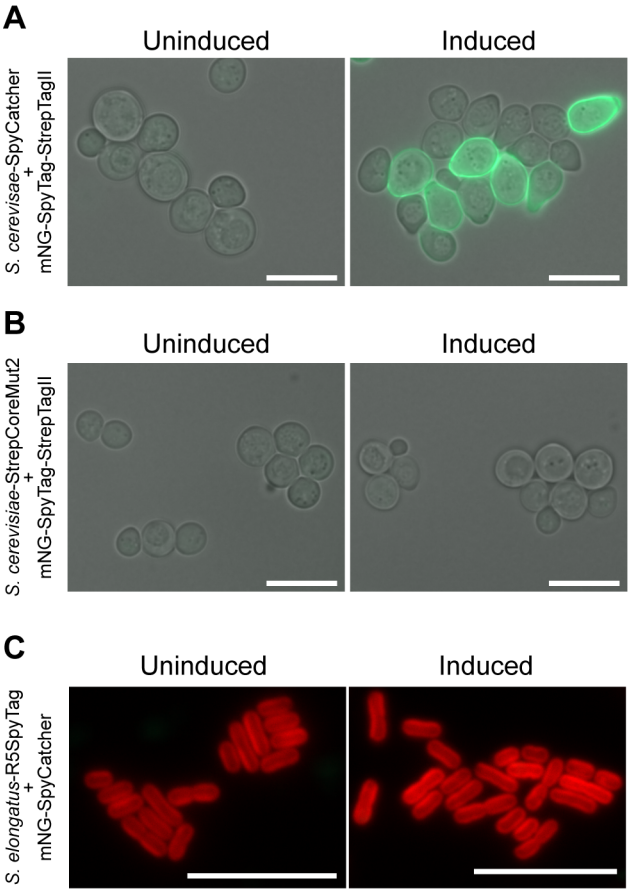

Figure 2.2.5: Preliminary testing of *S. cerevisiae* and *S. elongatus* strains with protein reagents

(A) Surface labeling of *S. cerevisiae* SpyCatcher with purified mNeonGreen-SpyTag-StrepTagII protein demonstrates that the surface displayed SpyCatcher domain is functional in this strain. (B) Testing of the *S. cerevisiae* StrepCoreMut2 with the same purified mNeonGreen-SpyTag-StrepTagII protein indicated that the expected interaction was not occurring despite indications that the recombinant surface protein is present on the cell surface. (C) Attempts at labeling of the *S. elongatus* SomA-R5SpyTag strain with the purified mNeonGreen-SpyCatcher protein also indicate that the reaction is inhibited by either the protein orientation or other steric hindrances on the cyanobacterial surface.

Discussion

In this chapter, I show preliminary data on the diversification of peptide sequences utilized in the cyanobacterial surface display system described in Chapter 2.1 and the development of heterotrophic strains capable of displaying the corresponding protein

domains that can interact with those peptide sequences. Utilizing the cyanobacterial surface display system I developed in Chapter 2.1, we were able to generate cyanobacterial strains that translocate the engineered SomA proteins containing both the SpyTag and Strep-tag II peptide sequence to the cell surface (Figure 2.2.1B). The heterotrophic strains of *E. coli* and *S. cerevisiae* appear to express their respective SpyCatcher domains without issue (Figure 2.2.2B). In the case of the *S. cerevisiae* Aga2p-SpyCatcher display strain, the SpyCatcher domain is shown to be active and able to recruit and bind the SpyTag-Fluorophore fusion protein purified in this work (Figure 2.2.4B). While surface display in *S. cerevisiae* has become quite routine (Pepper et al. 2008), surface expression of the SpyCatcher domain could be a novel mechanism to recruit and permanently adduct protein based products to the cell surface.

However, it appears in the case of the *S. elongatus* SomA-R5SpyTag strain, the accessibility of the SpyTag sequence is restricted such that a fluorophore with the SpyCatcher domain is unable to interact with it (Figure 2.2.4D). Surface layer stripping of the cyanobacteria strains was performed prior to removing extracellular material that might directly occlude the surface of the cyanobacteria's outer membrane (see Chapter 2.1 methods). This would suggest that the location and/or orientation of the SpyTag within the extracellular loop of the recombinant SomA may be playing a role in the inaccessibility of the sequence.

The results of Chapter 2.1 and the preliminary data presented here in Chapter 2.2, suggest that this system, with further refinement, has the potential to facilitate interspecies adhesion. We are working toward interspecies adhesion to artificially aggregate different species together to examine whether this physical association can stabilize engineered

commensal or symbiotic interactions. Previous work has shown that adhesion between cross-feeding strains is preferred under some conditions (Marchal et al. 2017), but not others (Kim et al. 2008). Thus, having the ability to induce tight and specific associations between co-cultured species would provide a unique mechanism by which to gauge the compatibility of two species. However, cell-adhesion systems could be applied in other capacities beyond co-culture. A relevant example is the sedimentation of planktonically grown cyanobacteria. One of the most significant costs in microalgal and cyanobacterial bioindustry is accrued during the harvesting of biomass (Sharma et al. 2011). An active area of research is in the use of biologically-based microbial flocculants to sediment cells from industrial scale cultures (Tong et al. 1999). By creating a specific adhesion mechanism, it may be possible to improve the overall cell capture efficiency of future bioflocculants.

Materials and Methods

Strains and culture conditions

Monocultures of *S. elongatus* and *S. cerevisiae* were cultivated as previously described (Chapter 2.1). *E. coli* strains were grown in Luria Bertani (LB) medium with 25 mg/mL of either Chloramphenicol (pAIDA1 vector) or Carbenicillin (pET-11b vector) to maintain selection for the respective plasmids, and incubated at 37°C.

Construct/strain development

The NSIII-SomA-R5Strep-tagII construct was synthesized using primers (F-Strep-tagII and R-Strep-tagII) that amplified a new fragment containing the Strep-tagII sequence

that targeted the original NSII-SomA-R5F construct (Chapter 2.1) as a template. Amplified fragments were re-circularized using Gibson assembly described in (Chapter 2.1). The NSIII-SomA-R5SpyTag construct was synthesized by amplifying the NSIII-SomA-R5 construct with R-NS3 and F-NS3, and then performing a Gibson Assembly with at DNA fragment containing insert sequence (Figure 2.2.1A) (Source: IDT). Transformation of WT *S. elongatus* PCC 7942 was performed as described in (Chapter 2.1.) Two iterations of both SpyCatcher and Streptavidin Core Mut 2 (*E. coli* or *S. cerevisiae* codon optimized) sequences were synthesized by IDT and incorporated into either pETCON-pAga2p or pAIDA1 via Gibson assembly (Gibson et al. 2009). The pETCON-ProteinA vector was cut with NdeI and BamHI to excise the ProteinA sequence from the plasmid, the backbone was then purified by agarose gel extraction (Qiagen). The purified backbone was then used in Gibson Assembly reactions with either the SpyCatcher or StrepCoreMut2 gene fragments to create the respective plasmids. The pAIDA1 vector was similarly processed, cutting the vector with the KpnI restriction enzyme, gel purifying the backbone, and assembled via Gibson reaction with the *E. coli* codon optimized SpyCatcher gene fragment. These vectors were

New #	Pseudonym	Primer Direction	Primer Sequence (5'->3')	Function	5' Homology Target (if applicable)
1	R-NS3	Reverse	TCTAGACATATGTTTTTCCTCCTTGTGTGAAATTGTTATCCGC	PCR NSIII Vector with homology to *somA* insert	*somA* insert
2	F-NS3	Forward	CGGCCGCGTAGGATCCGATCGGCACGTAAGAG	PCR NSIII Vector with homology to *somA* insert	*somA* insert
3	F-Strep-tag II	Forward	GGAGCCACCCCCAGTTCGAGAAGGGAGGAGGATCCTCTGAAG ACACTGGTTCCTTTG	SomA Lp7 Strep II Tag Insertion Forward Primer	*somA* insert
4	R-Strep-tag II	Reverse	CTCGAACTGGGGGTGGCTCCAGTTGGATCCACCGCCCGAACG GTTAGAAGCGCTG	SomA Lp7 Strep II Tag Insertion Reverse Primer	*somA* insert
Bold = (5' Homology); Underline= (3' Binding Region)					

Table 2.2.1: Chapter 2.2 Primer list

transformed into their respective chemically competent hosts (*S. cerevisiae* EBY100 (Lu 2011) or *E. coli* W cscR (Inoue et al. 1990).

Immunostaining and western blotting

Immunostaining for the *S. elongatus* and *E. coli* strains was performed as described for the cyanobacterial immunostaining performed in Chapter 2.1. Immunostaining of the *S. cerevisiae* strains were also performed as described in Chapter 2.1. Western blotting was also performed as in Chapter 2.1. The relevant antibodies used in this chapter are: α-FLAG tag monoclonal mouse IgG2b (LT0420; Lifetein), α–Strep-tag II Mouse/IgG1 (OAAF04751:Aviva Systems Biology), α-cMyc Tag Mouse/IgG2a (JP_A000704-100;GenScript), and goat α-mouse IgG Alexa Fluor® 488 (35502; Thermo).

Protein reagent purification

Protein purification was performed using the Ni-NTA Purification System (Novex/LifeTechnologies). Briefly, *E. coli* BL21 D3 cells carrying either the pET-11b mNeonGreen-SpyCatcher or pET-11b mNeonGreen-SpyTag-Strep-tagII plasmids (Figure 2.2.4A), were inoculated from single colonies into 125-mL baffled flasks filled with 50 mL of LB medium and 1 mM IPTG. These flasks were incubated ~12 hours in a Multitron Pro (Infors) incubator at 32°C with rotary shaking at 150 rpm. The cultures were then collected in 50 mL conical tubes and the cells were pelleted via centrifugation in a swing-bucket centrifuge for 45 min at 3,500×g, while maintaining a temperature of 4°C. The supernatant was removed and the cells were resuspended in 25 mL of chilled PBS by vortexing for >10 min. These cells were then lysed utilizing a One Shot system cell disrupter (Constant Systems Limited) set to a pressure level of 32 kpsi, and passed through the sapphire aperture three times. The cell lysates were then centrifuged once more to pellet cellular debris in an RC 5C Plus ultracentrifuge (Sorvall) using the SS-34 rotor (Sorvall). The lysates

were centrifuged for 1 hour at 16,500 rpm maintained at a temperature of 4°C. After the centrifugation, this lysate was transferred to a pre-chilled 50-mL conical tube

CHAPTER 3: BIOTRANSFORMATION OF 2,4-DINITROTOLUENE IN A PHOTOTROPHIC CO-CULTURE OF ENGINEERED *SYNECHOCOCCUS ELONGATUS* AND *PSEUDOMONAS PUTIDA*

This work has been prepared for submission to Applied and Environmental Microbiology

Authors:

Derek T. Fedeson, Pia Saake, Patricia Calero, Pablo Iván Nikel, & Daniel C. Ducat

Author Contributions:

DTF, PIN, and DCD designed and directed the project and experiments. PC designed and engineered the *P. putida* strains utilized in this work. DTF, PS, and PC performed the experiments and recorded the results. DTF, PS, PIN, and DCD analyzed and interpreted the data. DTF, PIN, and DCD prepared the manuscript and figures. DTF, PS, PC, PIN, and DCD edited the manuscript and figures.

Abstract

In contrast to the current paradigm of using microbial monocultures in most biotechnological applications, increasing efforts are being directed towards engineering mixed-species consortia to perform functions that are difficult to program into individual strains. Additionally, the division of labor between specialist species found in natural consortia can lead to increased catalytic efficiency and stability relative to a monoculture or a community composed of generalists. In this work, we have designed a synthetic co-culture for phototrophic degradation of xenobiotics, composed of a cyanobacterium, (*Synechococcus elongatus* PCC 7942) and a heterotrophic bacterium (*Pseudomonas putida* EM173). Cyanobacteria fix CO_2 through photosynthetic metabolism and secrete sufficient carbohydrates to support the growth and active metabolism of *P. putida*, which has been engineered to consume sucrose as the only carbon source and to degrade the environmental pollutant 2,4-dinitrotoluene (2,4-DNT). The synthetic consortium is able to degrade 2,4-DNT with only light and CO_2 as inputs for the system, and it was stable over time through repeated backdilutions. Furthermore, cycling this consortium through low nitrogen medium promoted the accumulation of polyhydroxyalkanoate (PHA)–an added-value biopolymer–in *P. putida*, thus highlighting the versatility of this production platform. Altogether, the synthetic consortium allows for simultaneous bioproduction of PHA and remediation of the industrial pollutant 2,4-DNT, using light and CO_2 as inputs.

Importance

In this study, we have created an artificial consortium composed of two bacterial species that enables the degradation of the industrially-produced environmental pollutant 2,4-DNT while simultaneously producing PHA bioplastic. In these co-cultures, the photosynthetic cyanobacteria fuel an engineered *P. putida* strain programmed both to use sucrose as a carbon source and to perform the biotransformation of 2,4-DNT. The division of labor in this synthetic co-culture is reminiscent of that commonly observed in microbial communities and represents a proof-of-principle example of how artificial consortia can be employed for bioremediation purposes. Furthermore, this co-culture system enabled the utilization of freshwater sources that could not be utilized in classical agriculture settings, reducing the potential competition of this alternative method of bioproduction with current agricultural practices, as well as remediation of contaminated water streams.

Introduction

In nature, bacteria typically co-exist in communities with hundreds to thousands of other microorganisms, creating a complex web of inter-species metabolic reactions (Little et al. 2008; Saxena 2015; Dolinšek et al. 2016; Goldford et al. 2017). Most consortia exhibit a high degree of "division of labor," where individual species have specialized metabolisms and exchange metabolites and signals with neighbors (Gestel et al. 2015; Tan et al. 2015). Interactions range from the cooperative degradation of toluene (Nikel et al. 2014; Tecon and Or 2017) to the consumption of metabolic waste products (Wilkinson et al. 1974). Compartmentalization of metabolism across distinct species can confer metabolic capabilities on a consortium that may be difficult to engineer within any one individual. Additionally, natural microbial consortia frequently exhibit a high degree of robustness in the face of dynamic environmental conditions and are resilient to invasive microbes (Kumar and Jagadeesh 2016; Blasche et al. 2017). Thus, there has been increasing interest in rationally engineering microbial consortia for desired outputs by dividing metabolic pathways across species (Ortiz-Marquez et al. 2013).

Previous work from our laboratory and others has focused on the utility of strains of cyanobacteria engineered to export photosynthetically-generated sucrose through the heterologous expression of the *cscB* gene from *Escherichia coli*, encoding sucrose permease (Ducat et al. 2012; Du et al. 2013; Song et al. 2016). In one study utilizing this engineered strain of *Synechococcus elongatus* PCC7942 (hereafter, *S. elongatus* CscB), sucrose secretion was such that hypothetical scaled production would significantly exceed current productivities of traditional sugar crops like sugar cane, sugar beet, and corn (Ducat et al.

2012). As such, the strain has been utilized on numerous occasions as a photosynthetic module in synthetic co-cultures as a supplier of fixed carbon for heterotrophic partners (Smith and Francis 2016, 2017; Hays et al. 2017; Li et al. 2017; Löwe et al. 2017a), including a recent report where co-cultures were maintained for longer than 5 months of continuous co-culture (Weiss et al. 2017). Communally, these works have demonstrated that the *S. elongatus* CscB strain can be flexibly paired with a variety of heterotrophic bacteria [*Escherichia coli* W (Hays et al. 2017), *Bacillus subtilis* (Hays et al. 2017), *Azotobacter vinelandii* (Smith and Francis 2016, 2017), *Halomonas boliviensis* (Weiss et al. 2017), and *Pseudomonas putida* (Löwe et al. 2017a)] and yeasts [*Saccharomyces cerevisiae* (Ducat et al. 2012; Hays et al. 2017), *Cryptococcus curvatus* (Li et al. 2017), and *Rhodotorula glutinis* (Li et al. 2017)] and demonstrated that these co-cultures can be used to photosynthetically produce valued biological products, *e.g.,* α-amylase (Hays et al. 2017), fatty acids (Li et al. 2017), and polyhydroxyalkanoates (PHA) [*e.g.,* poly(3-hydroxybutyrate) (PHB) (Smith and Francis 2016, 2017; Löwe et al. 2017a; Weiss et al. 2017)]. In work from Smith and Francis (Smith and Francis 2017) as well as our lab (Weiss et al. 2017) it was shown that *S. elongatus* CscB could be immobilized within hydrogels; this both enhanced carbon flux into sucrose production and allowed the cyanobacteria to exchange diffusible metabolites in medium, while enabling the heterotrophic cells to be readily harvested separately. Taken together, this co-culture approach has potential as a platform to enable the modular photosynthetic production of a flexible array of bioproducts.

A primary concern when considering large-scale aquatic based bioproduction, is that global potable water supplies are coming under increasing strain; scaled applications

of algae or cyanobacteria would be more sustainable if they can utilize marginal waters not suitable for other agricultural purposes (Barry et al. 2016). Industrial wastewater streams are one such example, as they are often contaminated with chemical compounds toxic to both flora and fauna. 2,4-Dinitrotoluene (2,4-DNT) is a nitroaromatic compound and is one of a diverse array of xenobiotics that have been released into the environment due to industrial synthetic chemistry and other manufacturing processes (Ju et al. 2010). While 2,4-DNT is produced as a by-product during polyurethane and pesticide synthesis, one of the most significant sources of these contaminants is explosive manufacturing (Spain 1995). One 2,4,6-trinitrotoluene (TNT)-manufacturing plant can contaminate five hundred thousand gallons of water with TNT and other nitroaromatics in a single day (Yinon 1990), and at some munitions manufacturing and processing sites, soil contamination is as high as 200 g of TNT per kilogram of soil (Hooker and Skeen 1999). These compounds are highly stable within the environment, and remediation costs via incineration are estimated near $400 USD per cubic yard of soil (Griest et al. 1998).

Despite the fact that these nitroaromatic compounds have only recently been introduced into the environment, a number of bacterial strains capable of mineralizing these unusual chemical structures have been isolated (Spain 1995; Symons and Bruce 2006; Ju et al. 2010). The most common mechanism by which 2,4-DNT is processed is through one or two-electron reduction via non-specific nitroreductases (French et al. 2001). Enzymes containing a redox-active flavin or iron center are especially prone to perform these reactions (Bryant and McElroy 1991). Single electron reductions temporarily reduces the nitro group but it is then immediately re-oxidized in the presence of molecular oxygen resulting in the generation of a superoxide, the accumulation of which

can lead to the ROS stress response (Park et al. 2006). Two electron reductions result in the production of a toxic hydroxylamino derivative that can react with DNA and cause subsequent mutations (Bryant and McElroy 1991). The nitroso- and hydroxylamino-derivatives are even more toxic than their parent molecule, able to form DNA and protein adducts that lead to mutagenesis and cellular damage (Spain 1995; Padda et al. 2003). Additionally, the derivatives from reduced nitroaromatics continue to persist in the environment (Achtnich et al. 1999), further emphasizing the need for alternative methods of degradation that allow for the complete biotransformation of these compounds.

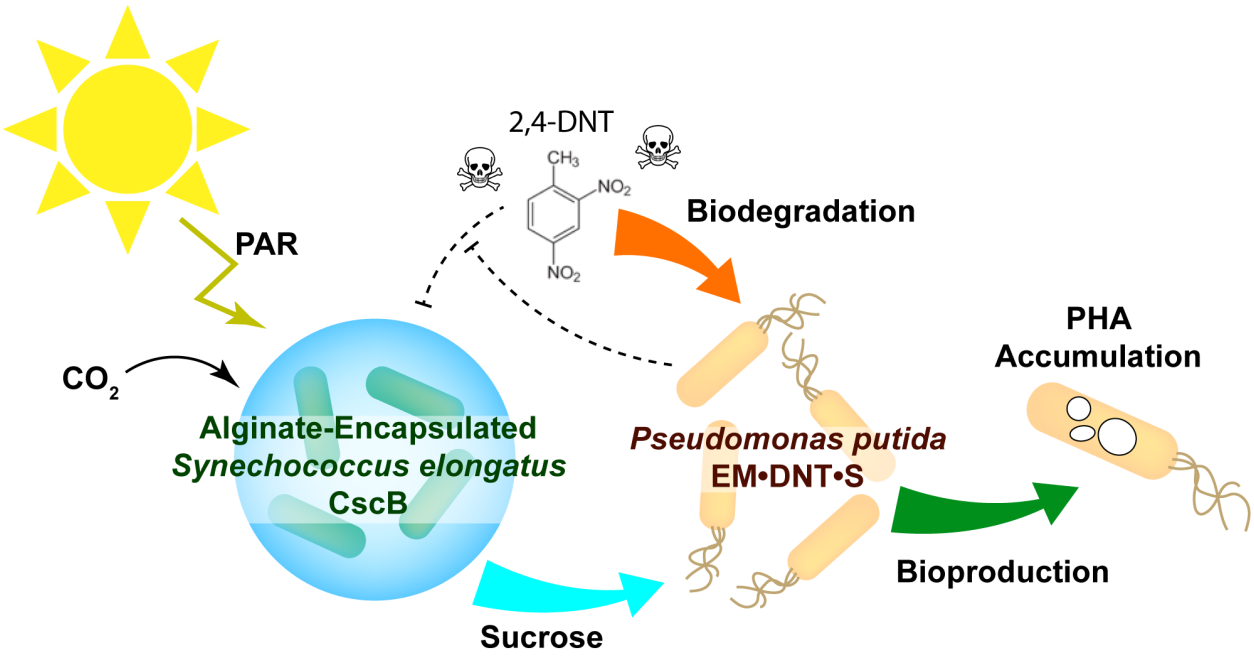

Figure 3.1: Conceptual design of the photosynthetic co-culture designed for simultaneous biodegradation and bioproduction

This co-culture of alginate-encapsulated *S. elongatus* CscB and *P. putida* EM•DNT•S photosynthetically drives the biodegradation of the toxin 2,4-dinitrotoluene (2,4-DNT) and simultaneously produce the bioplastic polyhydroxyalkanoate (PHA). The *S. elongatus* CscB embedded within alginate beads, perform photosynthesis, fixing carbon dioxide from the air using photosynthetically active radiation (PAR). This fixed carbon is converted into sucrose that is then exported from the cells in to the culture. There the sucrose is consumed by the *P. putida* EM•DNT•S which uses this energy to biodegrade the toxin 2,4-DNT. Additionally, the *P. putida* EM•DNT•S can also be directed to accumulate PHA in their biomass, making this system multifunctional.

A separate, oxidative pathway for degrading 2,4-DNT was identified in *Burkholderia* sp. R34, a strain isolated from surface water contaminated by an ammunition waste plant (Spanggord et al. 1991). The gene cluster responsible for processing 2,4-DNT has been identified (Spanggord et al. 1991; Haigler et al. 1994; Nishino and Paoli 2000) and contains 7 genes. Enzymes within the *dnt* degradation pathway are homologs of enzymes that function as part of an existing naphthalene degradation pathway in *Burkholderia sp*. R34 and proceed through oxidative steps that release nitrite. This suite of genes has since been chromosomally integrated into a strain of *Pseudomonas putida* EM173 via a Tn*7* construct to facilitate the analysis of this pathway (Pérez-Pantoja et al. 2013; Akkaya et al. 2018). *P. putida* is generally considered a reliable *chassis* for studying the biodegradation of organic compounds due to its tolerance of organic solvents (Ramos et al. 2002) and versatile central metabolism (Nelson et al. 2002; Nikel et al. 2016).

In this study, we explore whether the aforementioned synthetic consortium method (Weiss et al. 2017) can be engineered to utilize and remediate water streams contaminated with the environmental pollutant 2,4-DNT while also producing the bioplastic polyhydroxyalkanoate (PHA) (Figure 3.1). This was accomplished through the pairing of an engineered strain of *P. putida*, containing the genes needed to both metabolize sucrose and to degrade 2,4-DNT with the sucrose-exporting *S. elongatus* CscB encapsulated in alginate hydrogel beads. Approaching the bioremediation of this compound via the synthetic consortium method allows for the bioprocess to be photosynthetically powered while avoiding the complexities of introducing a new enzymatic pathway into photosynthetic cyanobacteria. We demonstrated that these co-cultures can successfully execute the biotransformation of 2,4-DNT via the engineered pathway and are also able to accumulate

PHA as a secondary function. This work is proof of principle for the use of synthetic cyanobacteria/heterotroph consortia for combined bioremediation and bioproduction applications.

Results

Alginate-encapsulated *S. elongatus* CscB can tolerate 2,4-DNT at higher concentrations than planktonic cultures

As 2,4-DNT is known to be highly toxic to a range of biological organisms (Yoon et al. 2006; Rocheleau et al. 2010), we first characterized the effect of this industrial byproduct on the growth and viability of cultures of *S. elongatus* CscB. We measured culture density and the level of chlorophyll *a* (Chl *a*) in planktonic *S. elongatus* CscB cultures in the presence of increasing concentrations of 2,4-DNT (Figure 3.2AB). Even the lowest concentration of 2,4-DNT examined (8 μM) caused a ~60% growth impairment in planktonic cyanobacterial cultures (Figure 3.2A), and a near cessation of growth in the first 48 h was observed at 2,4-DNT concentrations ≥ 15 μM (Figure 3.2A). The toxicity of this compound at these concentrations is highly relevant as leachates from soil contaminated with TNT and its breakdown products have been recorded as high as 98 μM (Griest et al. 1995). Chl *a* concentration is commonly measured as a proxy for physiological stress in cyanobacteria and is influenced by a variety of conditions (Sauer et al. 2001; Latifi et al. 2009; Korosh et al. 2018). Cultures at concentrations of 2,4-DNT ranging from 31 μM to 125 μM exhibited an overall loss of Chl *a* (Figure 3.2B). This progressive loss of Chl *a* aligned with visual chlorosis and bleaching of these cultures; this observation was consistent at multiple 2,4-DNT concentrations and at higher starting culture densities

(Figure 3.S1 in the Supplemental Materials). These preliminary experiments indicated that planktonic cyanobacteria are highly sensitive to even low concentrations of 2,4-DNT, which would complicate their ability to be engineered to directly degrade this nitroaromatic. Further, the viability loss of planktonic *S. elongatus* CscB would need to be mitigated for any co-culture applications targeting the remediation of these compounds.

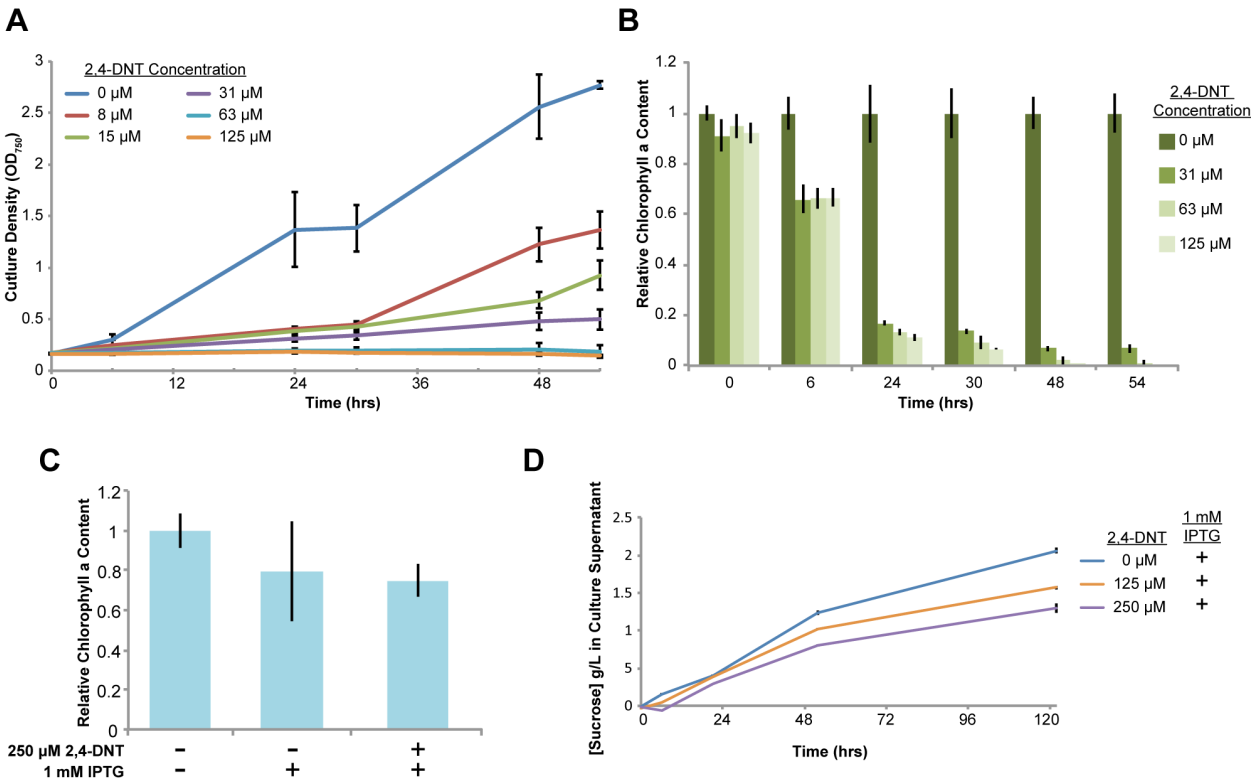

Figure 3.2: Growth and physiological parameters of planktonic and alginate-encapsulated *S. elongatus* CscB

(A) Planktonic cultures of *S. elongatus* CscB inoculated at OD_{750} = 0.2 were added with 2,4-DNT at 0 µM-125 µM and incubated for 54 h. Bacterial growth was estimated from OD_{750} readings. (B) Chlorophyll *a* content of cultures normalized to the values in control cultures with no added 2,4-DNT at each time point. (C) Chlorophyll *a* content of encapsulated *S. elongatus* CscB cells normalized to the values in uninduced (–), control cultures with no added 2,4-DNT. (D) Total sucrose concentration in the culture supernatant of induced (1 mM IPTG) alginate-encapsulated *S. elongatus* CscB while grown with 2,4-DNT at either 0 µm, 125 µM, or 250 µM. For the experiments shown in (A-C), the mean values for n = 3 are indicated, and error bars represent standard deviations; for the experiment indicated in

Figure 3.2 (cont'd)
(D), the mean values for n = 3 with 3 technical replicates per condition are indicated, and error bars represent standard deviations.

In previous work (Weiss et al. 2017), we utilized alginate hydrogel encapsulation of *S. elongatus* CscB to stabilize a co-culture with *Halomonas boliviensis* under prolonged nitrogen stress conditions. Encapsulation has been used for the immobilization of a variety of cell types, and has often led to increased stress tolerance, cell longevity, and metabolic flux toward target end products (Bailliez et al. 1985; Gillet et al. 2000; Srinivasulu et al. 2003; Leino et al. 2012; Therien et al. 2014; Ruiz-güereca and Sánchez-saavedra 2016). Alginate-encapsulated *S. elongatus* CscB cells did not exhibit chlorosis in the presence of 2,4-DNT, even when the concentration was raised to 250 μM, near the solubility limit for this compound (Figure 3.S2 in the Supplemental Materials). We then exposed encapsulated *S. elongatus* CscB cells to 2,4-DNT at 250 μM for 7 days while simultaneously inducing expression of the CscB exporter. Chl *a* was extracted from the beads and measured via spectrophotometry (Figure 3.2C). The data show that while the induction of *cscB* expression leads to a slight decrease in relative Chl *a* levels, the addition of 2,4-DNT to alginate-encapsulated cyanobacteria did not further decrease Chl *a* concentration. Similarly, the Chl *a* concentration per cell was maintained at a level similar to that of planktonic cells grown under our laboratory conditions (Figure 3.S3 in the Supplemental Materials). Finally, we measured sucrose export rates from IPTG-induced, encapsulated *S. elongatus* CscB in the presence of increasing 2,4-DNT concentrations (Figure 3.2D). Sucrose export was maintained for multiple days despite exposure to 125 or 250 μM 2,4-DNT. Altogether, alginate encapsulation appears to stabilize *S. elongatus* when exposed to high levels of 2,4-DNT over long time periods.

Engineering *P. putida* EM173 for sucrose consumption and evaluation of growth parameters in the presence of alginate-encapsulated *S. elongatus* CscB

We next set to construct strains of *P. putida* that can utilize sucrose as the only carbon source and are capable of degrading 2,4-DNT. *P. putida* does not normally utilize sucrose as a carbon substrate. The specific strains we used are derivatives of the genetically-tractable, prophage-less *P. putida* strain EM173 (Martínez-García et al. 2015). To enable sucrose consumption by *P. putida* EM173, we first transformed this strain with plasmid pSEVA221-*cscRABY* (Löwe et al. 2017b, 2018), bearing the sucrose utilization genes from *P. protegens* Pf-5 (Figure 3.3A). Specifically, this plasmid constitutively expresses genes encoding a sucrose hydrolase (CscA, PFL_3237) and a sucrose permease (CscB, PFL_3238), along with a cognate transcriptional regulator (CscR, PFL_3236). The introduction of pSEVA221-*cscRABY* into strain EM173 (giving rise to *P. putida* EM·S) enabled catabolism of sucrose and bacterial growth from the disaccharide. Separately, a synthetic mini-Tn*7* transposon, carrying the functions required for 2,4-DNT degradation in *Burkholderia* sp. R34 (Figure 3.3A) was constructed as described elsewhere (Akkaya et al. 2018). The *dnt* gene cluster in this transposon was delivered into the unique att·Tn*7* site within the chromosome of *P. putida* EM·S, resulting in a stable, engineered strain designed for 2,4-DNT degradation and sucrose consumption (*P. putida* EM·DNT·S). To test for successful catabolism of sucrose by these strains, we performed an initial characterization of sucrose catabolism in an experiment in which M9 minimal medium with 20 g/L sucrose was inoculated with either *P. putida* EM·S or *P. putida* EM·DNT·S at an optical density measured at 600 nm (OD_{600}) = 0.1. These cultures were followed over the course of 24 h, monitoring both culture density (OD_{600}) and soluble sucrose concentrations (Figure 3.3B).

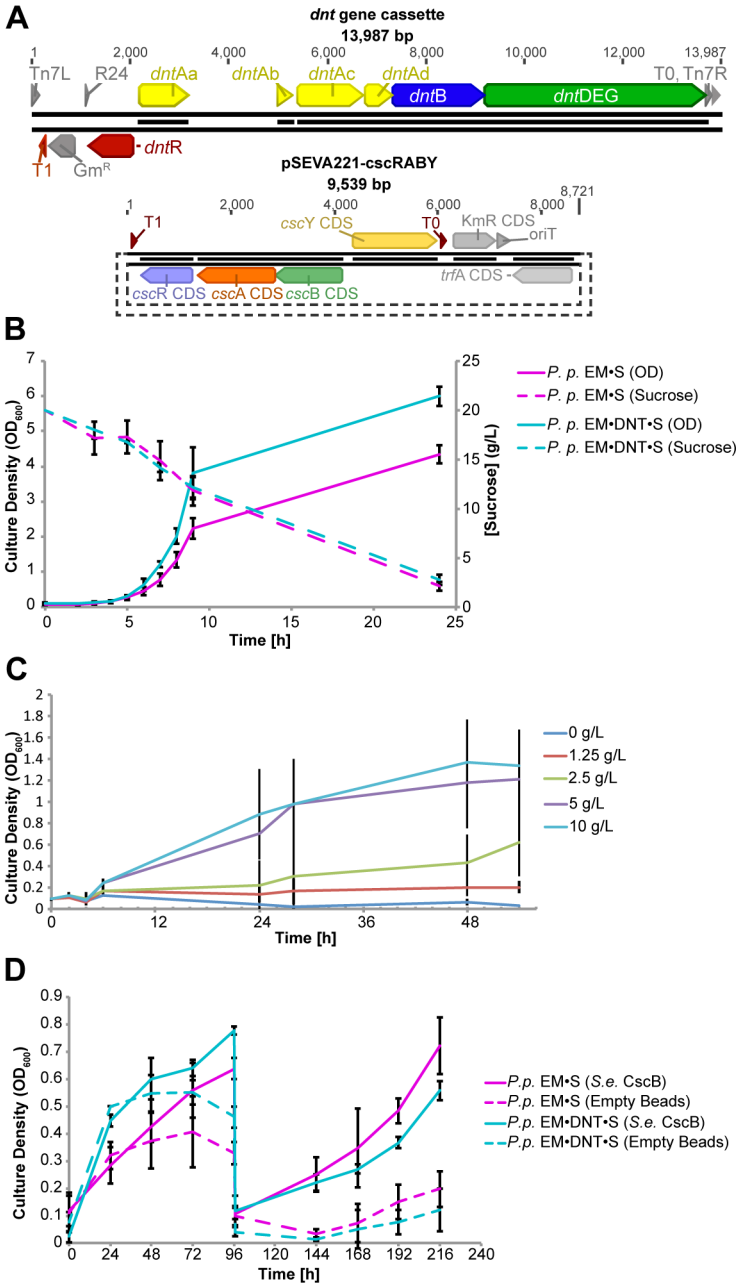

Figure 3.3: Construction of *P. putida* EM·DNT·S and characterization of sucrose-dependent growth alone or in co-cultures

(A) The 2,4-DNT degradation gene cluster from *Burkholderia* sp. R34. (B) Growth of *P. putida* EM·DNT·S at different concentrations of sucrose (0, 1.25, 2.5, 5, and 10 g/L) in M3 medium. (C) *P. putida* strains EM·S and *P. putida* EM·DNT·S were grown in M3 media with 20 g/L sucrose overnight and then inoculated at OD_{600} ~ 0.1 into flasks containing alginate beads with or without encapsulated *S. elongatus* CscB, all cultures contained 1 mM IPTG for induction of sucrose export. OD_{600} measurements were taken over the course of 216 hours, tracking the growth of the *P. putida* strains in the co-culture. At 96 h post-inoculation, all of the M3 media was removed and replaced with fresh medium, allowing the residual *P. putida* cells on the surface of the alginate beads to repopulate the culture. For the

Figure 3.3 (cont'd)
experiments shown in (B) and (C), the mean values for n = 3 are indicated, and error bars represent standard deviations.

Both *P. putida* EM·S or *P. putida* EM·DNT·S grew exponentially over the course of the first 9 h post-inoculation and by 24 h had reached final densities of OD_{600} = 4.3 and 6 respectively. During this time, sucrose concentration had declined in a near linear fashion from 20 g/L to < 3 g/L at 24 h. As sucrose was the only added carbon source and we could clearly observe the consumption of sucrose over time, these data definitively demonstrate that the pSEVA221-*cscRABY* vector enabled sucrose utilization in these two strains.

We cultured our doubly-modified *P. putida* EM·DNT·S in the presence of a range of sucrose concentrations to determine if this strain is capable of growing on a minimal medium designed for cyanobacterial growth with sucrose as a sole carbon source. For this purpose, we generated a phosphate buffered minimal medium derived from BG-11, herein referred to as M3 medium (Table S1 in the Supplemental Material). To gauge the growth capacity of *P. putida* EM·DNT·S under these conditions, we inoculated M3 medium that did not contain a carbon source, and incubated cells overnight. This promoted acclimation to the medium and depletion of internal carbon storage compounds that could confound the accurate determination of growth in the M3 medium. These cells were washed with fresh M3 medium before being inoculated into culture flasks with a range of sucrose concentrations (0 g/L to 10 g/L) and growth was tracked for 54 h (Figure 3.3C). Bacterial growth was evident at sucrose concentrations ranging from 1.25-10 g/L (Figure 3.3C), though carbon may have been growth-limiting at concentrations lower than 2.5 g/L (Figure 3.3C). These results confirm that the heterologous expression of the *cscRABY* genes from *P. protegens* Pf-5 is sufficient to confer sucrose utilization on *P. putida* in our background

strain bearing the 2,4-DNT degradation gene cluster, and indicated that the engineered *P. putida* strain can grow in the cyanobacterial M3 medium— setting the basis for conducting co-cultures.

Growth of engineered *P. putida* strains is supported by sucrose-rich cyanobacterial exudates in a synthetic consortium system

We next explored how the engineered *P. putida* strains (*P. putida* EM·S and *P. putida* EM·DNT·S) behaved in co-culture. The *P. putida* strains, grown overnight in M3 medium with 20 g/L sucrose, were inoculated at $OD_{600} \sim 0.1$ into culture flasks containing either empty alginate beads or alginate beads with encapsulated *S. elongatus* CscB (Figure 3D). In the first 48 h, both *P. putida* strains the OD_{600} continued to increase in all flasks, despite the absence of a carbon source in the flask containing empty alginate beads. Internal stores of carbon likely drove this residual growth in *P. putida*. However, these carbon stores appeared to be depleted after this period of time as the optical density of the cultures containing empty alginate beads declined over the next 24 h (Figure 3.3D). At 96 h, the culture supernatant was removed from all co-cultures, leaving the *S. elongatus* CscB alginate beads in place. Fresh medium was added and the co-culture densities were tracked for another 120 h (Figure 3.3D). Only the *P. putida* strains in flasks with alginate beads containing *S. elongatus* CscB showed signs of regrowth after the medium exchange, with OD_{600} increasing from 0.1 at 96 h to 0.5-0.6 at 216 h. These results demonstrate the *P. putida* strains tolerate and can utilize the exudates from the beaded *S. elongatus* CscBs, and are not significantly utilizing the alginate beads as a carbon source. These results are in agreement with previous work that utilized *P. putida* EM·S and *S. elongatus* CscB (Löwe et

al. 2017a), indicating that these species are compatible under light-driven co-culture conditions.

Biotransformation of 2,4-DNT by engineered *P. putida* EM·DNT·S in both monoculture and co-culture

We next examined the functionality of the 2,4-DNT degrading gene cluster in *P. putida* monocultures in M3 medium supplemented with 2 g/L sucrose as the sole carbon source. The *dnt* cluster is of significant interest to numerous research groups due to the fact that it is an actively evolving pathway (de las Heras et al. 2011; Nikel and Chavarrı 2013) and its unique biological processing of 2,4-DNT (Symons and Bruce 2006). This enzymatic pathway enables the oxidative degradation of 2,4-DNT, relying on two key successive dioxygenations of the 2,4-DNT substrate mediated by DntA and DntB (Figure 3.4A). 2,4-DNT is first dioxygenated by DntA to form 4-methyl-5-nitrocatechol (4M5NC), a compound with a strong absorption peak at 420 nm (de las Heras et al. 2011). 4M5NC is the substrate of DntB, which catalyzes another oxygenation reaction, transforming 4M5NC into 2-hydroxy-5-methylquinone (2H5MQ), an intermediate with an absorption peak at 485 nm (de las Heras et al. 2011). 2H5MQ is then processed by a number of additional enzymes encoded by genes in the pathway allowing for the complete mineralization of 2,4-DNT (Figure 3.4A) (Spanggord et al. 1991; Nishino and Paoli 2000).

We examined the transformation of 2,4-DNT by either *P. putida* EM·S or *P. putida* EM·DNT·S strains over time (Figure 3.4B-E). Flasks containing *P. putida* EM·S or *P. putida* EM·DNT·S were inoculated at OD_{600} ~ 0.1 and 2,4-DNT was added at 250 μM to the cultures. The supernatant of the *P. putida* EM·DNT·S cultures was visibly changed during

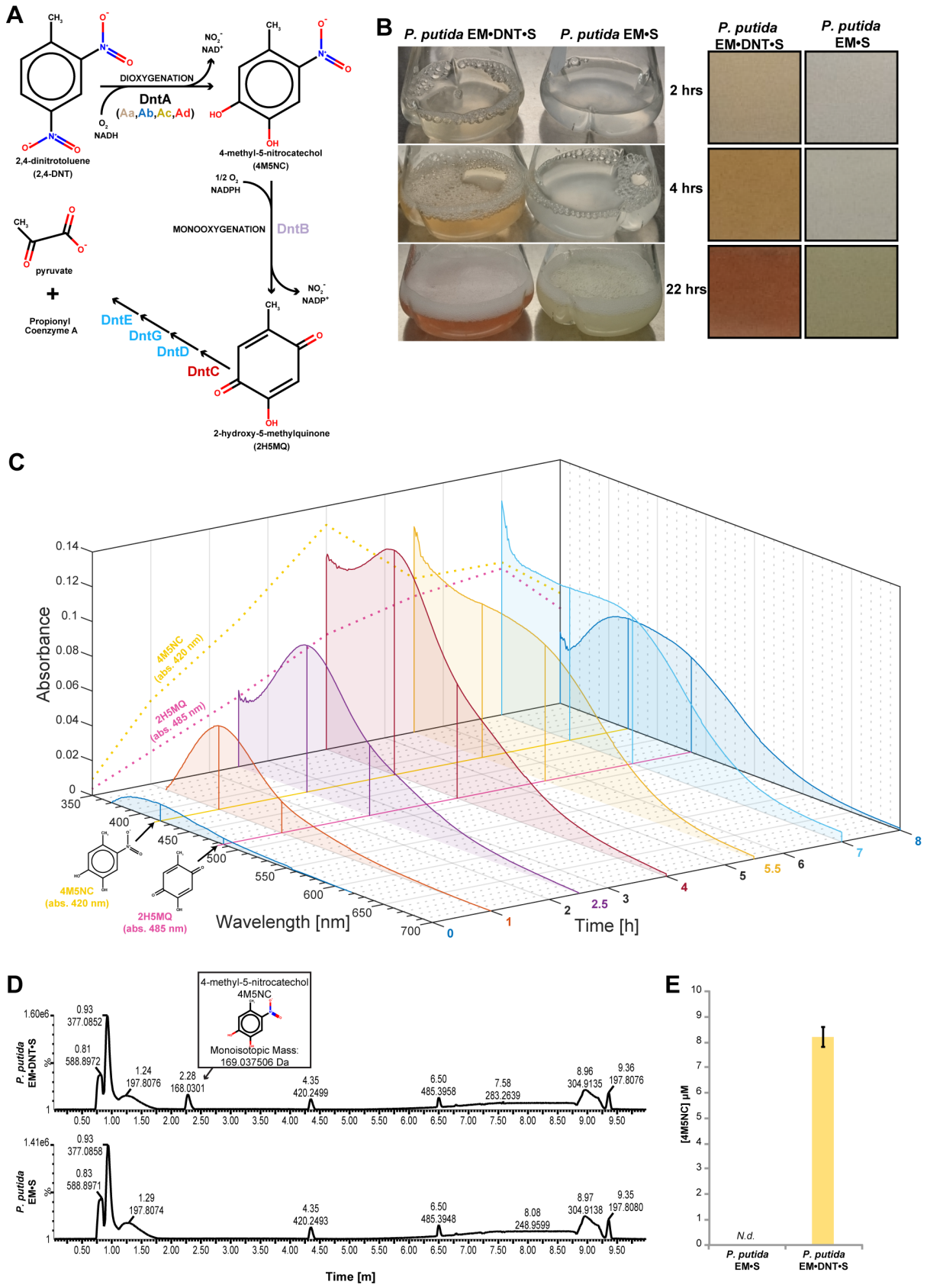

Figure 3.4: 2,4-DNT biotransformation in monocultures of engineered *P. putida*

Figure 3.4 (cont'd)

Figure 3.4: 2,4-DNT biotransformation in monocultures of engineered *P. putida*

(A) Exogenous pathway for the oxidative degradation of 2,4-DNT. (B) (Left) Representative flask cultures of monocultures of *P. putida* EM•DNT•S and *P. putida* EM•S over 22 h in M3 medium with 20 g/L sucrose with the addition of 250 μM 2,4-DNT. (Right) Enhanced side-by-side comparison of the cultures. (E) The select time points displayed of average culture supernatant spectrum (n = 3) of *P. putida* EM•DNT•S measured via scanning spectrophotometry. (D) Representative LC/MS elution profile of *P. putida* EM•DNT•S and *P. putida* EM•S supernatant after 4 hours of incubation M3 medium with 2 g/L sucrose and 250 μM 2,4-DNT. 4M5NC elutes from the column after 2.3 min negative ion mode. (E) Quantification of 4M5NC in supernatants of both *P. putida* EM•S and *P. putida* EM•DNT•S monocultures at the 4 h via LC/MS. *P. putida* EM•S strain did not generate any detectable amount of 4M5NC, while the *P. putida* EM•DNT•S strain accumulated 4M5NC. (F) Disappearance of 2,4-DNT in *P. putida* monocultures grown in M3 medium with 20 g/L sucrose and 250 μM 2,4-DNT measured by GC/MS (n = 3, reps error bars represent standard deviations).

the experiment (Figure 3.4B), and these spectroscopic shifts were consistent with the accumulation of intermediates of 2,4-DNT breakdown through the exogenous oxidative pathway (Figure 3.4A). As soon as 2 h after addition of 2,4-DNT to the culture medium at 250 μM, the supernatant turned yellow (Figure 3.4B), which is consistent with the accumulation of the first pathway intermediate, 4M5NC (de las Heras et al. 2011). Four hours later, the supernatant became visibly orange (Figure 3.4B), suggestive of accumulation of the second intermediate, 2H5MQ (de las Heras et al. 2011). These changes in supernatant coloration were not observed in the control reactions with the non-degrading *P. putida* EM·S strain (Figure 3.4B).

We further verified that the colorimetric changes in the supernatant of *P. putida* EM·DNT·S exposed to 2,4-DNT could be attributed to breakdown of the compound through the heterologous *dnt* pathway. An 8h time-course experiment was performed with additional time points in which both strains of *P. putida* were grown in M3 medium with 2 g/L sucrose during which the cultures were sampled and the supernatant extracted. The

absorbance spectra of *P. putida* EM·DNT·S supernatants exhibited a characteristic rise in an absorption peak at 420 nm over time until 4 h, at which time a second absorption peak at 485 nm became evident (Figure 3.4C). No defined peaks were evident in the visible wavelength absorption spectra of the non-degrading control strain (*P. putida* EM·S) (Figure 3.S4 in the Supplemental Materials). Although spectroscopic analysis is well-supported in the literature as a metric for measuring activity of this oxidative pathway (de las Heras et al. 2011), a more direct method of quantification was desirable to confirm the appearance of the pathway intermediates. Hence, supernatant samples from both *P. putida* EM·S and EM·DNT·S cultures at the 4h time point were evaluated for the presence of 4M5NC by liquid chromatography coupled to mass spectrometry (LC/MS). Figure 3D shows a representative LC/MS profile from one of the *P. putida* EM·DNT·S cultures, the peak representing 4M5NC is indicated. This peak matches that of the 4M5NC standard included for quantification (Figure 3.S5 in the Supplemental materials), and comparison to cultures of the non-degrading strain indicate that there was no 4M5NC generated by the control strain (Figure 3.4D-E).

To confirm specific degradation of the 2,4-DNT, culture supernatants were periodically sampled over two days. 2,4-DNT was observed to be rapidly lost from *P. putida* EM·DNT·S cultures over the course of the first 4 h, as measured by tandem gas chromatography coupled to mass spectrometry (GC-MS), and had dropped to undetectable levels by 22 h, a kinetic pattern of 2,4-DNT transformation similar to what has been reported for *Burkholderia* sp. R34 (Pérez-Pantoja et al. 2013) and other engineered *P. putida* strains (Akkaya et al. 2018) (Figure 3.S6A in the Supplemental Materials). 2,4-DNT concentrations in cultures containing the *P. putida* EM·S strain appeared to decrease at a

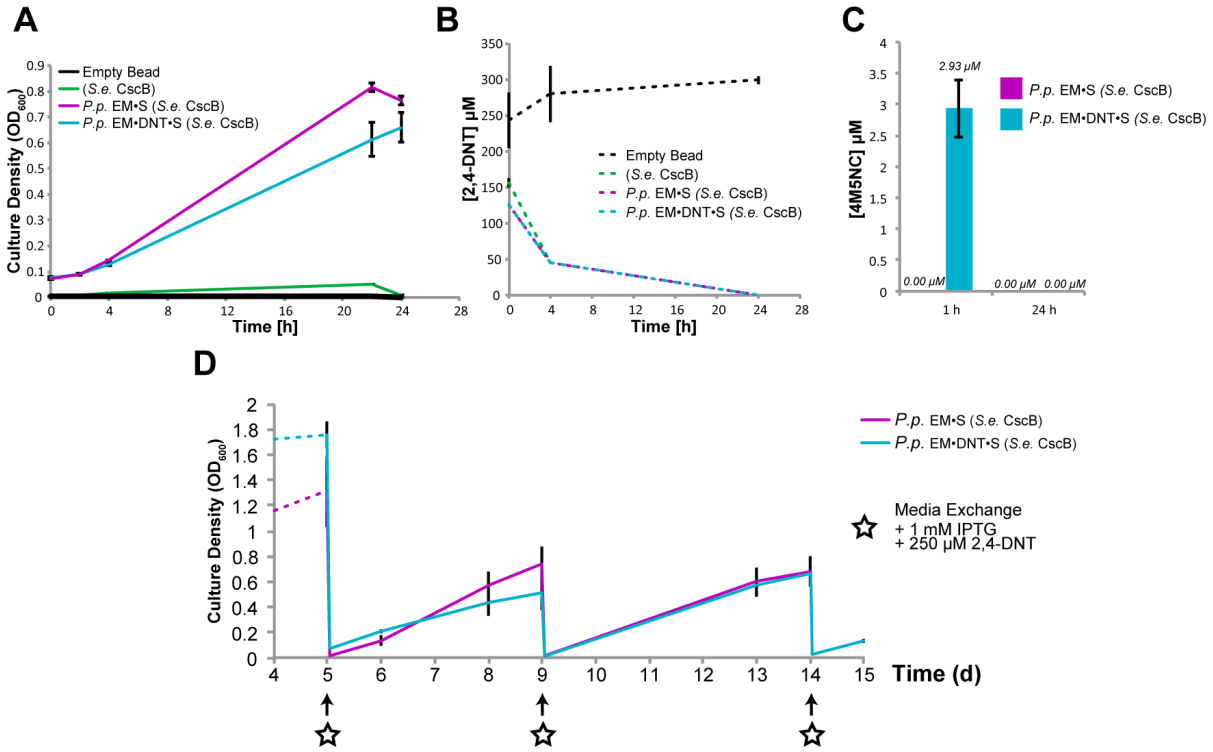

Figure 3.5: Degradation of 2,4-DNT in co-culture and long-term co-culture cycling
(A) Growth of *P. putida* strains in co-culture with alginate bead encapsulated *S. elongatus* CscB with 250 µM 2,4-DNT present in the media. (B) GC/MS analysis of the supernatants from the 24 hr co-culture demonstrates that presence of living cells triggers the transformation of 2,4-DNT via either the non-specific reductive pathway or exogenous oxidative pathway such that the concentration of 2,4-DNT has dropped to undetectable levels by 24 hours post inoculation. (C) In a separate experiment, we performed LC/MS quantification of 4M5NC in beaded co-cultures. Within 1 h of adding 2,4-DNT into beaded co-cultures, *P. putida* EM•DNT•S cultures accumulated 4M5NC that is been fully degraded by 24 h. (D) Optical density of a long-term co-culture of *P. putida* strains with encapsulated *S. elongatus* CscB with 250 µM 2,4-DNT. This displayed segment of this two week long co-culture shows stable cycling of the *P. putida* every 4-5 days. At each cycling, the culture supernatant containing the *P. putida* is removed and fresh media is added back to the culture along with 1 mM of IPTG, to maintain induction of cyanobacteria sucrose export, and 250 µM 2,4-DNT. For (A-C), $n = 3$, error bars represent standard deviations.

similar rate (Figure 3.S6A in the Supplemental Materials). This loss of 2,4-DNT may be attributed to the adsorption of the 2,4-DNT to cell surfaces, a known property of nitroaromatic compounds that makes them difficult to extract from biological substrate

(Achtnich et al. 1999), and/or the reduction of the compound by non-specific nitroreductases. Previous work by Akkaya et al. (Akkaya et al. 2018) with the *P. putida* EM strain indicated that the reductive pathway (Figure 3.S6C in the Supplemental Materials) is not likely a major contributor to 2,4-DNT transformation. We assessed our supernatant samples for the presence of 2-amino-4-nitrotoluene/4-amino-2-nitrotoluene (2A4NT/4A2NT), intermediates in the non-specific reductive pathway (Figure 3.S6D in the Supplemental Materials). These compounds were detected in minor amounts (< 3 μM) in both the *P. putida* EM·DNT·S and *P. putida* EM·S cultures (Figure 3.S6D in the Supplemental Materials). While it is difficult to quantify the flux attributable to the reductive pathway, the accumulation of 2A4NT/4A2NT compounds was reduced by 22% in *P. putida* EM·DNT·S cultures compared to the *P. putida* EM·S (Figure 3.S6D in the Supplemental Materials).

Degradation of 2,4-DNT by a synthetic consortium of *P. putida* EM·DNT·S and alginate-encapsulated *S. elongatus* CscB and long-term culture potential

We introduced 2,4-DNT into co-cultures of *P. putida* and encapsulated *S. elongatus* CscB. Both the *P. putida* EM·S and *P. putida* EM·DNT·S strains were able to grow with the beaded *S. elongatus* CscB in the presence of 250 μM 2,4-DNT (Figure 3.5A). Cultures containing only encapsulated *S. elongatus* CscB or empty alginate beads served as controls for both optical density measurements as well as any potential 2,4-DNT adsorption. GC-MS analysis for 2,4-DNT content of these cultures demonstrated that cultures containing *P. putida* or *S. elongatus* cells removed 2,4-DNT from the culture (Figure 5B), in line with previous results. In contrast, 2,4-DNT concentrations did not decrease in the flasks containing only empty beads (Figure 3.5B). Co-cultures containing *P. putida* EM·DNT·S

demonstrated a similar color change in the culture supernatant to that of *P. putida* EM·DNT·S monocultures, indicating that the exogenous pathway retained its function in the consortium system. These results demonstrate that this system can provide a directed method for the photosynthetically-driven degradation of 2,4-DNT. Subsequent LC-MS testing of co-culture supernatants shortly (1 h) and 24 h after inoculation of the co-culture with 2,4-DNT revealed that, as in previous monoculture experiments, the *P. putida* EM·DNT·S co-cultures accumulated 4M5NC (Figure 3.5C). This observation, again, indicates that 2,4-DNT is being degraded via the oxidative pathways in these co-cultures.

We initiated a longer duration co-culture in which we inoculated both strains of *P. putida* into culture flasks with encapsulated *S. elongatus* CscB cells and followed the cultures for 15 days, exchanging the culture supernatant every 4-5 days with fresh medium containing 250 μM 2,4-DNT (Figure 3.5D). Regrowth of *P. putida* strains following backdilution indicate stable repopulation, allowing for continual degradation of the 2,4-DNT (Figure 3.5D). The total mass of 2,4-DNT cleared by the *P. putida* EM·DNT·S strain over this period amounts to ca. 4 mg.

Simultaneous 2,4-DNT biodegradation and PHA bioproduction by engineered strains in a synthetic consortium.

P. putida accumulates PHA as a carbon storage, particularly under nitrogen-depleted conditions (Löwe et al. 2017a), providing the opportunity to both bioremediate 2,4-DNT and simultaneously produce a valuable byproduct. *P. putida* cells were inoculated into the encapsulated and induced *S. elongatus* CscB culture flasks at $OD_{600} \sim 0.5$ with 250 μM 2,4-DNT (Figure 3.6A). These flasks contained either M3 or M3-N medium, the latter of which

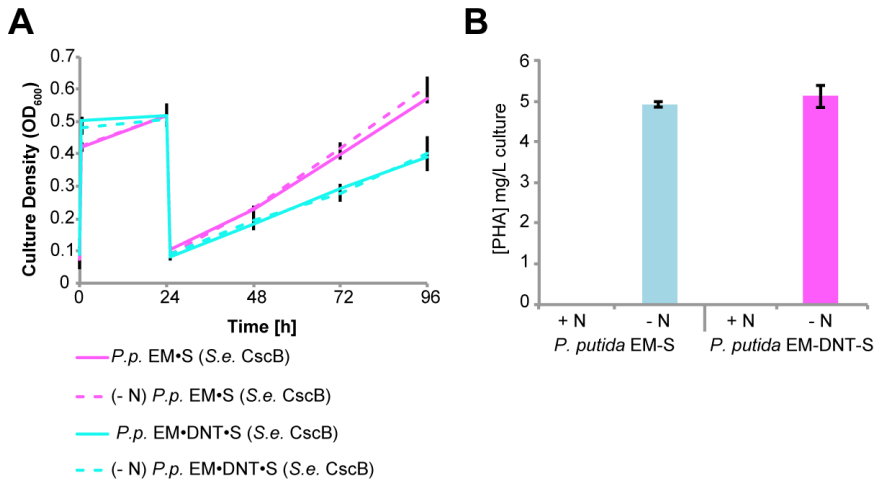

Figure 3.6: PHA accumulation in *P. putida* bioremediating co-cultures
(A) Co-cultures of beaded *S. elongatus* CscB and *P. putida* strains in the presence of 2,4-DNT with the standard or reduced concentration (2 mM) of nitrogen. Nitrogen scarcity triggers *P. putida* to allocate excess carbon into polyhydroxyalkanoate (PHA). (B) Quantification of PHA extracted from the *P. putida* biomass of co-cultures 24 h after inoculation into nitrogen replete (+ N) or nitrogen deplete (- N) medium.

has a reduced nitrogen content (2mM NH_4Cl) (Table 3.S1). Twenty four hours after cycling into the nitrogen deplete medium, cell culture was harvested, dried, and processed for quantification of methyl esters of alkanoic acids by high-pressure liquid chromatography (HPLC; see Methods). Processing of these samples showed that both *P. putida* EM·S and *P. putida* EM·DNT·S co-cultures in nitrogen deplete medium accumulated 4.9 and 5.1 mg PHA/L of culture, resulting in polymer contents of 22 and 23.4 mg of PHA/g cell dry weight, respectively.

Discussion

In this work, we demonstrate metabolic division of labor within an artificial microbial co-culture consisting of engineered strains of *S. elongatus* PCC 7942 and *P. putida* EM173. In this consortium, *S. elongatus* CscB produces soluble sugars using light and CO_2 as

inputs, providing sufficient organic compounds to promote the growth of co-cultivated strains of *P. putida.* In turn, we demonstrate that *P. putida* simultaneously degrades the environmental pollutant 2,4-DNT while producing the bioplastic precursor, PHA.

We have shown that encapsulation of *S. elongatus* CscB cells in alginate hydrogel beads allowed the cyanobacteria to persist in the presence of 2,4-DNT (Figs. 3.S1-S2 in the Supplemental Materials) and maintain consistent production of sucrose after culture back dilution. Encapsulated cyanobacteria tolerated concentrations of 2,4-DNT 5 times higher than could be tolerated by planktonic cyanobacterial cultures and did so without significantly changing chlorophyll *a* content (Figure 3.2BC). While there is precedence for the improved resilience of cells that are encapsulated within hydrogels (Bozeman et al. 1989; Romo and Perez-Martinez 1997; Weiss et al. 2017), it is evident in the literature that even species that share similar phototrophic lifestyles react to hydrogel encapsulation very differently, altering cell division rates, cell morphology, and key metabolic pathways (Moreno-Garrido 2008). Increased resistance to environmental toxins has been attributed to the physical properties of the encapsulating gel matrices (e.g. decreased diffusion of the toxin (Chen et al. 1993)), as well as to physiological changes within encapsulated cells (Bozeman et al. 1989). The mechanism by which the encapsulated cyanobacteria resist the effects of 2,4-DNT under these conditions has yet to be elucidated. Future work investigating how this encapsulation modulates cyanobacterium stress response to nitroaromatic compounds could yield genetic targets for modification to bolster the resilience of the cyanobacteria without the need for mechanical encapsulation.

P. putida is a gram-negative soil bacterium that has recently gained significant attention as a *chassis* for industrially-relevant synthetic biology. This is in part thanks to the

full sequencing (Nelson et al. 2002) and subsequent generation of *P. putida* strains (*e.g., P. putida* EM173 used in this work) with reduced genomes that demonstrate enhanced expression of heterologous proteins (Martínez-García et al. 2015). *P. putida*'s metabolic diversity and high tolerance of oxidative stress make it an ideal model organism for studying toxin remediation as well as bioproduction of added-value compounds (Nikel et al. 2016). The introduced oxidative 2,4-DNT degradation pathway (Figure 3.4A) is chromosomally integrated in this strain. While this pathway avoids generating highly reactive intermediates with hydroxylamino groups, the proteins in this pathway are not yet fully optimized for this new substrate (de las Heras et al. 2011; Pérez-Pantoja et al. 2013), leading to the production of oxidative stress in the *Burkholderia sp.* R34 from which the pathway originates (Pérez-Pantoja et al. 2013). This oxidative damage is thought to contribute to an increased rate of mutation and fosters a more rapid evolution of this strain to combat oxidative stress (Pérez-Pantoja et al. 2013). While *P. putida* has also been shown to experience increased oxidative stress when actively utilizing this pathway, this species does not exhibit the same rate of DNA damage and mutation (Akkaya et al. 2018). Thus, the physiological properties of *P. putida* allow for more efficient use of an imperfect 2,4-DNT degradation pathway. Evolving or engineering this pathway toward increased specificity for 2,4-DNT could allow for improved kinetics and reduced ROS generation. Conversely, the lower substrate specificity might allow this pathway to be redirected toward the degradation of other types of nitroaromatic pollutants from other industrial processes (Ju et al. 2010).

2,4-DNT as a compound represents a significant contaminant that poses a bioremediation challenge. 2,4-DNT in its solid state is very stable in the environment as it is

not bioavailable, where it often remains due to its low solubility. Once solubilized, 2,4-DNT can then be reduced to highly reactive hydroxylamino intermediates that damage cellular machinery and DNA as chemical adducts. Solid state 2,4-DNT has a high stability and low solubility, allowing this compound to persist in the environment and slowly disperse into surface and ground water. Furthermore, reduced derivatives of this compound do not readily mineralize in the environment and persist for extended periods of time in the soil (Achtnich et al. 1999). The longevity of this compound and its derivatives requires a long-term sustainable solution to remediate previous areas of contamination, as well as reduce contamination from industrial practices that are actively producing 2,4-DNT as a by-product. Previous works that propose alternative biologically based methods of degrading 2,4-DNT are limited either by the necessity to supply bioavailable carbon (Wang et al. 2011) or produce new biological substrate to perform the degradation (Oh et al. 2016).

Co-cultures of the 2,4-DNT degrading *P. putida* strain (*P. putida* EM·DNT·S) were successfully grown while solely supported by the fixed carbon provided by the encapsulated *S. elongatus* CscB. Furthermore, these cultures were able to successfully cycle over the two weeks as a demonstration of this system's stability and potential for long-term sustainable degradation of 2,4-DNT. While we demonstrate intermittent cycling of media in flask-based cultures here (Figure 3.5D), it is possible to conceive of a photobioreactor that would allow for continual introduction of 2,4-DNT-contaminated wastewater. Here, the full media exchanges associated with long-term flask-based co-cultures allowed us to demonstrate the ability of these co-cultures not only to remediate this compound but also produce the bioplastic precursor polyhydroxyalkanoate (PHA).

While sustainable production of PHA has been pursued in other contexts, this is, to our knowledge, the first report in which PHA formation has been concurrent with the degradation of a xenobiotic compound. In comparison to an independent report that aimed to optimize PHA production from batch cultures of *S. elongatus-P. putida* (Löwe et al. 2017a), we achieved a lower specific productivity in cultures simultaneously degrading 2,4-DNT. While this current system did not achieve the 90% PHA of Cell Dry Weight (CDW) value that is commonly regarded as a benchmark for viable industrial production strains, production of PHA in this system is secondary in importance relative to the bioremediation of 2,4-DNT. This production of PHA served to demonstrate the potential diversity of function inherent in this co-culture system. Furthermore, the conditions of this system could be further optimized for PHA production by modifying total nitrogen supplied, duration of nitrogen starvation, or concentration of 2,4-DNT.s Of note, we observed no appreciable difference in *P. putida* growth rates between co-cultures in nitrogen replete or in low nitrogen (2mM nitrate). This raises the possibility that *P. putida* may be able to utilize an unknown cyanobacterial by-product as a nitrogen source, and additional optimization may be required to fully activate PHA production pathways.

One question that arose as part of this work was whether the presence of *P. putida* EM·DNT·S provides a protective effect to *S. elongatus* CscB in co-cultures fed with 2,4-DNT contaminated medium. If this were the case, it would shift this relationship from a commensal to a more mutualistic relationship where each species benefits from the presence of the other. Pursuing longer-term cultures with even more rigorous exposure to 2,4-DNT could reveal whether *P. putida* EM·DNT·S might provide such a protective effect.

We show that these artificial co-cultures are not only capable of utilizing media contaminated with a toxic xenobiotic, but also of producing the bioplastic PHA. A scaled version of this system could hypothetically take wastewater effluent from industrial sources contaminated with 2,4-DNT, remediate the water allowing it to be utilized for other functions, and provide a mechanism by which PHA could be produced. The more immediately relevant take-away from this work is that photosynthetic co-cultures utilizing *S. elongatus* CscB are flexible both in its partnerships with other microbes as well as the intended functionality of the system. This creates opportunities for more advanced and complex co-cultures with new functions and constituents that we hope will not only provide solutions to modern conflicts, but also inform us on how nature of symbiotic relationships develop in the natural world.

Methods

Bacterial strains and culture conditions

Planktonic *S. elongatus* strains were grown as previously described (Weiss et al. 2017). Selection for the genomically-integrated *cscB* cassette was maintained during monoculturing with the addition of 12.5 ug/mL chloramphenicol to the medium. *P. putida* strains were streaked from frozen stocks onto selective LB plates and incubated at 32°C overnight. The following day, individual colonies were picked into LB media with appropriate antibiotics. Plasmid pSEVA221-cscRABY in both the *P. putida* EM·S and *P. putida* EM·DNT·S was maintained by addition of 50 ug/mL kanamycin, while *P. putida* EM·DNT·S, carrying a genomic integration of the *dnt* degradation gene cluster, was maintained with 25 µg/mL gentamicin. LB cultures were grown up overnight at 32°C in a

Multitron (Infors) incubatory with rotary agitation at 150 rpm. The next day, these were utilized to inoculate new overnight cultures in M3 defined medium (see Table S1 in the Supplemental Material) with either 20 g/L or 2 g/L sucrose, as indicated. These cultures were then used as inoculum for subsequent experiments.

Encapsulation of *S. elongatus* CscB in alginate beads

Alginate encapsulation was performed as previously described (Weiss et al. 2017) with minor adjustments. Briefly, planktonic *S. elongatus* CscB cells grown in BG-11 medium + 1g/L HEPES (pH 8.3; Sigma) were harvested at an optical density measured at 750 nm (OD_{750}) = 2 via centrifugation at 3,500×g for 30 min and concentrated in 3 mL of sulfur-free BG-11. These cells were then added to a sterile and degassed volume of 3% (wt/vol) sodium alginate and then gently mixed to a final OD_{750} = 5.0, making a roughly 2.75% (wt/vol) sodium alginate-*S. elongatus* CscB suspension. In a sterile hood, this solution was added dropwise to a ≥20-fold larger volume of 20 mM $BaCl_2$ using a vertically-oriented syringe pump (KD Scientific, Holliston, MA), 5 mL syringes (BD Biosciences), and 30 G needles. The drops traveled ~35 cm from needle to the slowly stirred $BaCl_2$ solution and were allowed to cure in the solution for at least 20 min before being rinsed once with BG-11 medium and then allowed to incubate overnight in M3 medium without the additional 100 mM NaCl. This medium was then exchanged the following day and refreshed again with M3 medium without added NaCl and transferred to 250-mL baffled Erlenmeyer flasks and placed into a Multitron Pro (Infors) Incubator with constant illumination (15W Grow-Lux; Sylvania; ~70 μmol m^{-2} s^{-1}), 2% CO_2 supplementation, and shaking (125 rpm) at 32°C overnight. The third day post encapsulation, the M3 medium was exchanged, and the

alginate beads were apportioned in ~10-mL aliquots into 125-mL baffled Erlenmeyer flasks. The medium was then replaced with M3 + 25 mM NaCl. The concentration of salt was then increased over the next two daily medium exchanges to 50 mM NaCl, and then to 100 mM NaCl. The medium was subsequently refreshed daily for 3-5 days prior to experiments, allowing the cells and alginate beads to fully stabilize. In the cases where the beads would be utilized in co-culture, CscB expression would be induced the day prior to inoculation of the *P. putida* cells, to prevent a lag in protein expression from influencing heterotrophic growth, and the media exchanged immediately prior to inoculation.

Analytical methods

Culture optical densities were measured with a Genesys 20 (Thermo Fisher Scientific, Waltham, MA) spectrophotometer. Planktonic *S. elongatus* CscB was measured at OD_{750}, and both co-culture experiments and *P. putida* monocultures were measured at OD_{600}. This spectrophotometer was also used to measure chlorophyll *a* concentrations of planktonic *S. elongatus* cultures as in (Zavřel et al. 2015). For chlorophyll *a* measurements in alginate-encapsulated *S. elongatus,* three technical replicates of four alginate beads were placed in 1.7 mL eppendorf tubes. Then, 1 mL of pre-chilled methanol was added to the beads which were then gently vortexed. These were then incubated at 4°C for 30 min in the dark. After briefly vortexing the tubes, the solution containing the chlorophyll *a* was removed, leaving the intact cell containing beads behind. Absorbance of the extracted chlorophyll *a* was measured in cuvettes at 720 nm and 665 nm to calculate the final chlorophyll *a* concentration as indicated elsewhere (Zavřel et al. 2015).

Sucrose concentration of beaded cultures was measured as indicated previously (Weiss et al. 2017) with a slight modification. At select timepoints, 1 mL of culture supernatant was withdrawn and pelleted at 17,000×g for 10 min. The supernatant was then transferred into a fresh tube for storage, 3 technical replicates of 100 µL were quantified via sucrose/D-glucose assay kit (Megazyme, Bray, Ireland) for each sample (Weiss et al. 2017).

Culture supernatant spectra were measured using a DU800 Spectrophotometer, (Beckman Coulter, CA, USA). Cell-free culture supernatant was obtained by centrifugation for 10 min at 17,000×g. The supernatant was then transferred to a cuvette for spectral analysis.

GC/MS and LC/MS detection and quantitation were performed with machinery housed in the Michigan State University Mass Spectrometry and Metabolomics Core. 2,4-DNT measurements were made using a Agilent 5975 GC/single quadrupole MS (Agilent). Culture samples were centrifuged at 17,000×g for 10 min and 10 µL of cell free supernatant were removed to a new tube. 50 µL of ethyl acetate was added to the supernatant and allowed to incubate at room temperature for 30 min. The 50 µL of ethyl acetate was then transferred to a GC vial and injected into the GC machine (injection volume 1 µL). Samples were separated with a 5% phenyl-methyl capillary column (Agilent) and measured by Mass Selective Detector (MSD). A temperature of 275°C was set for the split/splitless injector (ratio of 10:1). Helium gas was used as the carrier gas at a flow rate of 1 mL/min.

LC/MS measurements were made using a Waters Xevo G2-XS UPLC/MS/MS (Waters). Culture samples were harvested and pelleted via centrifugation (17,000×g for 10 min). A 100-µL aliquot of the supernatant was then transferred to a clean tube and

lyophilized. This was then resuspended in 1 mL deionized water. Supernatant samples were harvested from culture and HPLC Measurements of PHA accumulation were made with a Waters 2695 HPLC in Dr. Cheryl Kerfeld's lab at Michigan State University. Samples were process and analyzed as previously described (Weiss et al. 2017). Briefly, cells were centrifuged at 17,000×g for 10 min, the supernatant decanted, and the pellet was lyophilized. The cell biomass was dissolved in 1 mL of concentrated sulfuric acid, heated to 90 °C for 1 h, cooled to room temperature, and then diluted 100-fold with deionized water. A 20-µL aliquot was injected onto an Aminex 300-mm HPX-87H (Bio-Rad Laboratories, Hercules, CA) column, and 0.028 N H2SO4 was used as the mobile phase at a flow of 1 mL/min. The column temperature was maintained at 60 °C and UV- absorption was monitored at 210 nm. Two standards of commercial PHB (Sigma-Aldrich) were similarly treated and used for quantification purposes.

APPENDIX

Appendix: Chapter 3 Supplemental Materials

		BG-11	M3
Chemical Name	**Chemical Formula**	**Molarity**	**Molarity**
Ammonium iron(III) citrate	C6H8FeNO7	2.29E-05	2.29E-05
Calcium chloride dihydrate	CaCl2 x 2H2O	2.45E-04	2.45E-04
Citric acid	C6H8O7	3.12E-05	3.12E-05
Cobalt(II) nitrate hexahydrate	$Co(NO3)_2$ x 6H2O	1.70E-07	1.70E-07
Copper(II) sulfate pentahydrate	CuSO4 x 5H2O	3.16E-07	3.16E-07
Dibasic potassium phosphate	K2HPO4	2.30E-04	4.73E-03
Dihydrogen borate	H2BO3	4.70E-05	4.70E-05
Ethylenediaminetetraacetic acid (EDTA)	C10H16N2O8	3.42E-06	3.42E-06
Magnesium sulfate septahydrate	MgSO4 x 7H2O	3.04E-04	3.04E-04
Manganese (II) Chloride Hydrate	MnCl2 x 4H2O	9.15E-06	9.15E-06
Sodium Carbonate	Na2CO3	1.89E-04	1.89E-04
Sodium molybdate dihydrate	Na2MoO4 x 2H2O	1.61E-06	1.61E-06
Sodium nitrate	NaNO3	1.76E-02	1.76E-02
Zinc sulfate heptahydrate	ZnSO4 x 7H2O	7.72E-07	7.72E-07
Ammonium chloride	NH4Cl	-	4.00E-03
Sodium chloride	NaCl	-	0.1

Table 3.S1: Media composition

Chemical composition of BG-11, M3, and M3 -N media used in this study. Between standard BG-11 medium and M3 medium the only significant additions to this media are: a ~2 fold increase in dibasic potassium phosphate, for buffering the pH; 0.1 M sodium chloride to stimulate sucrose production in the *S. elongatus* CscB; and additional nitrogen in the form of ammonium chloride, which we have found stimulates the growth of some heterotrophs in co-culture. This additional nitrogen is not added in the M3 –N condition in which the sodium nitrate concentration is also reduced to $2x10^{-3}$ M or 2 mM to trigger the accumulation of polyhydroxyalkanoate (PHA) in the *P. putida* strains.

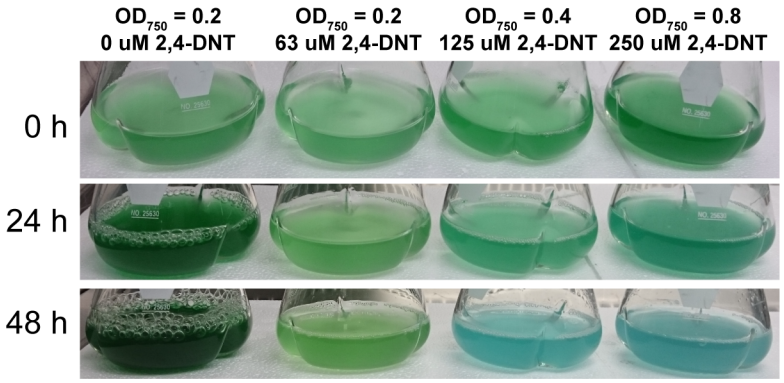

Figure 3.S1: Influence of 2,4-DNT on the growth of *S. elongatus* PCC 7942

(A) Following the growth, or lack thereof, in wild type cultures of *S. elongatus* PCC 7942 grown in BG-11 with varying concentrations of 2,4-DNT and inoculated at varying initial densities over the course of 48 hours (hrs). The concentration of 2,4-DNT added to these cultures corresponds with the estimated cell density as extrapolated from optical density (OD750). *E.g.,* OD_{750}(0.2) + 62.5uM 2,4-DNT compared to OD_{750}(0.4) + 120 µM 2,4-DNT.

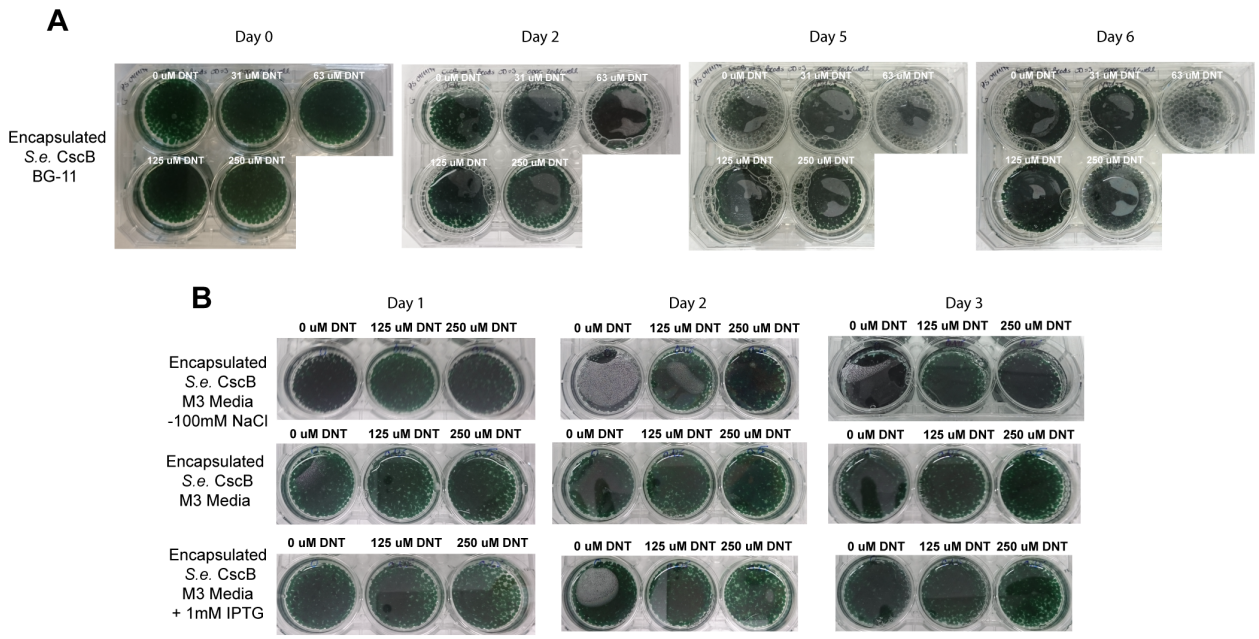

Figure 3.S2: Encapsulated *S. elongatus* CscB in different media with 2,4-DNT

(A) Encapsulated *S. elongatus* CscB cells in BG-11 with different added concentrations of 2,4-DNT [0 μM - 250 μM] were followed over the course of 6 days. In contrast to the planktonic cultures of *S. elongatus* PCC 7942, these cultures did not demonstrate the same bluing and bleaching transition associated with the toxic effects of the 2,4-DNT. (B) Encapsulated *S. elongatus* CscB cells were tested with this same range of 2,4-DNT concentrations [0 μM - 250 μM] in the modified co-culture media (M3) - 100 mM NaCl, in M3 media triggering the accumulation of sucrose with the *S. elongatus* CscB cells, and in M3 Media + 1 mM IPTG, the fully induced condition that allows for the accumulation and export of sucrose into the culture supernatant. This last condition is the one utilized for all co-cultures unless otherwise stated. Again no bleaching of the cells was observed.

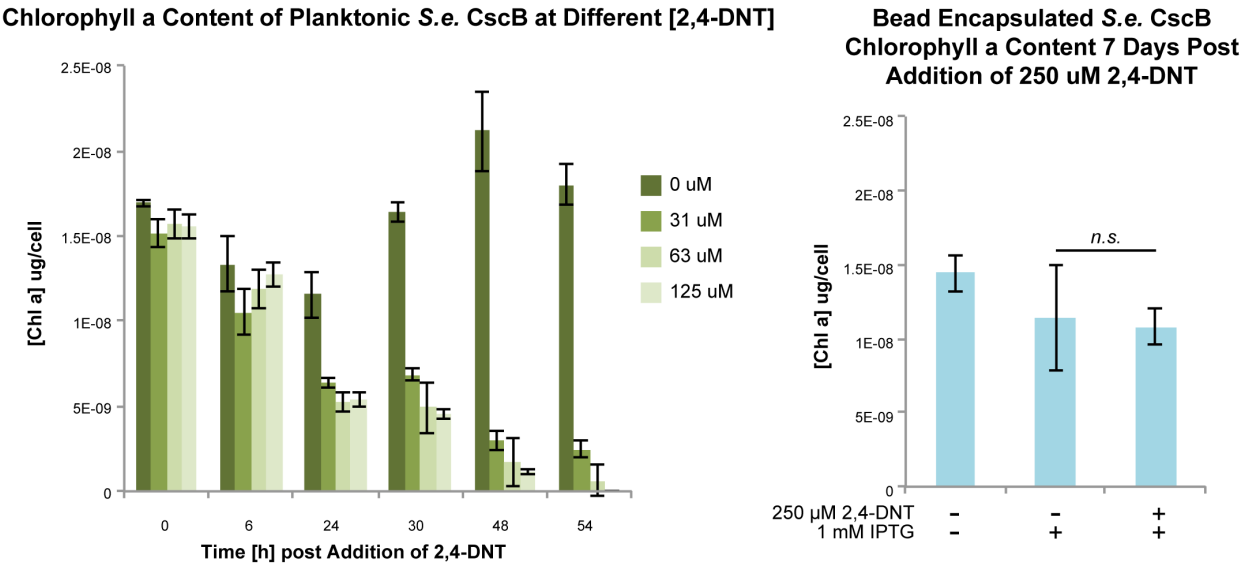

Figure 3.S3: Calculated chlorophyll *a* per cell comparison between planktonic and encapsulated *S. elongatus* CscB

(A) The calculated Chl *a* content of planktonic cells while exposed to a range of concentrations of 2,4-DNT. The 0 uM control cultures exhibit a slight decrease of Chl *a* per cell as they are actively dividing over the first 24 hours, diluting the existing Chl *a* between daughter cells. After 30 hours, however, these cells begin to increase the concentration of Chl *a* as self-shading of the culture increases the demand for light absorption. All of the cultures that have any concentration of 2,4-DNT exhibit a steady decline in Chl *a* per cell as the cells react to the 2,4-DNT. (B) In order to calculate the chlorophyll A concentration per cell for the alginate encapsulated cyanobacteria, it was necessary to make some estimations as to the number of beads in a given flask as well as the distribution of cells within those beads. The number of beads was calculated based on the apparent diameter of the alginate beads (~2.6 mm) as well as the total volume of alginate beads in each flask which was established as 10 mL of beads suspended in 20 mL of medium. These numbers brought us to the estimate of ~1086 beads per flask. In making the alginate beads, the final OD_{750} of the cells resuspended in the alginate is ~5.0 OD_{750}. With an estimated $3.3x10^8$ *S. elongatus* PCC 7942 cells per OD_{750} per 1 mL, we were then able to calculate that each bead upon formation should have approximately $1.52x10^7$ cyanobacteria cells. As previous work has shown that almost no divisions occur within these hydrogels over an extended period of time (Weiss et al. 2017), we assumed this initial cell count remained unchanged for the purposes of these estimates. From these calculations we were then able to give a final estimate on the Chl *a* content per cell. Interestingly, the per cell concentration of the beaded cyanobacteria is very much aligned with the initial Chl *a* content of the cells in the planktonic cultures. We believe this indicates these estimates are within a reasonable range of the actual per cell Chl *a* content.

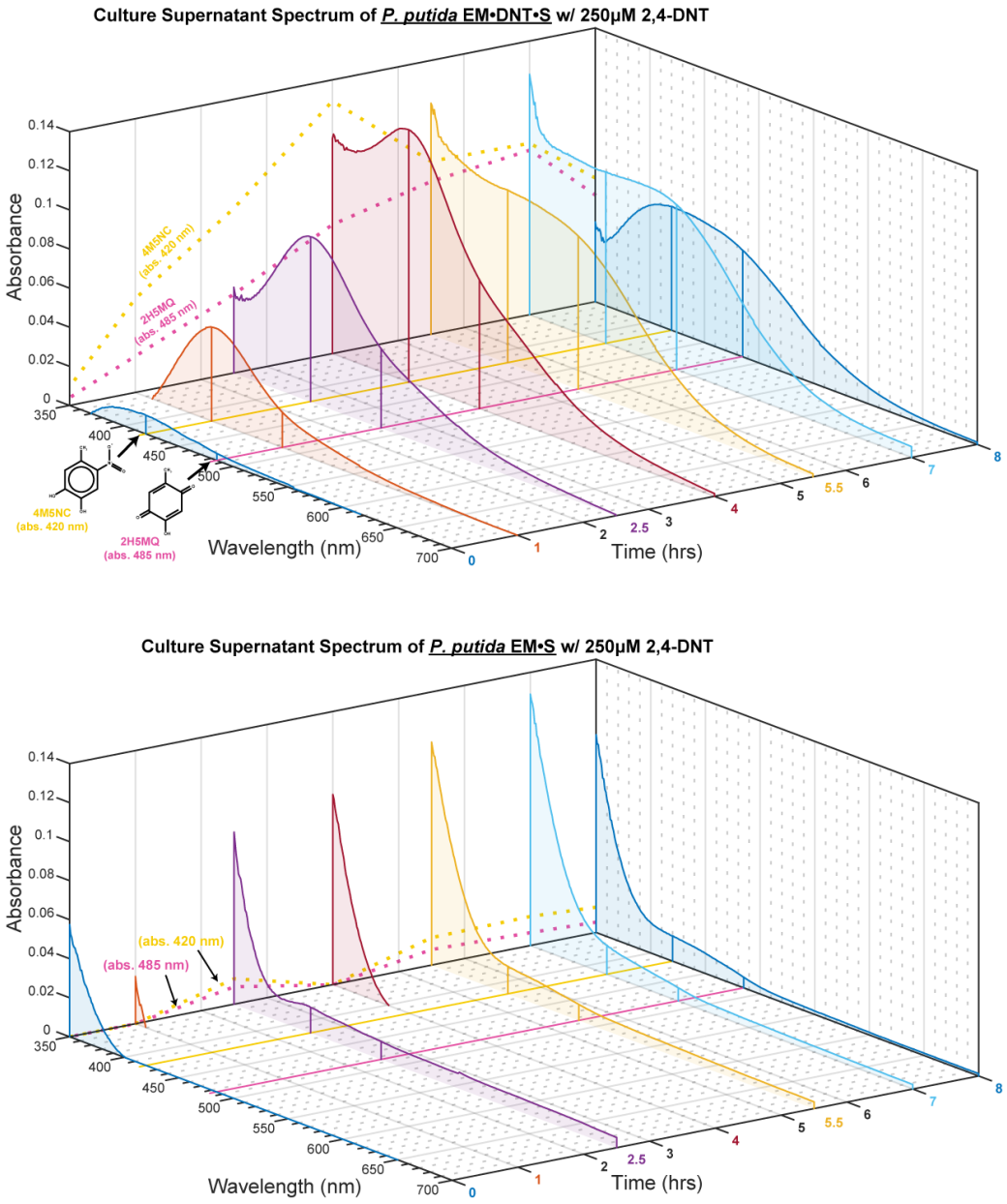

Figure 3.S4: Comparing *P. putida* supernatant spectra over time

(Top) The *P. putida* EM•DNT•S spectrum from Figure 3 included for comparison. (Bottom) The *P. putida* EM•S spectrum from the same experiment shows no significant accumulation of any colored products. This further illustrates that the observed color change is specific to the oxidative pathway degradation products. The selected spectra are an average of n = 3.

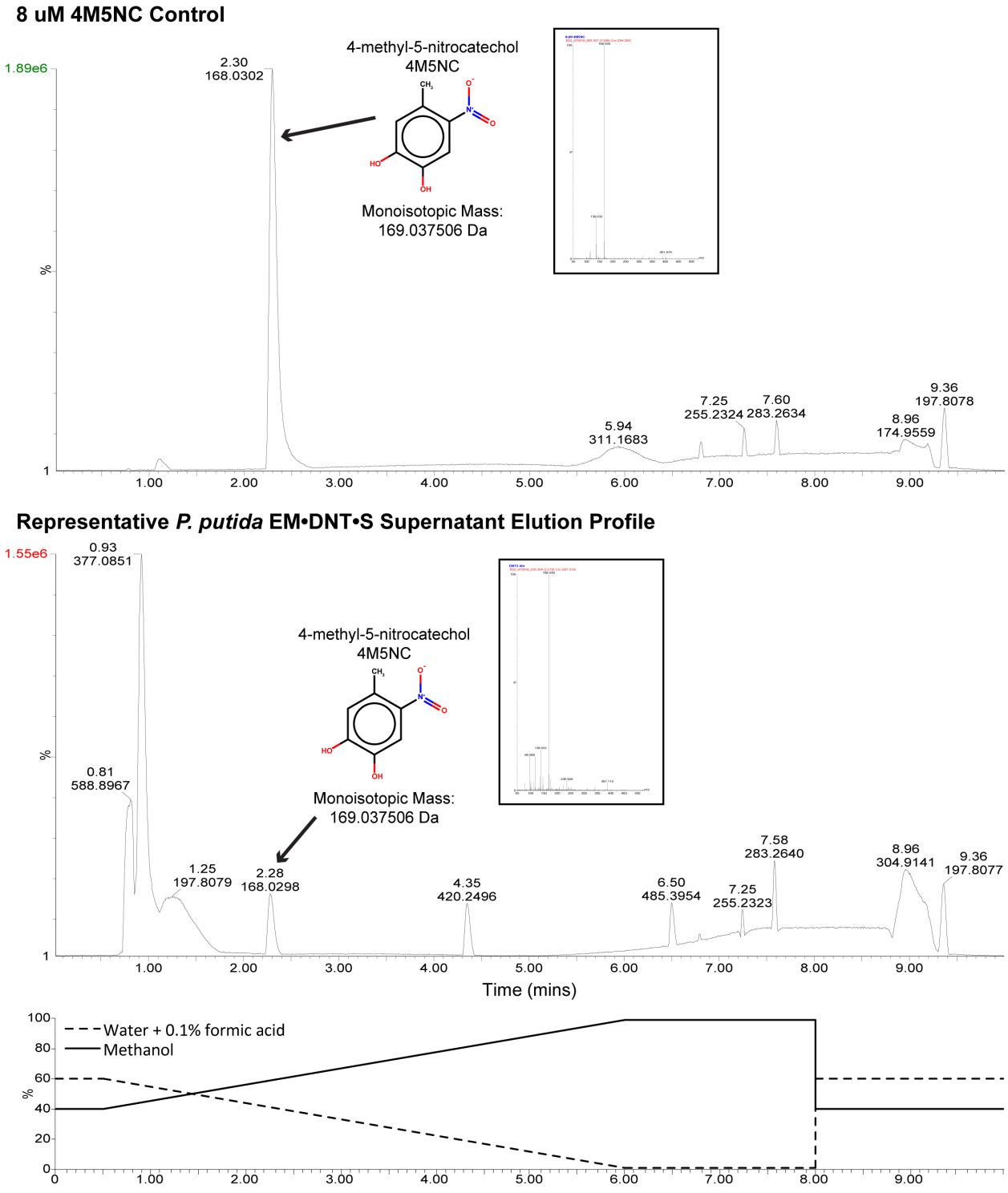

Figure 3.S5: 4M5NC control elution profile and m/z

(Top) Elution profile of 8 uM 4M5NC standard with inset m/z chromatograph of 4M5NC peak. (Middle) Elution profile of *P. putida* EM□DNT□S supernatant elution profile with inset m/z chromatograph of 4M5NC peak. (Bottom) Solvent split for LC/MS methods.

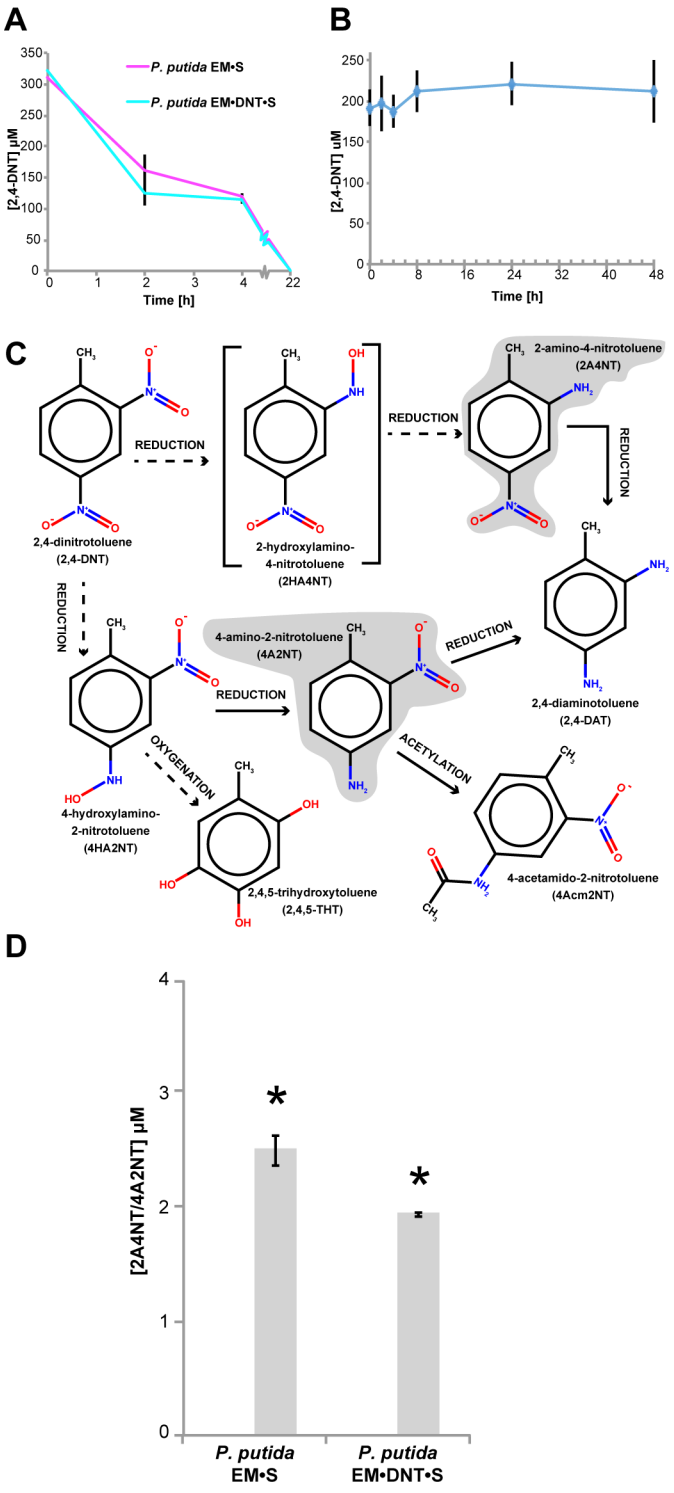

Figure 3.S6: Loss of 2,4-DNT from *P. putida* monocultures and reductive pathway analysis

(A) Disappearance of 2,4-DNT in *P. putida* monocultures grown in M3 medium with 20 g/L sucrose and 250 µM 2,4-DNT measured by GC/MS (n = 3, error bars represent standard deviations). (B) 2,4-DNT media controls were run under both the *P. putida* growth

Figure 3.S6 (cont'd)

conditions as well as under the *S. elongatus*/co-culture conditions. In all cases there was no apparent loss of 2,4-DNT by GCMS over the course of 48 hrs. (C) Reductive degradation of 2,4-DNT [adapted from (Shemer et al. 2018)]. Molecules in brackets are hypothetical. (D) LC/MS measurements of 2-amino-4-nitrotoluene/4-amino-2-nitrotoluene [2A4NT/4A2NT] from the supernatants of monocultures at the 4 h timepoint. Statistical analysis showed that this decrease was statistically significant (p-value = 0.02568) from *P. putida* EM•S to the *P. putida* EM•DNT•S indicating that there is decreased accumulation of this first measurable intermediate of the reductive pathway.

CHAPTER 4: DIRECTED EVOLUTION OF *ESCHERICHIA COLI* W CSCR WITH ALGINATE ENCAPSULATED *SYNECHOCOCCUS ELONGATUS* CSCB

The work presented in this chapter is unpublished.

Introduction

How interspecies microbial interactions arise and become fixed into stable symbiotic interactions in nature is a fundamental ecological question. Cyanobacteria are particularly prolific in their establishment of mutualistic interactions with a wide array of different organisms, including archaea, other prokaryotes, fungi, plants, and animals. These interactions are often shaped by millions, or even billions (*e.g.,* chloroplast endosymbiosis) of years of co-evolution of the partner species. It is challenging to deduce the origins of symbioses relying only on observations of existing natural systems because such symbioses are the legacies of a history of interactions between their ancestral populations. A pivotal question about the evolution of interacting microorganisms is to what extent their metabolic exchange networks emerge early as a result of fortuitous encounters between biochemically-compatible species, versus a product of long-term stable associations that increasingly drive a tighter integration of the communities' "interactome." In Chapter 1, we discussed the natural interactions that have evolved between the cyanobacterium *Prochlorococcus* and α-proteobacterium SAR11 as an example of a cyanobacterium/heterotroph relationship. *Prochlorococcus* has lost the ability to mitigate ROS and due to the high light intensity, excretes fixed carbon as a mechanism of balancing the cells redox state (Morris et al. 2011; Braakman et al. 2017). SAR11 has evolved the capacity to utilize that excreted carbon and improved its ROS mitigation capacity (Giovannoni 2005; Morris et al. 2011; Zinser 2018). While we can observe these current interactions and determine which factors are important to maintaining this relationship, it is very difficult to ascertain the evolutionary path that eventually led to this result due to

the dynamic genetic landscape in both of these organisms and the extended period of time over which they have co-evolved.

One of the primary advantages of utilizing synthetic microbial consortia, as discussed in Chapter 1, is that the interacting species in these systems do not need to have a prior evolutionary history with one another, permitting an opportunity to study the early stages of evolution between symbiotic partners from the "bottom up." This is a burgeoning field of research that is still in its infancy, but has already shown that synthetic consortia are potentially reflective of natural consortia. For example in (Hays et al. 2017), *S. cerevisiae* W303 and *B. subtilis* 3610 experienced significant growth impairment at high cyanobacterial cell concentrations while the *E. coli* W cscR thrived under the same conditions. It was also discovered that the *E. coli* W cscR strain could subsist in this environment off of unknown component(s) in the cyanobacterial exudates. The differences in performance under identical environmental conditions and with the same phototrophic partner by these organisms, suggests that underlying metabolic differences makes each species more or less compatible in a consortium. Elucidating these interactions found within these synthetic consortia may provide insight into important metabolisms that exist in natural consortia. Furthermore, these interactions are also significant to the development of productive synthetic consortia and may provide mechanisms by which bioproduction from these consortia could be enhanced. However, disentangling the various consortium-relevant metabolic differences between the three species presented in this example presents a significant challenge.

One method by which we may obtain both insight into metabolic pathways relevant to phototrophic co-culture as well as potentially improved heterotrophic bioproduciton

chassis is through directed evolution of heterotrophic strains under co-culture conditions. Numerous laboratory evolution studies have been conducted upon isolated model microbial species (Lenski et al. 1991; Boder et al. 2000; Gore et al. 2009; Kawecki et al. 2012; Ratcliff et al. 2012; Johnson et al. 2016; Pandey et al. 2016; Lenski 2017). Some of these experiments have been particularly impactful for theory development, as they allow real-time observation of the molecular mechanisms that propel an organism across an evolutionary landscape towards higher fitness under a given selective pressure. One of the conditions required in directed experimental evolution is that the selective pressure on the organisms remains consistent. To minimize environmental variation, most instances of experimental evolution focus on a single organism and apply consistent abiotic stressors or other artificial methods of selection on that species (Lenski et al. 1991; Boder et al. 2000; Maharjan et al. 2006; Johnson et al. 2016; Tizei et al. 2016). There are relatively few examples of laboratory co-evolution where selective pressures are applied to mixtures of two or more species and adaptation of both species is looked at simultaneously (Brockhurst and Koskella 2013; Koskella and Brockhurst 2014). A common quandary of analyzing co-evolved species is that each species has independent influence on the environment, thereby shaping the selective pressure. This can give rise to increased variability between separate populations that are evolved under identical experimental protocols, and raises "chicken or egg" style questions about observed adaptations. That is, did a mutation in species A arise as result of a change in species B or did it trigger the change in species B? Given that it is difficult to verify causative adaptive mutations even in well-studied model organisms such as *E. coli* (Lenski et al. 1998), determination of the selective forces shaping co-evolved species can be quite challenging.

In this chapter, I initiated experiments designed to gain insight into the dominant selective pressures facing the heterotrophic species partnered with *S. elongatus* CscB in the engineered co-cultures discussed previously (see Chapter 3). It is preferable to avoid the complications of co-evolution of both species mentioned above and it would also be possible that negative selection on the sucrose-production cassette in *S. elongatus* CscB would decrease the stability of the co-culture in the long term. The work of Weiss et al. (2017) demonstrated that *S. elongatus* CscB can be encapsulated in alginate hydrogels, remaining viable and capable of sucrose export for long time periods (>5 months). Cell division of the encapsulated cyanobacteria is dramatically slowed (Weiss et al. 2017), decreasing the likelihood of genetic changes that would alter culture conditions experienced by the partnered heterotroph. I therefore decided to utilize alginate encapsulated *S. elongatus* CscB as a platform with which I could expose a heterotrophic strain to the selective pressures of co-cultivation with a naïve cyanobacterial strain for a sufficient number of generations to permit adaptation of enhanced fitness traits.

Results

Selection and engineering of the ancestral strain

It has been previously shown that *E. coli* W can metabolize sucrose (Archer et al. 2011; Sabri et al. 2013a) and that it can be stably co-cultivated over long time periods with *S. elongatus* CscB, subsisting on cyanobacterial exudates as the sole source of organic carbon (Hays et al. 2017). Furthermore, *E. coli* has a well-developed molecular toolkit and has been routinely used for laboratory evolution studies (Lenski et al. 1998; Yang et al. 2013). The *E. coli* W cscR strain has had the sucrose catabolism repressor gene deleted

from its genome, which further enhances its utilization of sucrose (Arifin et al. 2011). This strain has been previously co-cultivated with *S. elongatus* CscB for weeks in planktonic co-culture (Hays et al. 2017), therefore it was an appropriate background to begin directed evolution studies.

I next incorporated differential fluorescent reporter tags into the ancestral strain that could be later used to facilitate the differentiation of the evolved and ancestral strains of *E. coli* W. I believed that use of fluorescence would provide the most utility, allowing for easy identification of the strains by fluorescent microscopy as well as flow cytometry for quantitative measurements. Many examples of this strategy can be found in the co-culture oriented literature (Kerner et al. 2012; Tecon and Or 2017). Because of the extra metabolic burden to retain plasmids, we opted to incorporate the fluorescent protein expression cassettes into the genome of our strain via the method developed in (Sabri et al. 2013b). This was to increase genetic stability of expression, eliminating the possibility of plasmid loss during the experimental evolution. We generated two variants of the pKIKOlacZCm plasmid, pKIKOlacZCm-mKOK and pKIKOlacZCm-mNG, encoding the orange mKOK (Tsutsui et al. 2008) and mNeonGreen (Shaner et al. 2013) proteins, respectively (Figure 4.1A). Expression of these proteins is driven by the constitutive J23100 promoter, which was selected as the strongest driver of expression from the Registry of Biological Parts: Anderson Promoter Collection (Figure 4.1A). These constructs were then transformed and integrated into the *E. coli* W cscR strains to generate the base strains of *E. coli* W cscR ΔlacZ::mKOK (*E. coli* W cscR mKOK) and *E. coli* W cscR ΔlacZ::mNeonGreen (*E. coli* W cscR mNG) (see methods). Fluorescent microscopy of these strains shows uniform expression of both proteins (Figure 4.1B) though the relative intensity of the mKOK appears lower than

that of mNeonGreen which may be due to the difference in absorbance spectra (515nm vs 505nm) and quantum yield (0.61 vs 0.80) (Tsutsui et al. 2008; Shaner et al. 2013). Multiple clonal stocks of these strains were made such that either could be used as the ancestral strain.

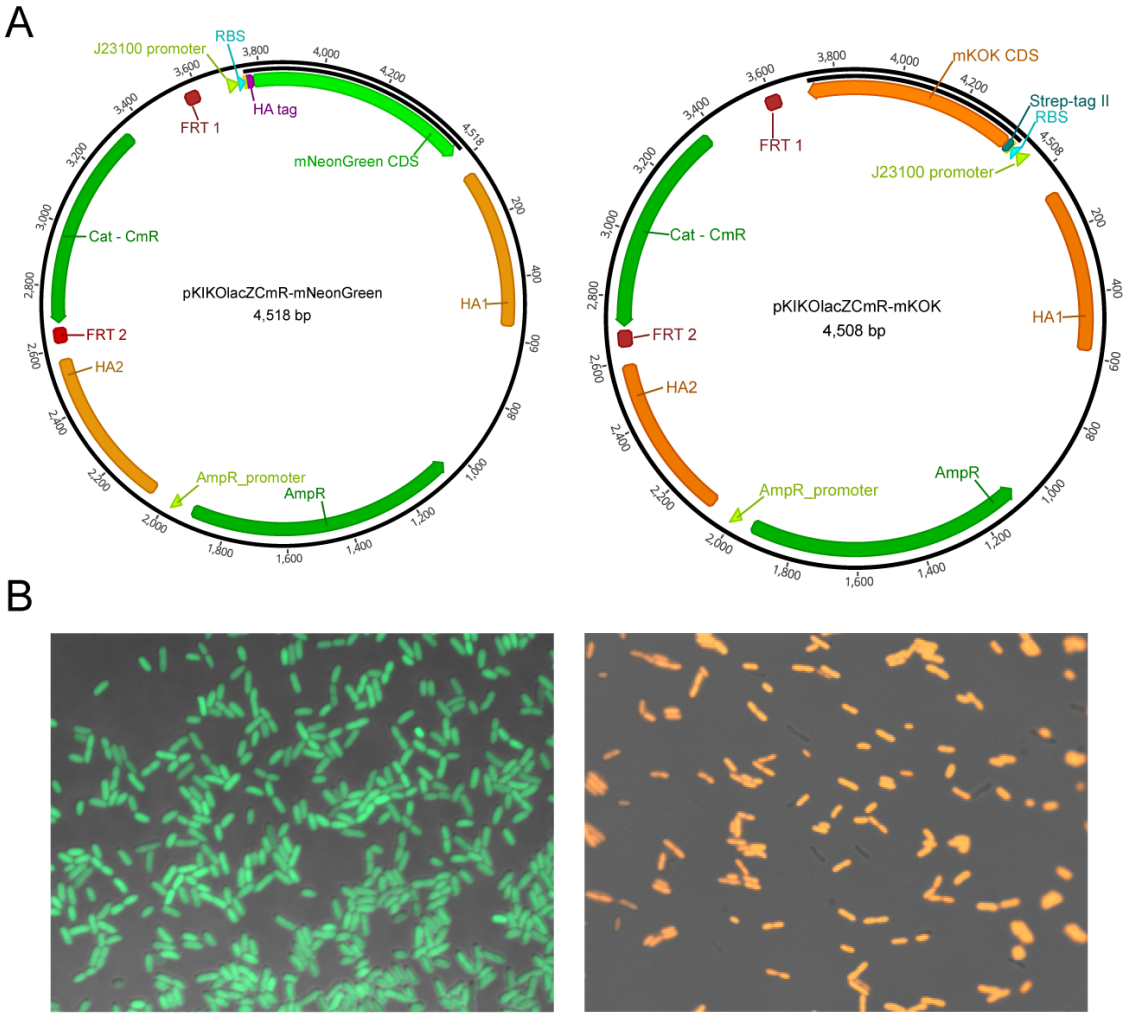

Figure 4.1 *E. coli* W cscR lacZ::Fluorophore lines.
(A) pKIKO vector maps of the plasmids used in this work to genomically integrate expression cassettes of the fluorophores, mNeonGreen (Left) or mKOK (Right). (B) Fluorescent microscopy images of *E. coli* W cscR lacZ::mNeonGreen (Left) and *E. coli* W cscR lacZ::mNeonGreen (Right).

Experimental selection conditions for photosynthetic co-culture

Once the strains were generated, we initiated a preliminary trial of experimental evolution with the *E. coli* W cscR ΔlacZ::mNeonGreen strain to determine whether this strain would be able to tolerate co-culture conditions. Alginate beads containing *S. elongatus* CscB were distributed into 16 flasks and inoculated with *E. coli* W cscR ΔlacZ::mNeonGreen immediately after the beads were fully cured (see Chapter 3 methods). These co-cultures were grown in phosphate buffered BG-11 in which we include an additional 4mM dibasic potassium phosphate (BG-11P). These cultures were then incubated in a photobioreactor and followed over the course of the next 50 days with frequent serial dilutions. Routine samples were collected to determine *E. coli* cell density (via CFUs) as well as screen for possible contaminants. The culture medium was removed and refreshed every 3-5 days and frozen stocks of the actively evolving cultures were made at each back dilution (Figure 4.2A). This method of experimental evolution could be considered a hybrid between continuous and serial transfer (Barrick and Lenski 2013). The alginate encapsulated cyanobacteria are constantly secreting photosynthetically-derived exudates the *E. coli* can metabolize (Hays et al. 2017), similar to continuous culture or bioreactor-based systems in which fresh carbon sources can be continually added to the culture. However unlike these systems, other nutrients (nitrogen, phosphate, *etc.,*) can become limited resources and waste products accumulate until the medium is completely refreshed upon back dilution, analogous to conventional serial transfer experiments. These back dilutions also function as genetic bottlenecks that randomly reduce the population size and improve beneficial mutation fixation rates (LeClair and Wahl 2017).

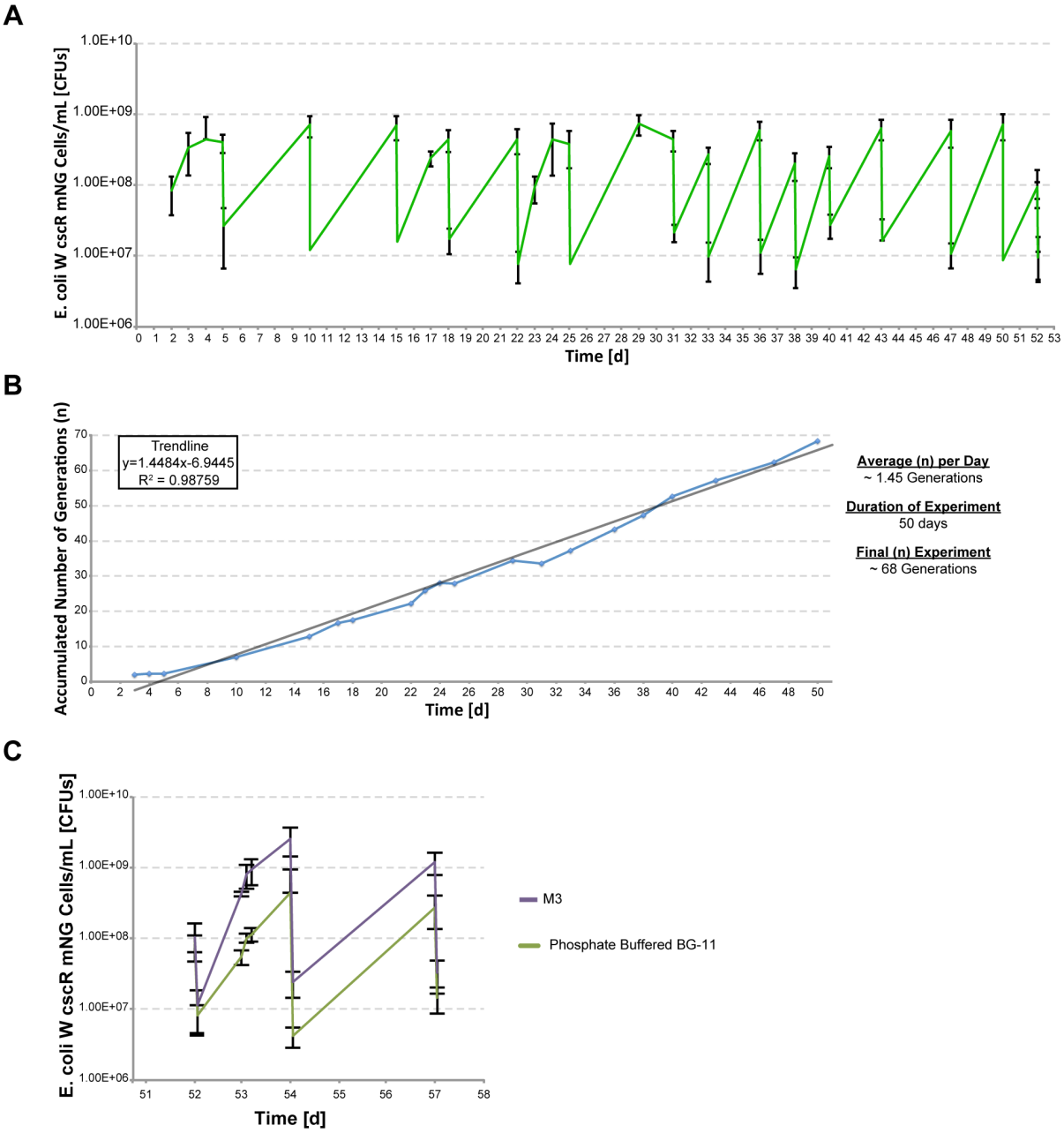

Figure 4.2: *E. coli* W cscR lacZ::mNeonGreen experimental evolution with alginate encapsulated *S. elongatus* CscB

(A) *E. coli* W cscR lacZ::mNeonGreen average density in co-culture over the course of the 50 day experiment (n=11 flasks, 5 were excluded due to contamination). Culture density was measured by serial dilution and counting colony forming units (CFUs). (B) This graph displays the accumulated total of generations from the course of this experiment. From this, we are able to calculate the estimated value of 1.45 generations per day, a value in line with previous estimates of planktonic co-culture growth (Ducat et al. 2012). (C) Splitting

Figure 4.2 (contt'd)
the existing 11 flasks into group A (n=5) and group B (n = 4), we examined the effect of adding an additional 4 mM nitrogen in the form of ammonium chloride NH_4Cl.

The population of *E. coli* W in the co-cultures stably oscillated between an initial cell concentration of $N_0 = \sim 10^7$ and a final cell concentration $N_F = \sim 10^9$ cells per mL over the course of this experiment. The generation turnover rate averaged ~ 1.45 generations per day and by the end of this experiment, we had accumulated ~70 generations over the course of 50 days (Figure 4.2B). During the course of our media analysis, we discovered that *E. coli* W could not efficiently utilize the nitrate that is supplied as the sole nitrogen source (Archer et al. 2011) in the co-culture buffer. We therefore modified this medium by supplementing 4mM NH_4Cl (M3 medium; Chapter 3 Methods), which increased the titer of *E. coli* by ~4 fold under co-culture conditions (Figure 4.2C). Higher total populations in experimental evolution studies have been shown to increase the overall pool of potential mutations, increasing rate beneficial mutation fixation (LeClair and Wahl 2017). Furthermore, removing nitrogen limitation as a selective pressure will allow additional evolutionary leeway to explore mutations related to sucrose utilization and ROS-mitigation.

Beyond the change in medium, there were a few other options to increase the *E. coli* W growth rates in co-culture. One option was to increase the dilution factor of co-culture to achieve higher generation turn over between back dilutions. The co-cultures were experiencing a roughly 100-fold reduction in population size with each back dilution. However, prior research that modeled the influence of bottlenecks on beneficial mutation fixation rates indicated that the dilution factor plays a significant role in random loss of beneficial mutations (Wahl et al. 2002). Wahl et al. calculated that a 10-fold dilution results

in a given beneficial mutation having an approximate 75% probability of fixation. Increasing this to the commonly utilized 10,000-fold dilution factor lowered the probability of fixation to 1% (Wahl et al. 2002). Thus, attempting to achieve a higher generation count between back dilutions would negatively impact the likelihood of beneficial mutations becoming fixed in our evolving populations. We therefore instead opted to increase the frequency of our back dilutions to once daily to increase turnover in our population.

Long-term co-culture to select for enhanced fitness

Making the necessary modifications to both the media and dilution protocol, I initiated a refined evolution experiment (Figure 4.3). 14 baffled culture flasks containing 10 mL of alginate bead encapsulated *S. elongatus* CscB were inoculated with M3 media with ~0.5 OD_{600} *E. coli* W cscR lacZ::mNeonGreen. After an initial 5 day adjustment period, these co-cultures were then back diluted daily for the remainder of the experiment and samples were taken every 7 days to make frozen stocks. Looking at a representative period of this experiment between day 13 and day 19 of co-culture, we can see that the *E. coli* cell density is oscillating between N_0 = ~10^7 and N_F ~10^9 cells/mL every 24 hours (Figure 4.3A). While this is roughly the same amplitude observed in the previous experiment (Figure 4.2A), the rate at which these densities are achieved is significantly increased, with a turn over of ~ 6.7 generations daily. This increased rate allowed for us to more than triple the number of generations accumulated by the end of this preliminary experiment, ~253 generations (Figure 4.3B) as compared to ~68 generations (4.2B). This rate of growth translates to roughly a 3.3 hour doubling time, ~ 1/3 the rate of *E. coli* W growth in rich medium

(Shiloach et al. 1975) indicating that these co-cultures are performing well, but there is still room for improvement.

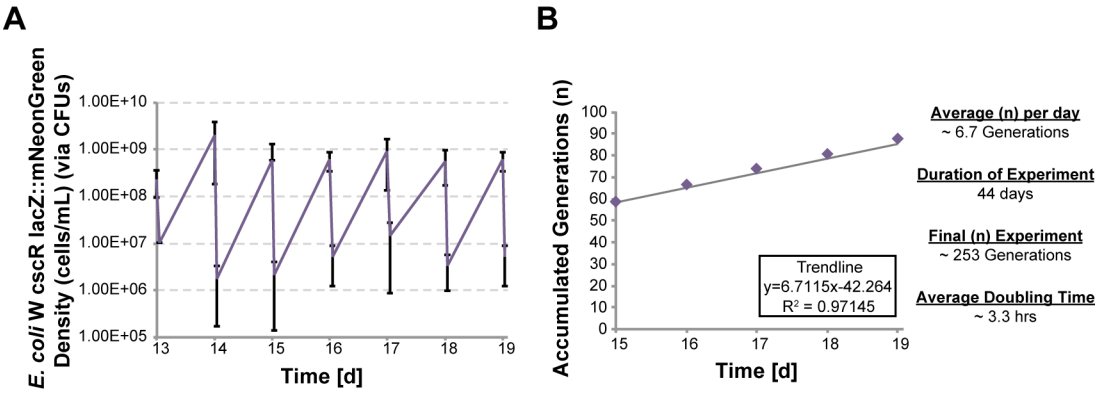

Figure 4.3: *E. coli* W cscR lacZ::mNeonGreen experimental evolution with daily dilutions

(A) A representative period of *E. coli* W density from day 13 to day 19 of the co-cultures. CFU's were measured by serial dilution subsequent colony counting. (B) Accumulated number of generations was plotted to create this graph, from which a linear trend line could be used to project future generation numbers as the experiment progressed. The average number of generations per day increased to 6.7 and the average doubling time was 3.3 hours.

Preliminary verification of enhanced fitness in evolved lines

One of our hypotheses was that consistent but diffuse levels of sucrose produced by the *S. elongatus* CscB would place a significant selective pressure on the *E. coli*, favoring mutations involved in improved sucrose uptake and/or catabolism. I therefore compared the capacity of ancestral and evolved strains to grow in defined media at decreasing sucrose content. To establishing a baseline for sucrose utilization, we first performed side-by-side inoculations of the ancestral and evolved strains of *E. coli* W cscR lacZ::mNeonGreen at ~0.4 OD_{600} into 15 mL culture tubes filled with M3 medium + 20 g/L sucrose (Figure 4.4A). As noted earlier, *E. coli* W cscR is naturally able to catabolize sucrose from the environment. Thus, in medium with 20 g/L of sucrose shows the ancestral

strain and evolved strains' optical densities increasing at similar rates. However, when the sucrose concentration was decreased to 1.25 g/L in a secondary experiment in which the

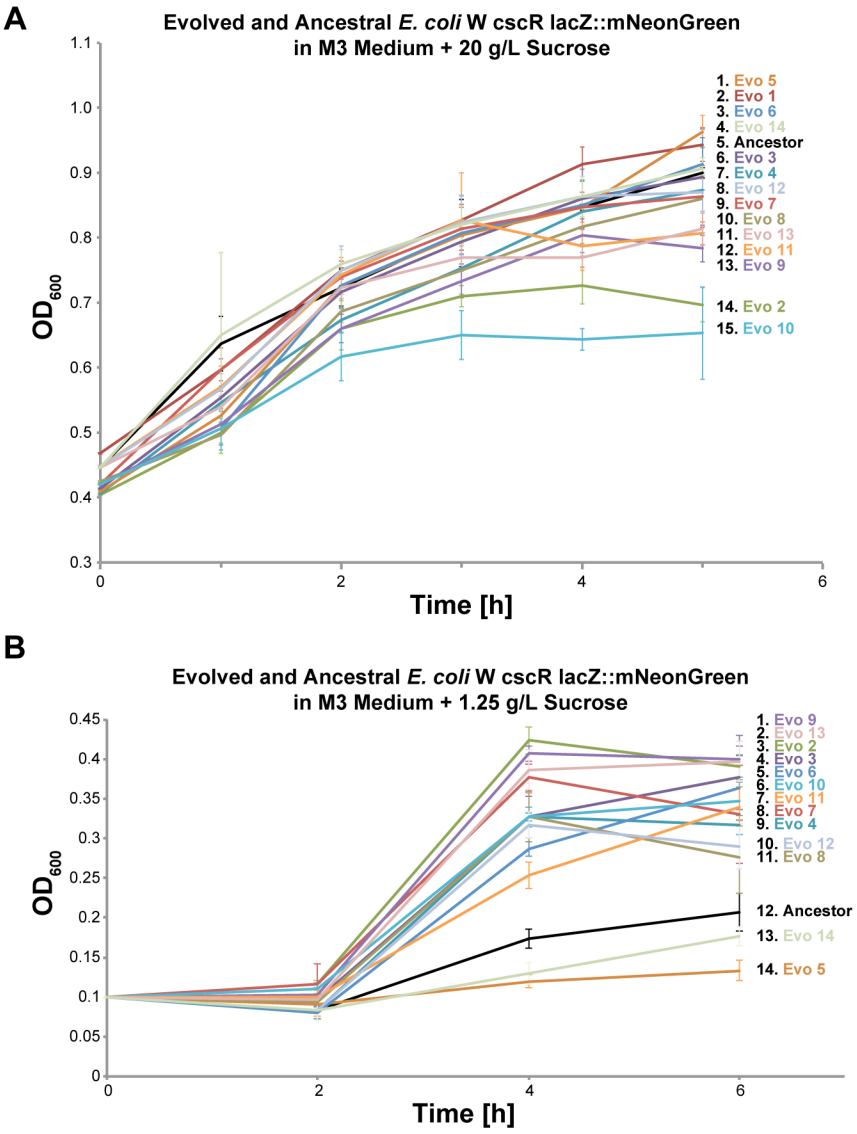

Figure 4.4: Preliminary evidence for enhanced fitness of evolved strains in low sucrose medium

(A) Baseline growth of both the ancestral and evolved strains demonstrated the ability to utilize sucrose as a carbon source. This experiment was performed in M3 medium + 20 g/L sucrose. Strains are listed along the right side of the graph in order of highest OD_{600} at the last measured time point. (B) Lowering the concentration of sucrose to 1.25 g/L demonstrated that a significant number of the evolved strains had improved fitness relative to the ancestral strain. (A & B) These experiments were performed in 15 mL culture tubes with $n = 3$.

strains were inoculated at 0.1 OD_{600}, the growth rates of the evolved strains and the ancestral strain begin to diverge (Figure 4.4B). These results suggest that over the course of 250 generations the majority of the experimentally co-evolved strains may have acquired mutations that enable them to better utilize low concentrations of sucrose.

Discussion

In this chapter I present my preliminary data on the long-term (>250 generations) directed evolution of *E. coli* W cscR in co-culture with alginate bead encapsulated *S. elongatus* CscB. Utilizing a fluorescently labeled *E. coli* W cscR strain, I performed proof-of-concept experiments to evolve heterotrophic strains better adapted to growing in the low concentrations of sucrose produced in phototrophic co-culture with *S. elongatus* CscB. While this work describes very preliminary testing of the evolved *E. coli* W strains the fact that we have observed significantly enhanced growth at low sucrose concentrations is promising data to support this system as a viable approach to experimental evolution.

Encapsulating the *S. elongatus* CscB in alginate severely limits cell division (Weiss et al. 2017), significantly reducing the likelihood that *S. elongatus* would spontaneously mutate in a way that eliminates sucrose export (*e.g.,* a cscB null mutation). Furthermore, this method of isolation allows the cells to interact with the supernatant as well as allows for facile removal of the planktonic heterotrophs without disrupting the cyanobacterial population. This facilitates the maintenance of consistent cyanobacterial based inputs into the co-cultures (*e.g.,* sucrose and other exudates), therefore stabilizing associated selective pressures for the heterotroph over time.

We hypothesized that two driving forces in this experimental evolution would be the hyperoxia and low abundance of carbon. This approach may generate *E. coli* mutants with enhanced fitness while growing in co-culture with cyanobacteria through multiple mechanisms. For example, we would expect increased fitness in strains with mutations that enhance utilization of sucrose or other secreted products from *S. elongatus*. Alternatively, *E. coli* mutants with increased resistance to hyperoxia may also be recovered. At high cyanobacterial densities in co-culture, they can inhibit the growth and viability of the partner heterotroph species. This effect is density dependent, is only observed in the light, and can result in instability or extinction of the heterotrophic microbe at high cyanobacterial densities (Hays et al. 2017). This effect may be multifaceted, but we strongly suspect hyperoxygenation and/or ROS production caused by oxygenic photosynthesis contributes to the heterotrophic viability loss. Additionally, other limited micronutrients that are only refreshed upon back dilution of the medium (phosphate, iron, *etc.,*) may also be a source of selective pressure. Nitrogen limitation may have been a significant selective pressure during the initial round of experimental evolution as there was a drastic improvement in *E. coli* growth after transitioning to the ammonium supplemented M3 medium. Interestingly, this also revealed that *E. coli* W was able to catabolize an as of yet unidentified cyanobacterial exudate as a source of nitrogen which may be a subject of future investigation.

Moving forward with this work, genome sequencing of the evolved strains can be used to identify mutations conferring fitness advantages. It is commonly accepted that the mutation rate of a given microbe is strongly correlated with the overall size of its genome with a calculated genomic mutation rate of ~0.0033 per DNA replication (Drake 1991).

This implies that per every 1000 replications we would expect to see ~3 mutants arise. However, our co-culture environment may be providing additional mutagenic stress in the form of ROS that has the potential to increase the rate of mutation in the *E. coli* strains. In conditions in which the mutation rate is relatively low, a beneficial mutation that arises often does so in isolation and undergoes a "selection sweep" in which this lineage quickly increases in frequency to dominate the culture (Desai and Fisher 2007). This property would facilitate identification of beneficial mutations within the evolved cultures as we would expect these mutations to rise to fixation quickly. It should also be noted that other examples of experimental evolution with *E. coli* witnessed the emergence of beneficial mutations in fewer than 50 generations (Marchal et al. 2017).

Future analyses of these evolved lines will include the quantification of relative fitness advantage over the ancestral strain in direct flask-based competitions, via flow cyotometry analysis, mediated by the genomically encoded mNeonGreen and mKOK fluorophores. Subsequent full-genome sequencing of these generated strains will allow for the identification of causative beneficial mutations. Areas of particular interest will be those in which a number of the independently generated lines converged on beneficial mutations in specific genes or pathways. These mutations can then be recapitulated in unevolved laboratory strains to verify whether these mutations do have a positive fitness effect under co-culture conditions. Additionally, by making regular frozen stocks of these evolving lines, we can trace the temporal origination of these mutations through the strains.

Ultimately, the lines generated by this approach may be used to gain "bottom up" insight into early adaptations that occur between microbes and cyanobacteria that increase

compatibility. Because of the modularity of this platform, there is the potential to examine multiple heterotrophic species in this manner and determine common pathways that mutate in ways important for adapting to a commensal lifestyle that is dependent upon cyanobacterial primary productivity.

Materials and Methods

Bacterial strains, media and growth conditions

S. elongatus CscB as cultured and alginate encapsulated as described in the Chapter 3 Methods. *E. coli* W cscR strains were regularly cultured in LB medium and were struck on rich medium LB plates from frozen stocks and grown at 32°C in an Multitron Pro (Infors). E. coli W cscR fluorescent lines were generated as in (Sabri et al. 2013b).

Co-culture conditions

Co-culture evolution of the *E. coli* strains were performed in 125-mL baffled flasks containing 10 mL of alginate encapsulated *S. elongatus* CscB and 20 mL of M3 medium with 1 mM IPTG (Chapter 3). These cultures were grown in a Multitron Pro (Infors) incubator with constant illumination by fluorescent bulbs (15W Gro-Lux; Sylvania; ~70 uml m-2 S-1), at 32°C, with supplemented 2% CO, and rotary shaking at 125 rpm. *E. coli* cell density was regularly checked via spot platting serial dilutions (dilution range 10^{-2}-10^{-7}) of the culture onto LB medium agarose plates, which were allowed to grow in an incubator overnight at 37°C. To generate frozen stocks of evolving cultures, 2 mL samples of the culture was taken and the cells were pelleted via centrifugation at 17,000×g for 10 mins. These cells were then resuspended in a mixture of LB and 30% glycerol and frozen at -80°C. Upon back

dilution, the entirety of the 20 mL of culture was removed from the baffled culture flasks, leaving the alginate beads in place. The flasks and beads were then rinsed with 20 mL of fresh M3 medium. After briefly shaking the flask, this medium was also removed and a fresh M3 medium was added back into the culture. 1 mM IPTG was then added to maintain the CscB expression of the alginate encapsulated *S. elongatus* CscB.

Imaging and spectrophotometery

These technologies and techniques were performed as previously described in Chapter 2 and Chapter 3.

CHAPTER 5: CONCLUSIONS AND FUTURE PROSPECTIVES

Overview

This dissertation works on developing tools and functions to enable artificial microbial consortia that include the photosynthetic cyanobacterium *S. elongatus* PCC 7942. In Chapter 2.1, we created a functional surface display system utilizing a recombinant internally tagged version of the endogenous outer membrane protein, SomA. We demonstrate that this surface display system allows these cyanobacteria to bind to functionalized abiotic beads and engineered *S. cerevisiae* (Fedeson and Ducat 2016). I then show preliminary data in Chapter 2.2 where I diversify the peptides displayed by the cyanobacteria and engineer both *E. coli* W cscR and *S. cerevisiae* strains to express surface bound protein domains to facilitate interspecies adhesion. Chapter 3 details our work in creating a bioremediating co-culture of the sucrose exporting strain of *S. elongatus CscB* and the 2,4-DNT degrading *P. putida* Suc+DNT+ strain. Encapsulation of the *S. elongatus* CscB cells within alginate hydrodel beads allows the cyanobacteria to endure the 2,4-DNT and maintain excretion of sucrose to support the *P. putida*. Engineered to express a suite of enzymes that specifically degrade 2,4-DNT via an oxidative pathway, measurement of colored intermediates indicated that the engineered strain was indeed oxidizing the 2,4-DNT and lowering the flux through the more damaging reductive pathway. Furthermore, the *P. putida* also accumulated the bioplastic precursor PHA when cultures were cycled into nitrogen deplete media. Finally, in Chapter 4, we perform a directed evolution experiment with co-cultured *E. coli* W cscR and alginate encapsulated *S. elongatus* CscB. Once optimized, this experiment achieved over 250 generations of *E. coli* W cscR in 14 independently evolved flasks, with preliminary competition results demonstrating that the evolved strains were outcompeting the ancestral strain in a sucrose only minimal medium.

Here, I discuss some of the broader questions and implications related to my work and the potential of synthetic microbial consortia.

Diffuse resources and spatial structure

An important component of cooperative microbial interactions that rely on diffusive public goods relates to how these microbes maintain partner specificity (Allen et al. 2013). These mechanisms include physical adhesion or local association (Momeni et al. 2013; Tecon and Or 2017) within a community, the exclusion or inhibition of competing species, and interspecies communication and translocation (Liaimer et al. 2015). In this dissertation, I have experimented with two approaches applicable to artificial consortia. The first involved creating a biological mechanism by which cyanobacteria could be induced to establish direct physical association with appropriately functionalized surfaces (Chapter 2). The second approach utilized alginate encapsulation to maintain a constant population of cooperating cyanobacteria to provide fixed carbon for heterotrophic species (Chapter 3 and Chapter 4). Both systems highlight the importance of spatial organization; one focused on bringing the species together, whereas the other emphasized the benefits of keeping the interacting species separate.

Spatial association is often used to overcome challenges associated with diffusible metabolite exchange. For example, experimental evolution of *S. cerevisiae* W303 to grow solely on low concentrations of diffuse sucrose resulted in the evolution of division mutants that allowed daughter cells to remain adhered to the mother cell, increasing the localized uptake of the resource by related cells (Koschwanez et al. 2013). Similarly, another study utilized auxotrophic strains of *E. coli* that engaged in passive cross-feeding,

allowing the two strains to grow in culture without supplementation. Over the course of 16 serial transfers of these co-cultures, mutations arose that resulted in aggregation of the cross-feeding strains in co-culture (Marchal et al. 2017). Convergence on adhesion in these experimental evolution studies supports the idea that spatial structuring of cooperative communities may be an important consideration in the development of synthetic consortia. This position is further strengthened by the observations that spatial organization of consortia favors the cooperating species, which provide positive feedback to culture growth (Chuang et al. 2009; Rossetti et al. 2010; Momeni et al. 2013). The work of Rossettie et al. modeled the evolution of cheater cells arising in unicellular and multicellular cyanobacteria, and found that in the aggregate/multicellular populations, these differentiated cells were unable to outcompete the cooperating vegetative cells without risking extinction. Thus, subdividing the population into structured aggregates, limits the evolution or invasion of cheating cell types.

Natural examples of structured consortia

These experiments echo the many existing associations that can be found in naturally occurring symbioses and consortia. Even the interactions between *Prochlorococcus* and SAR11 (discussed in Chapter 1), which are often separated by 100 or more cell lengths (Biller et al. 2015) in the highly turbulent surface layer of the open ocean, appear to have some level of spatial organization, with *Prochlorococcus* ecotypes stratifying in a niche-dependent manner (Johnson et al. 2017). Future research into this stratification may reveal additional features of community structure, potentially reflected in the specific "helper" microbes (*e.g.,* SAR11) that dominate a given stratum. If the association between

Prochlorococcus and SAR11 ecotypes were to represent a relatively unstructured and distant spatial organization, the other end of the spectrum of microbial interactions with high levels of physical and structural association could be represented by the holobiont, *Chlorochromatium aggregatum* (Liu et al. 2013). This consortium consists of the motile heterotrophic bacterium *Candidatus Symbiobacter mobilis*, with ~15 cells of adhered photolithoautotrophic bacterium *Chlorobium chlorochromatii*. The tight association between these two species has allowed for massive reductions in the *Ca S. mobilis* genome, rendering it entirely dependent on its epibionts and no longer capable of independent growth (Liu et al. 2013). This kind of genome reduction is reminiscent of that observed in plant and algal plastids (Howe et al. 2008). This lends credence to the hypothesis that the ancestral eukaryote and cyanobacteria may have also had a similarly strong physical association prior to the primary endosymbiotic event. Current evidence suggests that another important evolutionary transition, the colonization of land by plant life, was likely aided by interactions with symbiotic fungi (Delaux et al. 2015). Thus, the preadaptation of the ancestral eukaryotic and cyanobacterial species is an area of research that warrants further investigation to generate a more complete understanding of one of the most important evolutionary events of all time. While we are able to make some inferences through phylogenetic analysis of modern photosynthetic microorganisms, such as that of the primary endosymbiont likely belonging to the *Gloeomargaritales* (Ponce-Toledo et al. 2017), it is nearly impossible to accurately predict the nature of the environment and interactions that would have allowed for the primary endosymbiosis to occur solely from phylogenetic data. Additionally, although we are able to look at contemporary examples of natural eukaryotic and cyanobacterial symbioses for clues regarding what traits might

facilitate endosymbiotic events, as discussed in Chapter 1, it is often times difficult to disentangle highly integrated relationships. This and other similar avenues of research may benefit from the utilization of tailored synthetic consortia.

Artificial consortia and modularity

The usage of naïve and genetically tractable organisms to explore fundamental questions such as, "How do bacteria adapt to having photosynthetic neighbors? (Chapter 4)" allow for a significant level of control while sacrificing a variable amount of realism depending on the questions being pursued (Figure 1.1). However, direct co-cultures are not always suitable for every area of research. In Chapter 3, we found it necessary to encapsulate our sucrose exporting cyanobacteria in alginate hydrogels not only to maintain consistent sucrose production, but also to allow the cyanobacteria to withstand the toxic effects of 2,4-DNT in the co-culture medium. Furthermore, other examples of preliminary consortia have shown that some species are more or less compatible than others (Hays et al. 2017). One pertinent example is that of a tripartite culture of *Azotobacter vinelandii*, *Bacillus licheniformis*, and *Paenibacillus curdlanolyticus* that failed to thrive in isolation or in direct association were able to survive when grown in distantly connected microfluidics wells survived (Kim et al. 2008). Because this area of research is still developing, there is a lack of guiding principles to direct the construction of these synthetic consortia. Each new combination of species assembled into a consortium risks unanticipated metabolic interactions stymieing the consortium's productivity or even triggering its collapse. Thus, to enable the eventual expansion of potential species combinations, work is being done to

characterize or create strains to act as modular components that can be interchanged between consortia (Figure 1.2).

The pursuit of microbial strains with the potential for "plug-and-play" like functionality in artificial consortia is based on the same view that led to the creation of BioBricks™, the belief that by generating standardized modules, future researchers will have the diversity of components with which to design and explore consortia with new and unique functions. While my own dissertation work with consortia has been limited to utilizing strains of *E. coli*, *P. putida*, and *S. elongatus*, others have begun to explore a number of other species like *Azotobacter vinelandii* (Ortiz-Marquez et al. 2014; Smith and Francis 2016, 2017) with potential to become modular components.

Alginate encapsulation as a technique for artificial consortia

In both Chapter 3 and Chapter 4, the co-culture approach utilized entailed the encapsulation of the *S. elongatus* CscB strain within alginate hydrogels. Chapter 3 served as a direct demonstration of how applied synthetic ecology and rationally designed co-cultures could be utilized to address a pressing concern in our society. Chapter 4 focused on the experimental evolution of *E. coli* in a co-culture environment in which the only source of carbon was the cyanobacterial photosynthates from the alginate encapsulated *S. elongatus* CscB strain. The reasoning behind using this system in each of these projects is addressed in their respective chapters. However, there are additional features of this system relevant to the development of synthetic consortia that warrant discussion. One of the primary features of this system is that it physically separates the planktonic microbial species from the encapsulated species (in these cases, the cyanobacterium). While similar

in some respects to culture techniques that harness two chambers separated by membranes filter (Paul et al. 2013; Moutinho et al. 2017) or cultures separated by dialysis tubes/bags (Paul et al. 2009), these techniques do not maintain a fixed population as has been shown in the alginate hydrogel beads (Weiss et al. 2017). Cell density and growth phase can drastically influence how cells interact with their surroundings. This especially true in photosynthetic organisms like cyanobacteria that often regulate gene expression based on circadian rhythms (Markson et al. 2013; Piechura et al. 2017) or in microbes that utilize density dependent signaling mechanisms like quorum sensing (Waters and Bassler 2005). The use of alginate encapsulated cells thus acts as another level of control, reducing some of the variables related to the encapsulated species growth at the cost of exploring how changing the ratio between species influences consortia stability. Approaching this co-culture method with modularity in mind, one of the potential benefits is that it allows for the rapid one-sided testing of the encapsulated species on the planktonically grown species. Additionally, this influence is likely to be mediated by diffusible exudates which narrows the number of factors that need to be accounted for when trying to identify the causative metabolite(s).

The intersection of synthetic ecology and experimental evolution

My final discussion point focuses on how the intersection of rationally designed consortia and experimental evolution may present researchers with a unique tool to approach difficult questions. As alluded to earlier in this chapter, I believe that questions surrounding species adaptation to one another, especially in the context of symbiotic relationships, could be approached with a combination of these techniques. When we

identify a system or metabolic pathway that we believe is important for a symbiotic interaction, often times one of the first ways in which we attempt to understand it is by removing or altering its components. By methodically perturbing the system, we can establish what pathways are critical, redundant, or unnecessary. Furthermore, if that system shares homology with mechanisms in other related species we can also begin to determine how it has evolved over time. However, it is difficult to put these pieces back into their evolutionary context to explore how the interaction between these symbiotic organisms shaped their co-evolution. With experimental evolution of synthetic consortia, as opposed to removing functions from an existing symbiosis, you could instead work from the "bottom-up" by adding rationally defined functions (like cell adhesion) to a species in a co-culture and then observe how this change influences the development of these strains as they co-evolve.

The work presented here has significant potential to further increase awareness of and interest in cyanobacteria as well as synthetic microbial ecology. At the time of this writing, a second researcher group unaffiliated with my work has published a manuscript generating a surface display system similar to the one I describe in Chapter 2, for the cyanobacterium *Synechocystis* sp. 6803 (Cengic et al. 2018). It is my hope that others will continue to explore the potential of both cyanobacteria and artificial consortia.

REFERENCES

REFERENCES

Abramson BW, Kachel B, Kramer DM, Ducat DC. Increased photochemical efficiency in cyanobacteria via an engineered sucrose sink. Plant Cell Physiol. 2016;57(12):2451–60.

Achtnich C, Sieglen U, Knackmuss HJ, Lenke H. Irreversible binding of biologically reduced 2,4,6-trinitrotoluene to soil. Environ Toxicol Chem. 1999;18(11):2416–23.

Adams. Symbiotic Interactions. Springer; 2000.

Adams DG, Bergman B, Nierzwicki-Bauer SA, Duggan PS, Rai AN, Schüßler A. Cyanobacterial-plant symbioses. Prokaryotes Prokaryotic Biol Symbiotic Assoc. 2013. p. 359–400.

Aikens J, Turner RJ. Transgenic photosynthetic microorganisms and photobioreactor. 2013. p. 231pp.

Akkaya Ö, Pérez-pantoja DR, Calles B, Nikel PI, Lorenzo V de. The metabolic redox regime of Pseudomonas putida tunes its evolvability towards novel xenobiotic substrates. MBio. 2018;9:e01512-18.

Allen B, Gore J, Nowak MA. Spatial dilemmas of diffusible public goods. Elife. 2013;2013(2).

Altschul SF, Gish W, Miller W, Myers EW, Lipman DJ. Basic Local Alignment Search Tool. J Mol Biol. 1990;215:403–10.

Ambrosio R, Ortiz-Marquez JCF, Curatti L. Metabolic engineering of a diazotrophic bacterium improves ammonium release and biofertilization of plants and microalgae. Metab Eng. 2017;40:59–68.

Amin SA, Green DH, Hart MC, Kupper FC, Sunda WG, Carrano CJ. Photolysis of iron-siderophore chelates promotes bacterial-algal mutualism. Proc Natl Acad Sci. 2009;106(40):17071–6.

Andreu C, Del Olmo M. Yeast arming by the Aga2p system: effect of growth conditions in galactose on the efficiency of the display and influence of expressing leucine-containing peptides. Appl Microbiol Biotechnol. 2013;97(20):9055–69.

Andrianantoandro E, Basu S, Karig DK, Weiss R. Synthetic biology: new engineering rules for an emerging discipline. Mol Syst Biol. 2006;2:1–14.

Archer CT, Kim JF, Jeong H, Park JH, Vickers CE, Lee SY, et al. The genome sequence of E. coli W (ATCC 9637): comparative genome analysis and an improved genome-scale reconstruction of E. coli. BMC Genomics. 2011;12:9.

Arifin Y, Sabri S, Sugiarto H, Krömer JO, Vickers CE, Nielsen LK. Deletion of cscR in Escherichia coli W improves growth and poly-3-hydroxybutyrate (PHB) production from sucrose in fed batch culture. J Biotechnol. 2011;156(4):275–8.

Azam F, Malfatti F. Microbial structuring of marine ecosystems. Nat. Rev. Microbiol. 2007. p. 782–91.

Bailliez C, Largeau C, Casadevall E, Chimie L De, Physique O, Nationale E. Applied o . d Microbiology Biotechnology Growth and hydrocarbon production of Botryococcus braunii immobilized in calcium alginate gel. 1985;99–105.

Bais HP, Weir TL, Perry LG, Gilroy S, Vivanco JM. The role of root exudates in rhizosphere interations with plants and other organisms. Annu Rev Plant Biol. 2006;57:233–66.

Bar-On YM, Phillips R, Milo R. The biomass distribution on Earth. Proc Natl Acad Sci. 2018;201711842.

Barrick JE, Lenski RE. Genome dynamics during experimental evolution. Nat Rev Genet. 2013;14:827–39.

Barry A, Wolfe A, English C, Ruddick C, Lambert D. 2016 National Algal Biofuels Technology Review. Bioenergy Technol. Off. 2016.

Basu S, Gerchman Y, Collins CH, Arnold FH, Weiss R. A synthetic multicellular system for programmed pattern formation. Nature. 2005;434(7037):1130–4.

Baumdicker F, Hess WR, Pfaffelhuber P. The infinitely many genes model for the distributed genome of bacteria. Genome Biol Evol. 2012; 4:(4).443–56.

Bergman B, Ran L, Adams DG. Cyanobacterial-plant Symbioses: Signaling and Development. Cyanobacteria Mol Biol Genomics, Evol. 2008. 447–73.

Bertilsson S, Berglund O, Pullin MJ, Chisholm SW. Release of dissolved organic matter by Prochlorococcus. Vie Milieu. 2005;55(3–4):225–31.

Besingi RN, Clark PL. Extracellular protease digestion to evaluate membrane protein cell surface localization. Nat Protoc. 2015;10(12):2074–80.

Biller SJ, Berube PM, Lindell D, Chisholm SW. Prochlorococcus: The structure and function of collective diversity. Nat Rev Microbiol. 2015;13(1):13–27.

Biller SJ, Coe A, Chisholm SW. Torn apart and reunited: Impact of a heterotroph on the transcriptome of Prochlorococcus. ISME J. 2016;10(12):2831–43.

Biller SJ, Coe A, Roggensack SE, Chisholm SW. Heterotroph Interactions Alter

Prochlorococcus Transcriptome Dynamics during Extended Periods of Darkness. mSystems. 2018;3(3):e00040-18.

Blasche S, Kim Y, Oliveira AP, Patil KR. Model Microbial Communities for Ecosystems Biology. Curr Opin Syst Biol. 2017;(September):1–7.

van Bloois E, Winter RT, Kolmar H, Fraaije MW. Decorating microbes: Surface display of proteins on Escherichia coli. Trends Biotechnol. 2011;29(2):79–86.

Boder ET, Midelfort KS, Wittrup KD. Directed evolution of antibody fragments with monovalent femtomolar antigen-binding affinity. Proc Natl Acad Sci USA. 2000;97(20):10701–5.

Boder ET, Wittrup KD. Yeast surface display for screening combinatorial polypeptide libraries. Nat Biotechnol. 1997;15(6):553–7.

Boder ET, Wittrup KD. Yeast surface display for directed evolution of protein expression, affinity, and stability. Methods Enzymol. 2000 Jan;328:430–44.

Bohannan BJM, Lenski RE. The relative importance of competition and predation varies with productivety in a model community. Am Nat. 2000;156(4):329–40.

Bork P, Bowler C, De Vargas C, Gorsky G, Karsenti E, Wincker P. Tara Oceans studies plankton at Planetary scale. Science. 2015. p. 873.

Bozeman J, Koopman B, Bitton G. Toxicity testing using immobilized algae. Aquat Toxicol. 1989;14:345–52.

Braakman R, Follows MJ, Chisholm SW. Metabolic evolution and the self-organization of ecosystems. Proc Natl Acad Sci. 2017;114(15):E3091–100.

Brenner K, You L, Arnold FH. Engineering microbial consortia : a new frontier in synthetic biology. Trends Biotechnol. 2008;26(9):483–9.

Brockhurst MA, Koskella B. Experimental coevolution of species interactions. Trends Ecol Evol [Internet]. Elsevier Ltd; 2013;28(6):367–75.

Brussaard CPD, Bidle KD, Pedrós-Alió C, Legrand C. The interactive microbial ocean. Nat. Microbiol. 2016; 2

Bryant C, McElroy WD. Nitroreductases. In: Muller F, editor. Chem Biochem Flavoenzymes, Vol II. 1st ed. Boca Raton, Florida, USA: CRC Press, Inc.; 1991. p. 291–9.

Cameron DE, Bashor CJ, Collins JJ. A brief history of synthetic biology. Nat Rev Microbiol. 2014;12(5):381–90.

Carini P, Steindler L, Beszteri S, Giovannoni SJ. Nutrient requirements for growth of the extreme oligotroph "Candidatus Pelagibacter ubique" HTCC1062 on a defined medium. ISME J. 2013;7(3):592–602.

Carney LT, Lane TW. Parasites in algae mass culture. Front. Microbiol. 2014.

Carrieri D, Paddock T, Maness P-C, Seibert M, Yu J. Photo-catalytic conversion of carbon dioxide to organic acids by a recombinant cyanobacterium incapable of glycogen storage. Energy Environ Sci. 2012;5(11):9457.

Castenholz RW. Culturing Methods for Cyanobacteria. Methods Enzymol. 1988;167:68–93.

Cengic I, Uhlén M, Hudson EP. Surface display of small affinity proteins on Synechocystis sp. strain PCC 6803 mediated by fusion to the major type IV pilin PilA1. J Bacteriol. 2018;200(16):1–19.

Chaijarasphong T, Savage DF. Sequestered: Design and Construction of Synthetic Organelles. Synth Biol Parts, Devices Appl. John Wiley & Sons; 2018;8.

Chaparro JM, Sheflin AM, Manter DK, Vivanco JM. Manipulating the soil microbiome to increase soil health and plant fertility. Biol. Fertil. Soils. 2012. 489–99.

Chen D, Lewandowski Z, Roe F, Surapaneni P. Diffusivity of Cu2+ in Calcium Alginate Gel Beads. Biotechnol Bioeng. 1993;41:755–60.

Chisti Y. Biodiesel from microalgae. Biotechnol Adv. 2007;25(3):294–306.

Chisti Y. Constraints to commercialization of algal fuels. J Biotechnol. Elsevier B.V.; 2013;167(3):201–14.

Cho DH, Ramanan R, Heo J, Lee J, Kim BH, Oh HM, et al. Enhancing microalgal biomass productivity by engineering a microalgal-bacterial community. Bioresour Technol. 2015;175:578–85.

Chodkowski JL, Shade A. A new synthetic community system for probing microbial interactions driven by exometabolites. mSystems. 2017;2(6):4–7.

Chuang JS, Rivoire O, Leibler S. Simpson's paradox in a synthetic microbial system. Science. 2009;323(5911):272–5.

Chungjatupornchai W, Fa-aroonsawat S. Translocation of green fluorescent protein to cyanobacterial periplasm using ice nucleation protein. J Microbiol. 2009;47(2):187–92.

Chungjatupornchai W, Fa-Aroonsawat S. Biodegradation of organophosphate pesticide using recombinant cyanobacteria with surface- and intracellular-expressed organophosphorus hydrolase. J Microbiol. 2008;18(5):946–51.

Chungjatupornchai W, Kamlangdee A, Fa-Aroonsawat S. Display of organophosphorus hydrolase on the cyanobacterial cell surface using synechococcus outer membrane protein a as an anchoring motif. Appl Biochem Biotechnol. 2011;164(7):1048–57.

Connon SA, Giovannoni SJ. High-throughput methods for culturing microorganisms in very-low-nutrient media yield diverse new marine isolates. Appl Environ Microbiol. 2002;68(8):3878–85.

Cooper MB, Smith AG. Exploring mutualistic interactions between microalgae and bacteria in the omics age. Curr. Opin. Plant Biol. 2015. 147–53.

Costello EK, Stagaman K, Dethlefsen L, Bohannan BJM, Relman DA. The application of ecological theory toward an understanding of the human microbiome. Science. 2012;336(6086):1255–62.

Coyte KZ, Schluter J, Foster KR. The ecology of the microbiome: Networks, competition, and stability. Science. 2015;350(6261):663–6.

Delaux P-M, Radhakrishnan G V., Jayaraman D, Cheema J, Malbreil M, Volkening JD, et al. Algal ancestor of land plants was preadapted for symbiosis. Proc Natl Acad Sci. 2015;112(43):201515426.

Demmig-Adams B, Stewart JJ, Burch TA, Adams WW. Insights from placing photosynthetic light harvesting into context. J Phys Chem Lett. 2014;5(16):2880–9.

Desai MM, Fisher DS. Beneficial mutation-selection balance and the effect of linkage on positive selection. Genetics. 2007;176(3):1759–98.

Ding M-Z, Song H, Wang E-X, Liu Y, Yuan Y-J. Design and construction of synthetic microbial consortia in China. Synth Syst Biotechnol. 2016;6–11.

Dismukes GC, Carrieri D, Bennette N, Ananyev GM, Posewitz MC. Aquatic phototrophs: efficient alternatives to land-based crops for biofuels. Curr Opin Biotechnol. 2008;19(3):235–40.

Dodds WK, Gudder DA, Mollenhauer D. THE ECOLOGY OF NOSTOC. J Phycol. 1995;31(1):2–18.

Doebeli M, Hauert C. Models of cooperation based on the Prisoner's Dilemma and the Snowdrift game. Ecol Lett. 2005;8(7):748–66.

Dolinšek J, Goldschmidt F, Johnson DR. Synthetic microbial ecology and the dynamic interplay between microbial genotypes. FEMS Microbiol Rev. 2016;(January):1–19.

Drake JW. A constant rate of spontaneous mutation in DNA-based microbes. Proc Natl Acad

Sci. 1991;88(16):7160–4.

Du W, Liang F, Duan Y, Tan X, Lu X. Exploring the photosynthetic production capacity of sucrose by cyanobacteria. Metab Eng . 2013;19:17–25.

Duan Y, Luo Q, Liang F, Lu X. Sucrose secreted by the engineered cyanobacterium and its fermentability. J Ocean Univ China. 2016;15(5):890–6.

Ducat DC. Synthetic biology: molecular tools for engineering organisms. eLS. 2017

Ducat DC, Avelar-Rivas JA, Way JC, Silver PA. Rerouting carbon flux to enhance photosynthetic productivity. Appl Environ Microbiol. 2012;78(8):2660–8.

Ducat DC, Way JC, Silver PA. Engineering cyanobacteria to generate high-value products. Trends Biotechnol . 2011;29(2):95–103.

Dufresne A, Ostrowski M, Scanlan DJ, Garczarek L, Mazard S, Palenik BP, et al. Unraveling the genomic mosaic of a ubiquitous genus of marine cyanobacteria. Genome Biol. 2008;9(5).

Eiteman MA, Lee SA, Altman E. A co-fermentation strategy to consume sugar mixtures effectively. J Biol Eng. 2008;2.

Fedeson DT, Ducat DC. Cyanobacterial surface display system mediates engineered interspecies and abiotic binding. ACS Synth Biol. 2016;6(2):367–74.

Ferri S, Nakamura M, Ito A, Nakajima M, Abe K, Kojima K, et al. Efficient surface-display of autotransporter proteins in cyanobacteria. Algal Res. 2015;12:337–40.

Franzosa EA, Hsu T, Sirota-Madi A, Shafquat A, Abu-Ali G, Morgan XC, et al. Sequencing and beyond: Integrating molecular “omics” for microbial community profiling. Nat. Rev. Microbiol. 2015. p. 360–72.

French CE, Rosser SJ, Bruce NC. Biotransformations of Explosives. Biotechnol Genet Eng Rev. 2001;18(1):171–217.

Fuhrman JA, Cram JA, Needham DM. Marine microbial community dynamics and their ecological interpretation. Nat. Rev. Microbiol. 2015. p. 133–46.

Gestel J VaN, Vlamakis H, Kolter R. Division of Labor in Biofilms : the Ecology of Cell Differentiation. Microbiol Spectr Am Soc Microbiol. 2015;(May):1–24.

Ghirardi ML. Implementation of photobiological H2 production: The O2 sensitivity of hydrogenases. Photosynth. Res. 2015. p. 383–93.

Gibson DG, Young L, Chuang R-Y, Venter JC, Hutchison C a, Smith HO. Enzymatic assembly

of DNA molecules up to several hundred kilobases. Nat Methods. 2009 May;6(5):343–5.

Gillet F, Roisin C, Fliniaux MA, Dubreuil AJ, Barbotin JN. Immobilization of Nicotiana tabacum plant cell suspensions within calcium alginate gel beads for the production of enhanced amounts of scopolin. 2000;26:229–34.

Giovannoni SJ. Genome Streamlining in a Cosmopolitan Oceanic Bacterium. Science (80-). 2005;309(5738):1242–5.

Giovannoni SJ. SAR11 Bacteria: The Most Abundant Plankton in the Oceans. Ann Rev Mar Sci. 2017;9(1):231–55.

Glass DS, Riedel-Kruse IH. A Synthetic Bacterial Cell-Cell Adhesion Toolbox for Programming Multicellular Morphologies and Patterns. Cell. 2018;174(3):649–658.e16.

Goers L, Freemont P, Polizzi KM. Co-culture systems and technologies: taking synthetic biology to the next level. J R Soc Interface. 2014;11(96):20140065–20140065.

Golden SS, Brusslan J, Haselkorn R. [12] Genetic engineering of the cyanobacterial chromosome. Methods Enzymol. 1987;153(C):215–31.

Goldford JE, Lu N, Bajic D, Estrela S, Tikhonov M, Sanchez-Gorostiaga A, et al. Emergent Simplicity in Microbial Community Assembly. bioRxiv. 2017;474(August):205831.

Gopal M, Gupta A, Thomas G V. Bespoke microbiome therapy to manage plant diseases. Front Microbiol. 2013;4(DEC).

Gore J, Youk H, van Oudenaarden A. Snowdrift game dynamics and facultative cheating in yeast. Nature. 2009 May 14;459(7244):253–6.

Greenfield LK, Whitfield C. Synthesis of lipopolysaccharide O-antigens by ABC transporter-dependent pathways. Carbohydr Res. 2012 Jul 15;356:12–24.

Griest WH, Stewart AJ, Vass AA, Ho CH. Chemical and Toxicological Characterization of Slurry Reactor Biotreatment of Explosives-Contaminated Soils.pdf. Oak Ridge, Tennessee, USA; 1998.

Griest WH, Tyndall RL, Stewart AJ, Caton JE, Vass AA, Ho C -H, et al. Chemical characterization and toxicological testing of windrow composts from explosives-contaminated sediments. Environ Toxicol Chem. 1995;14(1):51–9.

Grima EM, Belarbi E, Fernández FGA, Medina AR, Chisti Y. Recovery of microalgal biomass and metabolites: process options and economics. Biotechnol Adv. 2003;20(7):491–515.

Gründel M, Scheunemann R, Lockau W, Zilliges Y. Impaired glycogen synthesis causes metabolic overflow reactions and affects stress responses in the cyanobacterium Synechocystis sp. PCC 6803. Microbiol (United Kingdom). 2012;158(12):3032–43.

Gupta PL, Lee SM, Choi HJ. A mini review: photobioreactors for large scale algal cultivation. World J Microbiol Biotechnol. 2015;31(9):1409–17.

Hagan CL, Silhavy TJ, Kahne D. β-Barrel membrane protein assembly by the Bam complex. Annu Rev Biochem. 2011 Jan;80:189–210.

Haigler BE, Nishino SF, Spain JC. Biodegradation of 4-Methyl-5-Nitrocatechol by Pseudomonas sp. Strain DNT. J Bacteriol. 1994;176(11):3433–7.

Hansel A, Pattus F, Ju UJ, Tadros MH. Cloning and characterization of the genes coding for two porins in the unicellular cyanobacterium Synechococcus PCC 6301. 1998;1399:31–9.

Hansel A, Tadros MH. Characterization of two pore-forming proteins isolated from the outer membrane of Synechococcus PCC 6301. Curr Microbiol. 1998;36(6):321–6.

Hanski I, Hanski I. Metapopulation dynamics. Nature. 1998;396(6706):41–9.

Hartmann M, Gomez-Pereira P, Grob C, Ostrowski M, Scanlan DJ, Zubkov M V. Efficient CO2 fixation by surface Prochlorococcus in the Atlantic Ocean. ISME J. 2014;8(11):2280–9.

Hays SG, Ducat DC. Engineering cyanobacteria as photosynthetic feedstock factories. Photosynth Res. 2015;123(3):285–95.

Hays SG, Patrick WG, Ziesack M, Oxman N, Silver PA. Better together: Engineering and application of microbial symbioses. Curr Opin Biotechnol. 2015;36:40–9.

Hays SG, Yan LLW, Silver PA, Ducat DC. Synthetic Photosynthetic Consortia Define Interactions Leading to Robustness and Photoproduction. J Biol Eng. 2017;11(4):1–36.

Hickman JW, Kotovic KM, Miller C, Warrener P, Kaiser B, Jurista T, et al. Glycogen synthesis is a required component of the nitrogen stress response in Synechococcus elongatus PCC 7942. Algal Res. 2013;2(2):98–106.

Holyoak M, Lawler SP. Persistence of an extinction-prone predator-prey interaction through metapopulation dynamics. Ecology. 1996;77(6):1867–79.

Hom EFY, Murray AW. Plant-fungal ecology. Niche engineering demonstrates a latent capacity for fungal-algal mutualism. Science. 2014 Jul 4;345(6192):94–8.

Hooker BS, Skeen RS. Transgenic phytoremediation blasts onto the scene. Nat Biotechnol.

1999;17(May):1999.

Howe CJ, Barbrook a C, Nisbet RER, Lockhart PJ, Larkum a WD. The origin of plastids. Philos Trans R Soc Lond B Biol Sci. 2008 Aug 27;363(1504):2675–85.

Inoue H, Nojima H, Okayama H. High efficiency transformation of Escherichia coli with plasmids. Gene. 1990;96(1):23–8.

Ispolatov I, Ackermann M, Doebeli M. Division of labour and the evolution of multicellularity. Proc R Soc B Biol Sci. 2012;279(1734):1768–76.

Ives AR, Carpenter SR. Stability and diversity of ecosystems. Science. 2007. p. 58–62.

Jarmander J, Gustavsson M, Do TH, Samuelson P, Larsson G. A dual tag system for facilitated detection of surface expressed proteins in Escherichia coli. Microbial Cell Factories; 2012;11(1):1.

Jessup CM, Forde SE, Bohannan BJM. Microbial Experimental Systems in Ecology. Adv Ecol Res. 2005;37(04):273–307.

Jessup CM, Kassen R, Forde SE, Kerr B, Buckling A, Rainey PB, et al. Big questions, small worlds: Microbial model systems in ecology. Trends Ecol. Evol. 2004. p. 189–97.

Johnson TJ, Halfmann C, Zahler JD, Zhou R, Gibbons WR. Increasing the tolerance of filamentous cyanobacteria to next-generation biofuels via directed evolution. Algal Res. 2016;18:250–6.

Johnson ZI, Zinser ER, Coe A, McNulty NP, Malcolm E, Woodward S, et al. Niche Partitioning among Prochlorococcus Ecotypes along Ocean-Scale Environmental Gradients. Science. 2017;311(5768):1737–40.

Jose J, Bernhardt R, Hannemann F. Functional display of active bovine adrenodoxin on the surface of E. coli by chemical incorporation of the [2Fe-2S] cluster. ChemBioChem. 2001;2(9):695–701.

Jose J, Bernhardt R, Hannemann F. Cellular surface display of dimeric Adx and whole cell P450-mediated steroid synthesis on E. coli. J Biotechnol. 2002;95(3):257–68.

Jose J, Zangen D. Autodisplay of the protease inhibitor aprotinin in Escherichia coli. Biochem Biophys Res Commun. 2005;333(4):1218–26.

Ju K-S, Parales R, E. Nitroaromatic Compounds, from Synthesis to Biodegradation. Microbiol Mol Biol Rev. 2010;74(2):250–72.

Kang HJ, Baker EN. Intramolecular isopeptide bonds: Protein crosslinks built for stress? Trends Biochem Sci. 2011;36(4):229–37.

Kashtan N, Roggensack SE, Rodrigue S, Thompson JW, Biller SJ, Coe A, et al. Single-Cell Genomics Reveals Hundreds of Coexisting Subpopulations in Wild Prochlorococcus. Science. 2014;344(April):416–20.

Kato S, Haruta S, Cui ZJ, Ishii M. Stable Coexistence of Five Bacterial Strains as a Cellulose-Degrading Community. Appl Environ Microbiol. 2005;71(11):7099–106.

Kawecki TJ, Lenski RE, Ebert D, Hollis B, Olivieri I, Whitlock MC. Experimental evolution. Trends Ecol Evol. 2012;27(10):547–60.

Kazamia E, Aldridge DC, Smith AG. Synthetic ecology - A way forward for sustainable algal biofuel production? J Biotechnol. 2012a;162(1):163–9.

Kazamia E, Czesnick H, Nguyen TT Van, Croft MT, Sherwood E, Sasso S, et al. Mutualistic interactions between vitamin B12-dependent algae and heterotrophic bacteria exhibit regulation. Environ Microbiol. 2012b;14(6):1466–76.

Kazamia E, Helliwell KE, Purton S, Smith AG. How mutualisms arise in phytoplankton communities: building eco-evolutionary principles for aquatic microbes. Ecol. Lett. 2016. p. 810–22.

Kelsic ED, Zhao J, Vetsigian K, Kishony R. Counteraction of antibiotic production and degradation stabilizes microbial communities. Nature. 2015;521(7553):516–9.

Kerner A, Park J, Williams A, Lin XN. A programmable scherichia coli consortium via tunable symbiosis. PLoS One. 2012;7(3):1–10.

Kerr B, Riley MA, Feldman MW, Bohannan BJM. Local dispersal promotes biodiversity in a real-life game of rock-paper-scissors. Nature. 2002;418(6894):171–4.

Kim HJ, Boedicker JQ, Choi JW, Ismagilov RF. Defined spatial structure stabilizes a synthetic multispecies bacterial community. Proc Natl Acad Sci U S A. 2008;105(47):18188–93.

Kinoshita S. Amino-acid Production by the Fermentation Process. Nature. 1972. p. 211.

Kiran B, Kumar R, Deshmukh D. Perspectives of microalgal biofuels as a renewable source of energy. Energy Convers Manag. 2014;88:1228–44.

Kondo a, Ueda M. Yeast cell-surface display--applications of molecular display. Appl Microbiol Biotechnol. 2004;64(1):28–40.

Korndorfer IP, Skerra A. Improved affinity of engineered streptavidin for the Strep-tag II peptide is due to a fixed open conformation of the lid-like loop at the binding site. Protein Sci. 2002;11:883–93.

Korosh TC, Dutcher A, Pfleger BF, McMahon KD. Inhibition of Cyanobacterial Growth on a Municipal Wastewater Sidestream Is Impacted by Temperature. mSphere. 2018;3(1):1–15.

Koschwanez JH, Foster KR, Murray AW. Improved use of a public good selects for the evolution of undifferentiated multicellularity. Elife. 2013(2):e00367.

Koskella B, Brockhurst MA. Bacteria-phage coevolution as a driver of ecological and evolutionary processes in microbial communities. FEMS Microbiol Rev. 2014;38(5):916–31.

Kumar KH, Jagadeesh KS. Microbial consortia-mediated plant defense against phytopathogens and growth benefits. South Indian J Biol Sci. 2016;2(4):395–403.

Kvennefors ECE, Sampayo E, Kerr C, Vieira G, Roff G, Barnes AC, et al. Regulation of Bacterial Communities Through Antimicrobial Activity by the Coral Holobiont. Microbial Ecology. 2012;63(3):605–18.

de las Heras A, Chavarría M, de Lorenzo V. Association of dnt genes of Burkholderia sp. DNT with the substrate-blind regulator DntR draws the evolutionary itinerary of 2,4-dinitrotoluene biodegradation. Mol Microbiol. 2011;82(2):287–99.

Latifi A, Ruiz M, Zhang CC. Oxidative stress in cyanobacteria. FEMS Microbiol Rev. 2009;33(2):258–78.

Latorre C, Lee JH, Spiller H, Shanmugam KT. Ammonium ion-excreting cyanobacterial mutant as a source of nitrogen for growth of rice: A feasibility study. Biotechnol Lett. 1986;8(7):507–12.

Law R, Daniel Morton R. Permanence and the assembly of ecological communities. Ecology. 1996;77(3):762–75.

LeClair JS, Wahl LM. The Impact of Population Bottlenecks on Microbial Adaptation. J Stat Phys. Springer US; 2017;172(1):1–12.

Leino H, Kosourov SN, Saari L, Sivonen K, Tsygankov AA, Aro EM, et al. Extended H_2 photoproduction by N2-fixing cyanobacteria immobilized in thin alginate films. Int J Hydrogen Energy. 2012;37(1):151–61.

Lenski RE. Convergence and Divergence in a Long-Term Experiment with Bacteria. Am Nat. 2017;190(S1):S57–68.

Lenski RE, Mongold JA, Sniegowski PD, Travisano M, Vasi F, Gerrish PJ, et al. Evolution of competitive fitness in experimental populations of E. coli: What makes one genotype a better competitor than another? Antonie van Leeuwenhoek, Int J Gen Mol Microbiol. 1998;73(1):35–47.

Lenski RE, Rose MR, Simpson SC, Tadler SC. Long-Term Experimental Evolution in Escherichia coli . I . Adaptation and Divergence During 2 , 000 Generations. Am Nat. 1991;138(6):1315–41.

Li T, Li C-T, Butler K, Hays SG, Guarnieri MT, Oyler GA, et al. Mimicking lichens: Incorporation of yeast strains together with sucrose-secreting cyanobacteria improves survival, growth, ROS removal, and lipid production in a stable mutualistic co-culture production platform. Biotechnol Biofuels. 2017;10(1):1–12.

Liaimer A, Helfrich EJN, Hinrichs K, Guljamow A, Ishida K, Hertweck C, et al. Nostopeptolide plays a governing role during cellular differentiation of the symbiotic cyanobacterium *Nostoc punctiforme*. Proc Natl Acad Sci. 2015;112(6):1862–7.

Lindemann SR, Bernstein HC, Song HS, Fredrickson JK, Fields MW, Shou W, et al. Engineering microbial consortia for controllable outputs. ISME J. 2016. p. 2077–84.

Little AE, Robinson CJ, Peterson SB, Raffa KF, Handelsman J. Rules of Engagement: Interspecies Interactions that Regulate Microbial Communities. Annu Rev Microbiol. 2008;62:375–401.

Liu Z, Müller J, Li T, Alvey RM, Vogl K, Frigaard N, et al. Genomic analysis reveals key aspects of prokaryotic symbiosis in the phototrophic consortium “Chlorochromatium aggregatum”. Genome Biol. 2013;14(11):R127.

Löwe H, Hobmeier K, Moos M, Kremling A, Pflüger-Grau K. Photoautotrophic production of polyhydroxyalkanoates in a synthetic mixed culture of Synechococcus elongatus cscB and Pseudomonas putida cscAB. Biotechnol Biofuels. 2017a;:1–11.

Löwe H, Schmauder L, Hobmeier K, Kremling A, Pflüger-Grau K. Metabolic engineering to expand the substrate spectrum of Pseudomonas putida toward sucrose. Microbiologyopen. 2017b;6(4):1–9.

Löwe H, Sinner P, Kremling A, Pflüger-Grau K. Engineering sucrose metabolism in Pseudomonas putida highlights the importance of porins. Microb Biotechnol. 2018;0(0):1–10.

Lu Y. Making Yeast Competent Cells and Yeast Cell Transformation. Bio-Protocol. 2011;1(14):4–6.

MacArthur R, Levins R. Competition, habitat selection, and character displacement in a patchy environment. Proc Natl Acad Sci. 1964;51(6):1207–10.

Maharjan R, Seeto S, Notley-McRobb L, Ferenci T. Clonal Adaptive Radiation in a Constant Environment. Science. 2006;313(5786):514–7.

Malmstrom RR, Coe A, Kettler GC, Martiny AC, Frias-Lopez J, Zinser ER, et al. Temporal dynamics of Prochlorococcus ecotypes in the Atlantic and pacific oceans. ISME J. 2010;4(10):1252–64.

Marchal M, Goldschmidt F, Derksen-Müller SN, Panke S, Ackermann M, Johnson DR. A passive mutualistic interaction promotes the evolution of spatial structure within microbial populations. BMC Evol Biol. 2017;17(1):106.

Markson JS, Piechura JR, Puszynska AM, O'Shea EK. Circadian control of global gene expression by the cyanobacterial master regulator RpaA. Cell. 2013;155(6):1396–408.

Martínez-García E, Jatsenko T, Kivisaar M, de Lorenzo V. Freeing Pseudomonas putida KT2440 of its proviral load strengthens endurance to environmental stresses. Environ Microbiol. 2015;17(1):76–90.

Mata TM, Martins AAA, Caetano NS. Microalgae for biodiesel production and other applications: A review. Renew Sustain Energy Rev. 2010;14(1):217–32.

May RM. Thresholds and breakpoints in ecosystems with a multiplicity of stable states. Nature. 1977. p. 471–7.

Mccann KS. The diversity–stability debate. Nature. 2000;405:228–33.

McEwen JT, Machado IMP, Connor MR, Atsumi S. Engineering Synechococcus elongatus PCC 7942 for continuous growth under diurnal conditions. Appl Environ Microbiol. 2013 Mar;79(5):1668–75.

McGrady-Steed J, Harris PM, Morin PJ. Biodiversity regulates ecosystem predictability. Nature. 1997;390(6656):162–5.

Meeks JC, Elhai J. Regulation of Cellular Differentiation in Filamentous Cyanobacteria in Free-Living and Plant-Associated Symbiotic Growth States. Microbiol Mol Biol Rev. 2002;66(1):94–121.

Messner P, Sleytr UB. Crystalline bacterial cell-surface layers. Adv Microb Physiol. 1992;33:213–75.

Messner P, Steiner K, Zarschler K, Schäffer C. S-layer nanoglycobiology of bacteria. Carbohydr Res. 2008;343(12):1934–51.

Minty JJ, Singer ME, Scholz SA, Bae C-H, Ahn J-H, Foster CE, et al. Design and characterization of synthetic fungal-bacterial consortia for direct production of isobutanol from cellulosic biomass. Proc Natl Acad Sci U S A. 2013;110(36):14592–7.

Momeni B, Chen CC, Hillesland KL, Waite A, Shou W. Using artificial systems to explore the ecology and evolution of symbioses. Cell. Mol. Life Sci. 2011. p. 1353–68.

Momeni B, Waite A, Shou W. Spatial self-organization favors heterotypic cooperation over cheating. Elife. 2013;2013(2).

Morel A, Ahn Y-H, Partensky F, Vaulot D, Claustre H. Prochlorococcus and Synechococcus - a Comparative-Study of Their Optical-Properties in Relation To Their Size and Pigmentation. J Mar Res. 1993;51:617–49.

Moreno-Garrido I. Microalgae immobilization : Current techniques and uses. Bioresour Technol. 2008;99:3949–64.

Morris JJ, Johnson ZI, Szul MJ, Keller M, Zinser ER. Dependence of the cyanobacterium Prochlorococcus on hydrogen peroxide scavenging microbes for growth at the ocean's surface. PLoS One. 2011;6(2).

Moutinho TJ, Panagides JC, Biggs MB, Medlock GL, Kolling GL, Papin JA. Novel co-culture plate enables growth dynamic-based assessment of contact-independent microbial interactions. PLoS One. 2017;12(8):1–13.

Mueller UG, Sachs JL. Engineering Microbiomes to Improve Plant and Animal Health. Trends Microbiol. 2015. p. 606–17.

Naeem S, Li S. Biodiversity enhances ecosystem reliability. Nature. 1997;390(6659):507–9.

Nai C, Meyer V. From Axenic to Mixed Cultures: Technological Advances Accelerating a Paradigm Shift in Microbiology. Trends Microbiol. 2018. p. 538–54.

Natrah FMI, Bossier P, Sorgeloos P, Yusoff FM, Defoirdt T. Significance of microalgal-bacterial interactions for aquaculture. Rev. Aquac. 2014. p. 48–61.

Nelson KE, Weinel C, Paulsen IT, Dodson RJ, Hilbert H, Santos VAPM, et al. Complete genome sequence and comparative analysis of the metabolically versatile Pseudomonas putida KT2440. Environ Microbiol. 2002;4(12):799–808.

Niederholtmeyer H, Wolfstädter BT, Savage DF, Silver P a, Way JC. Engineering cyanobacteria to synthesize and export hydrophilic products. Appl Environ Microbiol. 2010;76(11):3462–6.

Nikel PI, Chavarría M, Danchin A, de Lorenzo V. From dirt to industrial applications: Pseudomonas putida as a Synthetic Biology chassis for hosting harsh biochemical reactions. Curr Opin Chem Biol. 2016;34:20–9.

Nikel PI, Chavarrı M. Endogenous Stress Caused by Faulty Oxidation Reactions Fosters Evolution of 2,4-Dinitrotoluene- Degrading Bacteria. 2013;9(8).

Nikel PI, Silva-Rocha R, Benedetti I, de Lorenzo V. The private life of environmental

bacteria: Pollutant biodegradation at the single cell level. Environ Microbiol. 2014;16(3):628–42.

Nishino SF, Paoli GC. Aerobic Degradation of Dinitrotoluenes and Pathway for Bacterial Degradation of Aerobic Degradation of Dinitrotoluenes and Pathway for Bacterial Degradation of 2,6-Dinitrotoluene. Appl Environ Microbiol. 2000;66(5):2139–47.

Oh S, Seo Y, Ryu K. Reductive removal of 2,4-dinitrotoluene and 2,4-dichlorophenol with zero-valent iron-included biochar. Bioresour Technol. 2016;216:1014–21.

Ortiz-Marquez JCF, Do Nascimento M, Curatti L. Metabolic engineering of ammonium release for nitrogen-fixing multispecies microbial cell-factories. Metab Eng. 2014;23:154–64.

Ortiz-Marquez JCF, Do Nascimento M, Dublan MDLA, Curatti L. Association with an ammonium-excreting bacterium allows diazotrophic culture of oil-rich eukaryotic microalgae. Appl Environ Microbiol. 2012;78(7):2345–52.

Ortiz-Marquez JCF, Do Nascimento M, Zehr JP, Curatti L. Genetic engineering of multispecies microbial cell factories as an alternative for bioenergy production. Trends Biotechnol. 2013;31(9):521–9.

Padda RS, Wang C, Hughes JB, Kutty R, Bennett GN. Mutagenicity of nitroaromatic degradation compounds. Environ Toxicol Chem. 2003;22(10):2293–7.

Pande S, Kaftan F, Lang S, Svatoš A, Germerodt S, Kost C. Privatization of cooperative benefits stabilizes mutualistic cross-feeding interactions in spatially structured environments. ISME J. 2016;10(6):1413–23.

Pandey RP, Parajuli P, Koffas MAG, Sohng JK. Microbial production of natural and non-natural flavonoids: Pathway engineering, directed evolution and systems/synthetic biology. Biotechnol Adv. 2016;34(5):634–62.

Pankratov TA, Kachalkin A V, Korchikov ES, Dobrovol TG. Microbial Communities of Lichens. 2017;86(3):293–309.

Papini M, Salazar M, Nielsen J. Systems biology of industrial microorganisms. Adv Biochem Eng Biotechnol. 2010;120:51–99.

Park W, Peña-Llopis S, Lee Y, Demple B. Regulation of superoxide stress in Pseudomonas putida KT2440 is different from the SoxR paradigm in Escherichia coli. Biochem Biophys Res Commun. 2006;341(1):51–6.

Park Y, Je KW, Lee K, Jung SE, Choi TJ. Growth promotion of Chlorella ellipsoidea by co-inoculation with Brevundimonas sp. isolated from the microalga. Hydrobiologia. 2008;598(1):219–28.

Partensky F, Hess WR, Vaulot D. Prochlorococcus, a marine photosynthetic prokaryote of global significance. Microbiol Mol Biol Rev. 1999;63(1):106–27.

Paul C, Barofsky A, Vidoudez C, Pohnert G. Diatom exudates influence metabolism and cell growth of co-cultured diatom species. Mar Ecol Prog Ser. 2009;389(2007):61–70.

Paul C, Mausz MA, Pohnert G. A co-culturing/metabolomics approach to investigate chemically mediated interactions of planktonic organisms reveals influence of bacteria on diatom metabolism. Metabolomics. 2013;9(2):349–59.

Pepper L, Cho Y, Boder E, Shusta E. A decade of yeast surface display technology: where are we now? Comb Chem. 2008;11(2):127–34.

Pereira SB, Mota R, Vieira CP, Vieira J, Tamagnini P. Phylum-wide analysis of genes/proteins related to the last steps of assembly and export of extracellular polymeric substances (EPS) in cyanobacteria. Sci Rep. 2015 6;5:14835.

Pérez-Pantoja D, Nikel PI, Chavarría M, de Lorenzo V. Endogenous Stress Caused by Faulty Oxidation Reactions Fosters Evolution of 2,4-Dinitrotoluene-Degrading Bacteria. PLoS Genet. 2013;9(8).

Piechura JR, Amarnath K, Shea EKO. Natural changes in light interact with circadian regulation at promoters to control gene expression in cyanobacteria. 2017;1–37.

Ponce-Toledo RI, Deschamps P, López-García P, Zivanovic Y, Benzerara K, Moreira D. An Early-Branching Freshwater Cyanobacterium at the Origin of Plastids. Curr Biol. 2017;27(3):386–91.

Posewitz MC. Metabolism and Genetics of Algal Hydrogen Production. Microalgal Hydrog Prod. 2018. p. 167–88.

Prosser JI, Bohannan BJM, Curtis TP, Ellis RJ, Firestone MK, Freckleton RP, et al. The role of ecological theory in microbial ecology. Nat Rev Microbiol. 2007;5(5):384.

Rai a. N, Söderbäck E, Bergman B. Cyanobacterium±plant symbioses. New Phytol. 2000;147(3):449–81.

Rai AN, Bergman B, Rasmussen U. Cyanobacteria in symbiosis. Rai AN, Bergman B, Rasmussen U, editors. Kluwer Academic Pub.; 2002.

Ramos JL, Duque E, Maria-Trinidad G, Godoy P. Mechanisms of solvent tolerance in gram-negative bacteria. Annu Rev Microbiol. 2002;56:743–68.

Rastogi RP, Sinha RP. Biotechnological and industrial significance of cyanobacterial secondary metabolites. Biotechnol Adv. 2009;27(4):521–39.

Ratcliff WC, Denison RF, Borrello M, Travisano M. Experimental evolution of multicellularity. Proc Natl Acad Sci. 2012;109(5):1595–600.

Raven JA. Why Are There No Picoplanktonic O(2) Evolvers with Volumes Less-Than 10(-19) M(3). J Plankton Res. 1994;16(5):565–80.

Reddington SC, Howarth M. Secrets of a covalent interaction for biomaterials and biotechnology: SpyTag and SpyCatcher. Curr Opin Chem Biol. 2015. 29:94–9.

Rittmann BE. Opportunities for renewable bioenergy using microorganisms. Biotechnol Bioeng. 2008;100(2):203–12.

Rocheleau S, Kuperman RG, Simini M, Hawari J, Checkai RT, Thiboutot S, et al. Toxicity of 2 , 4-dinitrotoluene to terrestrial plants in natural soils. Sci Total Environ. 2010;408:3193–9.

Rollié S, Mangold M, Sundmacher K. Designing biological systems: Systems Engineering meets Synthetic Biology. Chem. Eng. Sci. 2012. p. 1–29.

Romo S, Perez-Martinez C. The Use of Immobilization in Alginate Beads for Long-Term Storage of Pseudanabaena galeata (Cyanobacteria) in the Laboratory. J Phycol. 1997;(33):1073–6.

Rossetti V, Schirrmeister BE, Bernasconi M V, Bagheri HC. The evolutionary path to terminal differentiation and division of labor in cyanobacteria. J Theor Biol. 2010;262(1):23–34.

Roy KD, Marzorati M, Van den Abbeele P, Van de Wiele T, Boon N. Synthetic microbial ecosystems: an exciting tool to understand and apply microbial communities. Environ Microbiol. 2014;16(6):1472–81.

Rubin BE, Wetmore KM, Price MN, Diamond S, Shultzaberger RK, Lowe LC, et al. The essential gene set of a photosynthetic organism. Proc Natl Acad Sci U S A. 2015;112(48):E6634-43.

Ruiz-güereca DA, Sánchez-saavedra MP. Growth and phosphorus removal by Synechococcus elongatus co-immobilized in alginate beads with Azospirillum brasilense. J Appl Phycol. Journal of Applied Phycology; 2016;1501–7.

Sabra W, Dietz D, Tjahjasari D, Zeng A-P. Biosystems analysis and engineering of microbial consortia for industrial biotechnology. Eng Life Sci. 2010;10(5):407–21.

Sabri S, Nielsen LK, Vickers CE. Molecular control of sucrose utilization in Escherichia coli W, an efficient sucrose-utilizing strain. Appl Environ Microbiol. 2013a;79(2):478–87.

Sabri S, Steen JA, Bongers M, Nielsen LK, Vickers CE. Knock-in/Knock-out (KIKO) vectors for rapid integration of large DNA sequences, including whole metabolic pathways, onto the Escherichia coli chromosome at well-characterised loci. Microb Cell Fact. 2013b;12(1):1.

Said S Ben, Or D. Synthetic microbial ecology: Engineering habitats for modular consortia. Front Microbiol. 2017;8(JUN).

Samuelson P, Gunneriusson E, Nygren PA, Ståhl S. Display of proteins on bacteria. J Biotechnol. 2002;96(2):129–54.

Sandor M, Langone J. Demonstration of high and low affinity complexes between protein A and rabbit immunoglobulin C antibodies depending on hapten density. Biochem Biophys Res. 1982;106(3):761–7.

Sauer J, Schreiber U, Schmid R, Völker U, Forchhammer K. Nitrogen starvation-induced chlorosis in Synechococcus PCC 7942. Low-level photosynthesis as a mechanism of long-term survival. Plant Physiol. 2001;126(1):233–43.

Savage VM, Webb CT, Norberg J. A general multi-trait-based framework for studying the effects of biodiversity on ecosystem functioning. J Theor Biol. 2007;247(2):213–29.

Saxena S. Diversity of Industrially Relevant Microbes. Appl Microbiol. New Delhi: Springer India; 2015. p. 1–11.

Schmidt TGM, Skerra A. One-step affinity purification of bacterially produced proteins by means of the “Strep tag” and immobilized recombinant core streptavidin. J Chromatogr A. 1994;676(2):337–45.

Schuster B, Sleytr UB. S-layer-supported lipid membranes. J Biotechnol. 2000;74(3):233–54.

Shaner NC, Lambert GG, Chammas A, Ni Y, Cranfill PJ, Baird MA, et al. A bright monomeric green fluorescent protein derived from Branchiostoma lanceolatum. Nat Methods. 2013;10(5):407–9.

Sharma NK, Tiwari SP, Tripathi K, Rai AK. Sustainability and cyanobacteria (blue-green algae): Facts and challenges. J Appl Phycol. 2011;23(6):1059–81.

Sheehan J, Dunahay T, Benemann J, Roessler P. Look Back at the U.S. Department of Energy’s Aquatic Species Program: Biodiesel from Algae; Close-Out Report. 1998;(July).

Shemer B, Yagur-kroll S, Hazan C, Belkin S. Aerobic Transformation of 2,4-Dinitrotoluene by Escherichia coli and Its Implications for the Detection of Trace Explosives. Appl Environ Microbiol. 2018;84(4):e01729-17.

Sher D, Thompson JW, Kashtan N, Croal L, Chisholm SW. Response of Prochlorococcus ecotypes to co-culture with diverse marine bacteria. ISME J. 2011. p. 1125–32.

Sherr EB, Sherr BF. Significance of predation by protists in aquatic microbial food webs. Antonie van Leeuwenhoek, Int J Gen Mol Microbiol. 2002;81(1–4):293–308.

Shevchenko A, Wilm M, Vorm O, Mann M. Mass Spectrometric Sequencing of Proteins from Silver-Stained Polyacrylamide Gels. Anal Chem. 1996;68(5):850–8.

Shiloach J, Bauer S, Chemistry B. High-Yield Growth of E. coli at Different Temperatures in a Bench Scale Fermentor. Biotechnol Bioeng. 1975;XVII:227–39.

Shong J, Jimenez Diaz MR, Collins CH. Towards synthetic microbial consortia for bioprocessing. Curr Opin Biotechnol. 2012;23(5):798–802.

Shou W, Ram S, Vilar JMG. Synthetic cooperation in engineered yeast populations. Proc Natl Acad Sci USA. 2007;104(6):1877–82.

Simkovsky R, Daniels EF, Tang K, Huynh SC, Golden SS, Brahamsha B. Impairment of O-antigen production confers resistance to grazing in a model amoeba-cyanobacterium predator-prey system. Proc Natl Acad Sci. 2012;109(41):16678–83.

Singh AP, Tiwari DN. Phenotypic expression of ammonia-excreting mutants of *Anabaena* 7120 under nitrogen limitation. World J Microbiol Biotechnol. 1998;14(4):591–3.

Šmarda J, Šmajs D, Komrska J, Krzyžánek V. S-layers on cell walls of cyanobacteria. Micron. 2002;33(3):257–77.

Smith MJ, Francis MB. A Designed A. vinelandii−S. elongatus Coculture for Chemical Photoproduction from Air, Water, Phosphate, and Trace Metals. ACS Synth Biol. 2016;5:acssynbio.6b00107.

Smith MJ, Francis MB. Improving metabolite production in microbial co-cultures using a spatially constrained hydrogel. Biotechnol Bioeng. 2017;114(6):1195–200.

Smith VH, Sturm BSM, deNoyelles FJ, Billings SA. The ecology of algal biodiesel production. Trends Ecol. Evol. 2010. p. 301–9.

Söding J, Biegert A, Lupas AN. The HHpred interactive server for protein homology detection and structure prediction. Nucleic Acids Res. 2005;33(SUPPL. 2):244–8.

Song H-S, Cannon W, Beliaev A, Konopka A. Mathematical Modeling of Microbial Community Dynamics: A Methodological Review. Processes. 2014a;2(4):711–52.

Song H, Ding M-Z, Jia X-Q, Ma Q, Yuan Y-J. Synthetic microbial consortia: from systematic

analysis to construction and applications. Chem Soc Rev. 2014b;

Song K, Tan X, Liang Y, Lu X. The potential of Synechococcus elongatus UTEX 2973 for sugar feedstock production. Appl Microbiol Biotechnol. 2016;(189).

Spain JC. Biodegradation of Nitroaromatic Compounds. Annu Rev Microbiol. 1995;49:2548-2523–55.

Spanggord RJ, Spain JC, Nishino SF, Mortelmans KE. Biodegradation of 2,4-dinitrotoluene by a Pseudomonas sp. Appl Environ Microbiol. 1991;57(11):3200–5.

Spiller H, Gunasekaran M. Ammonia-excreting mutant strain of the cyanobacterium Anabaena variabilis supports growth of wheat. Appl Microbiol Biotechnol. 1990;33(4):477–80.

Spiller H, Latorre C, Hassan ME, Shanmugam AKT. Isolation and Characterization of Nitrogenase-Derepressed Mutant Strains of Cyanobacterium Anabaena variabilist. J Bacteriol. 1986;165(2):412–9.

Srinivasulu B, Adinarayana K, Ellaiah P. Investigations on Neomycin Production With Immobilized Cells of Strep- tomyces marinensis Nuv-5 in Calcium Alginate Matrix. 2003;4(4):1–6.

Stapleton J a., Whitehead T a., Nanda V. Computational redesign of the lipid-facing surface of the outer membrane protein OmpA. Proc Natl Acad Sci. 2015;112(31):9632–7.

Stoodley P, Sauer K, Davies DG, Costerton JW. Biofilms as complex differentiated communities. Annu Rev Microbiol. 2002;56:187–209.

Sumper M, Berg E, Mengele R. Primary structure and glycosylation of the S-layer protein of Haloferax volcanii. J Bacteriol. 1990;172(12):7111–8.

Symons ZC, Bruce NC. Bacterial pathways for degradation of nitroaromatics. Nat Prod Rep. 2006;23(6):845.

Tan J, Zuniga C, Zengler K. Unraveling interactions in microbial communities - from co-cultures to microbiomes. J Microbiol. 2015;53(5):295–305.

Tandon P, Jin Q. Microalgae culture enhancement through key microbial approaches. Renew. Sustain. Energy Rev. 2017. p. 1089–99.

Tecon R, Or D. Cooperation in carbon source degradation shapes spatial self- organization of microbial consortia on hydrated surfaces. Sci Rep. 2017;7:1–11.

Temperton B, Giovannoni SJ. Metagenomics: Microbial diversity through a scratched lens. Curr. Opin. Microbiol. 2012. p. 605–12.

Therien JB, Zadvornyy OA, Posewitz MC, Bryant DA, Peters JW. Growth of Chlamydomonas reinhardtii in acetate-free medium when co-cultured with. 2014;1–8.

Tizei PAG, Csibra E, Torres L, Pinheiro VB. Selection platforms for directed evolution in synthetic biology. Biochem Soc Trans. 2016;44(4):1165–75.

Tong Z, Zhe L, Huai-lan Z. microbial flocculant and its application in environmental protection. J Env Sci. 1999;11(1):1–12.

Trautner C, Vermaas WFJ. The sll1951 gene encodes the surface layer protein of Synechocystis sp. strain PCC 6803. J Bacteriol. 2013;195(23):5370–80.

Tringe SG, Rubin EM. Metagenomics: DNA sequencing of environmental samples. Nat. Rev. Genet. 2005. p. 805–14.

Trivedi P, Delgado-Baquerizo M, Trivedi C, Hu H, Anderson IC, Jeffries TC, et al. Microbial regulation of the soil carbon cycle: Evidence from gene-enzyme relationships. ISME J. 2016;10(11):2593–604.

Tsimring L, Hasty J, Danino T, Mondrago O, Mondragón-Palomino O, Tsimring L, et al. A synchronized quorum of genetic clocks. Nature. 2010;463(7279):326–30.

Tsutsui H, Karasawa S, Okamura Y, Miyawaki A. Improving membrane voltage measurements using FRET with new fluorescent proteins. Nat Methods. 2008;5(8):683–5.

Umeda H, Aiba H, Mizuno T. SomA, a novel gene that encodes a major outer-membrane protein of Synechococcus sp. PCC 7942. Microbiology. 1996;142 (Pt 8:2121–8.

Usher KM, Bergman B, Raven JA. Exploring Cyanobacterial Mutualisms. Annu Rev Ecol Evol Syst. 2007;38(1):255–73.

Vaara T. The outermost surface structures in chroococcacean cyanobacteria. Can J Microbiol. 1982;28:929–41.

Vaishampayan A, Sinha RP, Häder DP, Dey T, Gupta AK, Bhan U, et al. Cyanobacterial biofertilizers in rice agriculture. Bot. Rev. 2001. p. 453–516.

Verseux CN, Baqué M, Lehto K, De Vera JPP, Rothschild LJ, Billi D. Sustainable life support on Mars - The potential roles of cyanobacteria. Int J Astrobiol. 2016. p. 65–92.

Verseux CN, Paulino-Lima IG, Baqué M, Billi D, Rothschild LJ. Synthetic biology for space exploration: Promises and societal implications. Ambivalences Creat Life Soc Philos Dimens Synth Biol. 2015. p. 73–100.

Voss S, Skerra a. Mutagenesis of a flexible loop in streptavidin leads to higher affinity for the Strep-tag II peptide and improved performance in recombinant protein purification. Protein Eng. 1997;10(8):975–82.

Wahl LM, Gerrish PJ, Saika-Voivod I. Evaluating the impact of population bottlenecks in experimental evolution. Genetics. 2002;162(2):961–71.

Waite AJ, Shou W. Adaptation to a new environment allows cooperators to purge cheaters stochastically. Proc Natl Acad Sci. 2012;109(47):19079–86.

Wang H, Zhang W, Chen L, Wang J, Liu T. The contamination and control of biological pollutants in mass cultivation of microalgae. Bioresour. Technol. 2013. p. 745–50.

Wang Z, Ye Z, Zhang M. Bioremediation of 2,4-dinitrotoluene (2,4-DNT) in immobilized micro-organism biological filter. J Appl Microbiol. 2011;(110):1476–84.

Waters CM, Bassler BL. Quorum Sensing : Communication in Bacteria. Annu Rev Cell Dev Biol. 2005;21(1):319–46.

Weiss TL, Ducat DC. Designing stable, synthetic, light-driven cyanobacteria-heterotroph consortia for bioproduction. Metab Eng. 2017;(44):236–45.

Weiss TL, Young EJ, Ducat DC. A synthetic , light-driven consortium of cyanobacteria and heterotrophic bacteria enables stable polyhydroxybutyrate production. Metab Eng. 2017;44:236–45.

Werner GDA, Strassmann JE, Ivens ABF, Engelmoer DJP, Verbruggen E, Queller DC, et al. Evolution of microbial markets. Proc Natl Acad Sci USA. 2014 Jan 28;111(4):1237–44.

Widder S, Allen RJ, Pfeiffer T, Curtis TP, Wiuf C, Sloan WT, et al. Challenges in microbial ecology: Building predictive understanding of community function and dynamics. ISME J. 2016. p. 2557–68.

Wilkinson TG, Topiwala HH, Hamer G. Interactions in a mixed bacterial population growing on methane in continuous culture. Biotechnol Bioeng. 1974;16(1):41–59.

Wintermute EH, Silver PA. Dynamics in the mixed microbial concourse. Genes Dev. 2010;24(23):2603–14.

Wyman CE, Goodman BJ. Biotechnology for production of fuels, chemicals, and materials from biomass. Appl Biochem Biotechnol. 1993 Sep;39–40(1):41–59.

Xu Y, Tiago Guerra L, Li Z, Ludwig M, Charles Dismukes G, Bryant D a. Altered carbohydrate metabolism in glycogen synthase mutants of Synechococcus sp. strain PCC 7002: Cell factories for soluble sugars. Metab Eng. 2012;16C:56–67.

Yang S, Sleight SC, Sauro HM. Rationally designed bidirectional promoter improves the evolutionary stability of synthetic genetic circuits. Nucleic Acids Res. 2013;41(1):e33.

Ye C, Zou W, Xu N, Liu L. Metabolic model reconstruction and analysis of an artificial microbial ecosystem for vitamin C production. J Biotechnol. 2014;182–183(1):61–7.

Yinon J. Toxicity and Metabolism of Explosives. Boca Raton, Florida, USA: CRC Press, Inc.; 1990.

Yoon JM, Oliver DJ, Shanks J V. Phytotransformation of 2,4-Dinitrotoluene in Arabidopsis thaliana : Toxicity , Fate , and Gene Expression Studies in Vitro. 2006;1524–31.

Zakeri B, Fierer JO, Celik E, Chittock EC, Schwarz-Linek U, Moy VT, et al. Peptide tag forming a rapid covalent bond to a protein, through engineering a bacterial adhesin. Proc Natl Acad Sci USA. 2012;109(12):E690-7.

Zavřel T, Sinetova MA, Červený J. Measurement of Chlorophyll a and Carotenoids Concentration in Cyanobacteria. Bio-Protocol. 2015;5(9):1–5.

Zengler K, Palsson BO. A road map for the development of community systems (CoSy) biology. Nat Rev Microbiol. 2012;10(5):366–72.

Zhang CC, Laurent S, Sakr S, Peng L, Bédu S. Heterocyst differentiation and pattern formation in cyanobacteria: A chorus of signals. Mol. Microbiol. 2006. p. 367–75.

Zhang Z, Meng L, Ni C, Yao L, Zhang F, Jin Y, et al. Engineering Escherichia coli to bind to cyanobacteria. J Biosci Bioeng. 2017;123(3):347–52.

Zinser ER. Cross-protection from hydrogen peroxide by helper microbes: The impacts on the cyanobacterium Prochlorococcus and other beneficiaries in marine communities. Environ Microbiol Rep. 2018;00:1–13.